The Journal of Fourier Analysis and Applications

Volume 5, Numbers 2/3, 1999

Fractal Differential Equations on the Sierpinski Gasket

Kyallee Dalrymple, Robert S. Strichartz, and Jade P. Vinson

Communicated by Stephane Jaffard

ABSTRACT. Let Δ denote the symmetric Laplacian on the Sierpinski gasket SG defined by Kigami [11] as a renormalized limit of graph Laplacians on the sequence of pre-gaskets G_m whose limit is SG. We study the analogs of some of the classical partial differential equations with Δ playing the role of the usual Laplacian. For harmonic functions, biharmonic functions, and Dirichlet eigenfunctions of Δ, we give efficient algorithms to compute the solutions exactly, we display the results of implementing these algorithms, and we prove various properties of the solutions that are suggested by the data. Completing the work of Fukushima and Shima [8] who computed the Dirichlet eigenvalues and their multiplicities, we show how to construct a basis (but not orthonormal) for the eigenspaces, so that we have the analog of Fourier sine series on the unit interval. We also show that certain eigenfunctions have the property that they are a non-zero constant along certain lines contained in SG. For the analogs of the heat and wave equation, we give algorithms for approximating the solution, and display the results of implementing these algorithms. We give strong evidence that the analog of finite propagation for the wave equation does not hold because of inconsistent scaling behavior in space and time.

1. Introduction

Kigami [11] defined a Laplacian on the Sierpinski gasket SG (see Fig. 1) as a renormalized limit of difference operators (graph Laplacians) on the sequence of pre-gaskets G_m whose limit is SG. The existence of such a Laplacian had been known previously through probabilistic constructions of Brownian motion type processes, but this was an indirect approach. Kigami also extended his construction to a wider class of fractals in [12]. This set the stage for a direct analytic study of the analogs of some of the classical partial differential equations on these fractals, which we propose to call *fractal differential equations*. Shima [21] and Fukushima and Shima [8] studied the spectrum

Math Subject Classifications. Primary 31C45, 42C99.

Keywords and Phrases. Fractal differential equations, analysis on fractals, Sierpinski gasket, eigenfunctions of the Laplacian, wave propagation on fractals.

Acknowledgements and Notes. Kyallee Dalrymple – Research supported by the Supercomputing Program for Undergraduate Research (SPUR) at the Cornell Theory Center, which received major funding from the National Science Foundation and New York State.

Robert S. Strichartz – Research supported in part by the National Science Foundation, Grant DMS–9623250.

Jade P. Vinson – Research supported by the National Science Foundation through the Research Experiences for Undergraduates (REU) Program.

ISSN 1069-5869

of the Dirichlet Laplacian, and determined explicitly the eigenvalues and their multiplicities for the analog of SG in all dimensions, using methods introduced in [20] and [19]. One of the main goals of this paper is to complete the process by determining explicitly all the Dirichlet eigenfunctions for the original SG. Thus, we have all the ingredients for the analog of Fourier sine series on SG.

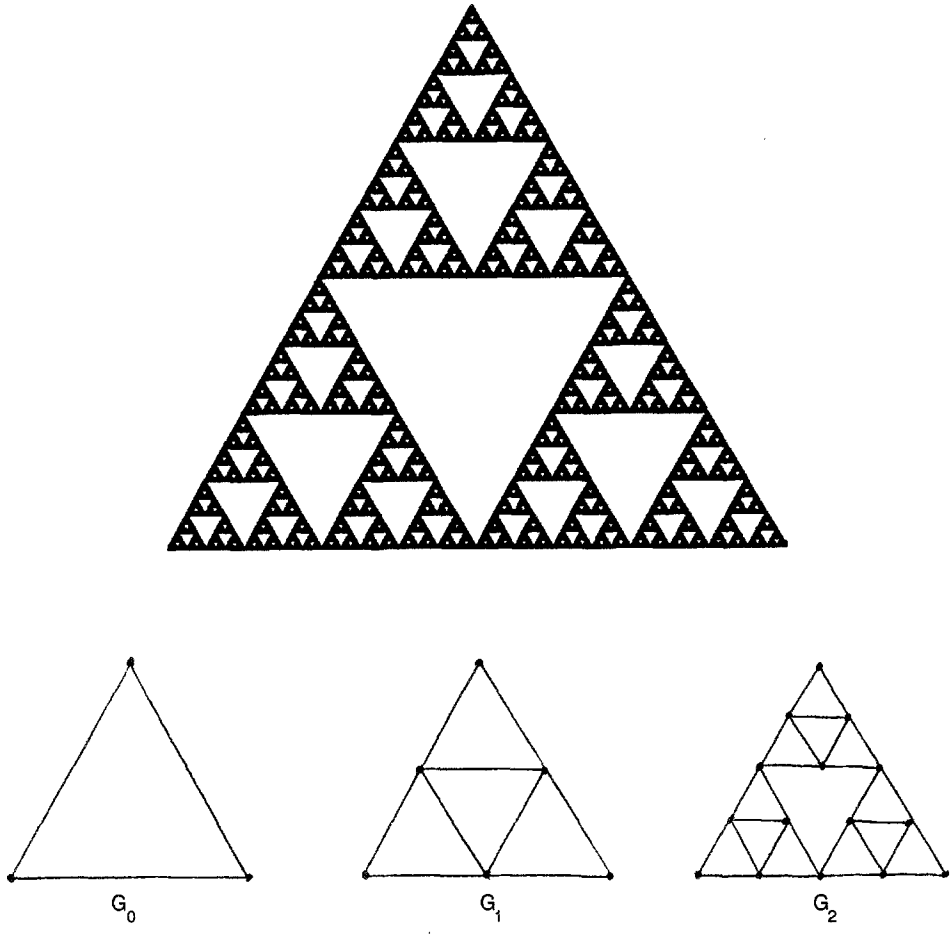

FIGURE 1 a) SG. b) G_0. c) G_1. d) G_2.

These eigenfunctions are important special functions on SG. Other important special functions include the harmonic functions and, more generally, the solutions of $\Delta^k f = 0$. (It is expected that a theory of splines built out of these pieces can be developed.) In Section 2 we give algorithms for the computation of these special functions. The algorithms are both exact and efficient, giving the values of these functions on the vertices of the graph G_m as a direct linear function of the values on three of the vertices of G_{m-1}. We also give some algorithms that allow the direct computation of the restrictions of these functions to line segments (edges in G_m) that occur in SG, without involving values of points not on the line segment. These latter algorithms have important theoretical consequences, but we did not use them in actual computations.

In Section 3 we display the data we obtained by implementing our algorithms. There is a wealth of information here, and we have only scratched the surface in trying to make sense of it. In Section 4 we give proofs of some of the observations that are apparent from the data. We also prove that the three families of Dirichlet eigenfunctions described and illustrated in Section 3 suffice to

generate a basis (not orthonormal, however) for all Dirichlet eigenfunctions. This is the analog of the single family $\sin \pi kx$ of Dirichlet eigenfunctions on the unit interval (the analog of SG in $\mathbb{R}$). In that case, all the eigenfunctions can be built up out of scaled copies of the ground state $\sin \pi x$. In the case of SG, the Dirichlet eigenfunctions reveal a much more complicated structure.

In Section 5 we discuss the heat equation $\frac{\partial}{\partial t}u = \Delta u$ and wave equation $\frac{\partial^2}{\partial t^2}u = \Delta u$, where $u(x,t)$ is a function of $x \in SG$ and time t. Properties of the heat equation are accessible to probabilistic methods, so we concentrate on the wave equation. We describe algorithms for the approximate solutions of both equations, and present data obtained via these algorithms. In contrast to the algorithms in Section 2, these are not exact; from the one-dimensional analog we cannot expect that the restriction of x to G_m will in any way simplify the problem. (Another approach would be to use the Dirichlet eigenfunction expansion, but at present this seems highly impractical.)

Certain properties of the wave equation, such as well-posedness of the Cauchy problem and conservation of energy, are routine consequences of abstract analysis. An obvious question is whether or not there is a maximum speed of propagation for solutions of the wave equation. We will show that this is impossible because of the different scaling properties in space and time. When measured on a smaller scale, the wave must travel faster. It remains remotely possible, but unlikely, that there could be a finite (but unbounded) propagation speed. This would require massive cancellation, of the sort that is ruled out in a more familiar context by the Lions–Titchmarsh Theorem on supports of convolutions of distributions in $\mathbb{R}^n$.

In describing some functions on the vertices of G_m we will simply draw figures with values of the functions at vertices labeled. In order to simplify the figures, we omit the label on vertices where the value is 0.

In this paper we have deliberately restricted our attention to the simplest example of a Laplacian on a fractal. There are obviously many more examples that need to be studied. We mention here a few directions for further research:

1) Describe all Neumann eigenfunctions.

2) Consider the analogous equations on fractal blowups of SG [23]. This was done in [8] for just one blowup, which has a single boundary point. But there are uncountably many non-congruent blow-ups, most of which have no boundary points.

3) Extend the results to higher dimensional Sierpinski gaskets. The results on eigenvalues in [8] are already done in this generality.

4) Extend the results to symmetric Laplacians on other nested fractals as discussed by Lindstrøm [17].

5) Extend the results to other Laplacians on SG.

6) It would be interesting to see the graphs of our functions using the harmonic metric on SG introduced in Kigami [13]. This metric embeds SG in the plane in such a way that the harmonic functions are just restrictions of linear functions on the plane.

Several recent papers on topics related to this work include [2, 3, 6, 7, 9, 15, 16, 24, 25, 26, 27].

Many of the programs used to generate the data presented here are available at the Web site `http://www.tc.cornell.edu/Edu/SPUR/SPUR96/Kyal/cover.html`. This site also contains related graphics.

2. Algorithms for Harmonic Functions and Eigenfunctions

In this section we describe algorithms for the exact computation of harmonic, biharmonic, and Dirichlet eigenfunctions for the symmetric Laplacian on the Sierpinski gasket. These algorithms allow for the computation of the values of these functions on the vertices of the graphs G_m, the pre-gaskets, that approximate SG. The key idea of Kigami [11] is that it is possible to define a Laplacian

Δ on SG as the renormalized limit

$$\Delta = \lim_{m\to\infty} 5^m \Delta_m \tag{2.1}$$

where Δ_m is the graph Laplacian on G_m, which we describe next. (We actually use a slightly different normalization constant than in [11]. Our choice is consistent with [8].)

We let G_0 be the graph whose vertices p_0, p_1, p_2 form an equilateral triangle in the plane, and whose edges are the three sides of the triangle. We let S_j denote the contractive similarities

$$S_j z = p_j + \frac{1}{2}(z - p_j), \quad j = 0, 1, 2,$$

with fixed points at the vertices of G_0 and contraction ratio $1/2$. The vertices V_m and edges E_m of G_m are defined inductively as the images under these contractions of the vertices and edges of G_{m-1}. We define the *boundary* of G_m to consist of the three vertices p_0, p_1, p_2 of G_0. Note that every vertex in G_m that is not in the boundary is the image of two different vertices in G_{m-1}, and has exactly four neighbors. We define a *minimal triangle* in G_m to be the image of G_0 under a contraction $S_{j_1} \cdots S_{j_m}$. It is understood that a function on G_m is a function (real or complex valued) defined on the vertices V_m.

We define the graph Laplacian Δ_m on G_m by

$$\Delta_m f(x) = \left(\sum_{(x,y)\in E_m} f(y) \right) - 4f(x) \tag{2.2}$$

for x in V_m not a boundary point. A *harmonic function* is a solution of $\Delta_m f = 0$ at all non-boundary points. A *biharmonic function* is a solution of $\Delta_m f = g$ at all non-boundary points, where g is harmonic (strictly speaking, $\Delta_m^2 f$ is not defined at points neighboring the boundary points). A *(Dirichlet) eigenfunction* with *eigenvalue* λ_m is a solution of

$$-\Delta_m f = \lambda_m f \tag{2.3}$$

at non-boundary points (that vanishes at the boundary points).

Suppose we have a function f defined on G_{m-1}, and we wish to extend it to G_m. Let T be any minimal triangle in G_{m-1}, with vertices v_0, v_1, v_2, and let v_{01}, v_{12}, v_{02} denote the midpoints of the edges of T, as shown in Fig. 2.

Then the vertices v_0, v_1, v_2 belong to V_{m-1}, so f is defined there, but v_{01}, v_{12}, v_{02} belong to G_m and not G_{m-1}. Thus, the extension problem is to define f at v_{01}, v_{12}, v_{02}. The following algorithm is given in Kigami [11], but we include the proof for completeness.

Algorithm 2.1. If f is harmonic on G_m and T is as in Fig. 2, then

$$f(v_{01}) = \frac{2}{5} f(v_0) + \frac{2}{5} f(v_1) + \frac{1}{5} f(v_2), \tag{2.4}$$

and similarly for $f(v_{12})$ and $f(v_{02})$. Conversely, if f is harmonic on G_{m-1} and we extend it to G_m using (2.4) on every minimal triangle in G_{m-1}, then the extension is harmonic on G_m.

Proof. According to Kigami [11], f is harmonic on G_m if and only if its restriction to G_{m-1} is harmonic and $\Delta_m f(x) = 0$ for every x in V_m but not in V_{m-1}. For each T this means

$$4f(v_{01}) = f(v_0) + f(v_1) + f(v_{12}) + f(v_{02}) \tag{2.5}$$

and similarly for the other two midpoints. It is elementary to check that (2.4) is equivalent to (2.5). □

This algorithm is analogous to the Poisson integral formula, since the values at the midpoints of the edges of T are obtained as weighted averages of the values at the vertices. It provides

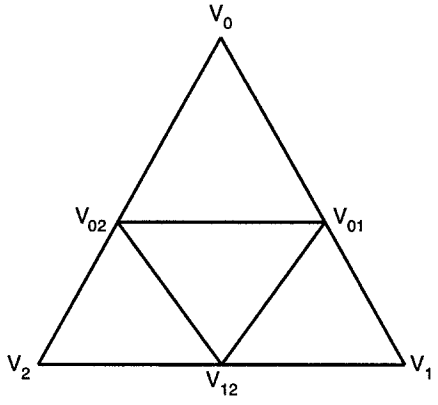

FIGURE 2 Labeling of vertices in G_m of a minimal triangle in G_{m-1}.

an effective procedure to inductively compute the exact values of harmonic functions from the Dirichlet data, namely the boundary values $f(p_0)$, $f(p_1)$, $f(p_2)$. It can also be interpreted as a statement of self-similarity. Specifically, suppose f is the harmonic function satisfying $f(p_0) = 1$, $f(p_1) = f(p_2) = 0$. If R is a 1/3 rotation, then $f \circ R$ and $f \circ R^{-1}$ take boundary values $(0, 1, 0)$ and $(0, 0, 1)$, respectively. Then $f \circ S_0^{-1} + \frac{2}{5} f \circ R \circ S_0^{-1} + \frac{2}{5} f \circ R^{-1} \circ S_0^{-1}$ is a harmonic function on $S_0(SG)$ taking the same values as f on the vertices of this triangle, and so must be equal to f on $S_0(SG)$. Similarly for $\frac{2}{5} f \circ S_1^{-1} + \frac{1}{5} f \circ R^{-1} \circ S_1^{-1}$ on $S_1(SG)$ and $\frac{2}{5} f \circ S_2^{-1} + \frac{1}{5} f \circ R \circ S_2^{-1}$ on $S_2(SG)$. If we ignore the three midpoints where these triangles overlap, we can add the three equations to obtain the self-similar identity

$$\begin{aligned} f &= f \circ S_0^{-1} + \frac{2}{5} f \circ R \circ S_0^{-1} + \frac{2}{5} f \circ R^{-1} \circ S_0^{-1} + \frac{2}{5} f \circ S_1^{-1} \\ &\quad + \frac{1}{5} f \circ R^{-1} \circ S_1^{-1} + \frac{2}{5} f \circ S_2^{-1} + \frac{1}{5} f \circ R \circ S_2^{-1} . \end{aligned}$$

Similar identities hold for $f \circ R$ and $f \circ R^{-1}$. Such identities make it easy to compute inner products of harmonic functions (with respect to normalized Hausdorff measure), as in [24].

The next algorithm enables us to study the restriction of a harmonic function to any straight line contained in SG. Let E be any edge in G_{m-2}. Denote the endpoints of E by v_0, v_1, the midpoint by v_{01}, and let v_{001} be the midpoint of the edge in G_{m-1} connecting v_0 and v_{01}, as in Fig. 3.

Algorithm 2.2. Let f be harmonic on G_m. Then

$$f(v_{001}) = \frac{4}{5} f(v_{01}) + \frac{8}{25} f(v_0) - \frac{3}{25} f(v_1) . \tag{2.6}$$

Proof. We can use (2.4) to solve for $f(v_2)$ in terms of $f(v_0)$, $f(v_1)$, and $f(v_{01})$, obtaining

$$f(v_2) = 5f(v_{01}) - 2f(v_0) - 2f(v_1) .$$

Then we can use this in the formula analogous to (2.4) for $f(v_{02})$, obtaining

$$\begin{aligned} f(v_{02}) &= \frac{1}{5} f(v_1) + \frac{2}{5} f(v_0) + \frac{2}{5} (5f(v_{01}) - 2f(v_0) - 2f(v_1)) \\ &= 2f(v_{01}) - \frac{2}{5} f(v_0) - \frac{3}{5} f(v_1) . \end{aligned}$$

Finally, we substitute this in the analog of (2.4) for the smaller upper triangle to obtain

$$\begin{aligned} f(v_{001}) &= \frac{2}{5} (f(v_0) + f(v_{01})) + \frac{1}{5} f(v_{02}) \\ &= \frac{2}{5} (f(v_0) + f(v_{01})) + \frac{1}{5} \left(2f(v_{01}) - \frac{2}{5} f(v_0) - \frac{3}{5} (v_1) \right) \end{aligned}$$

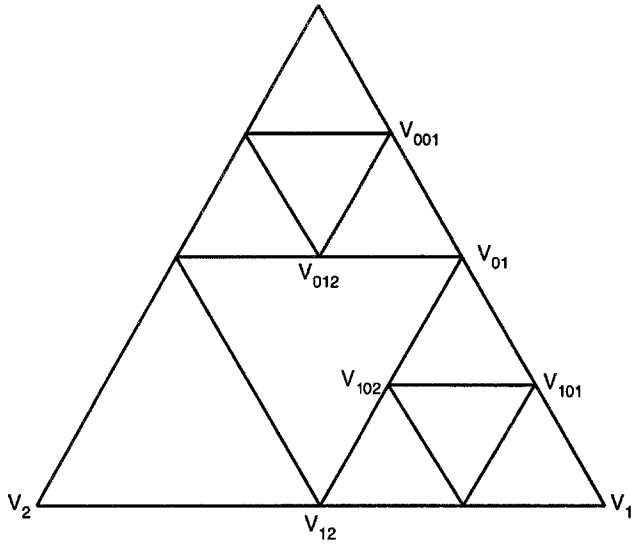

FIGURE 3 Labeling of some vertices in G_m of a minimal triangle in G_{m-2}.

which is (2.6). □

Note that the coefficients in (2.6) sum to 1, but the appearance of the negative sign in (2.6) is in contrast to (2.4).

Next we consider biharmonic functions, solutions of $\Delta g = f$ where f is harmonic. Because of (2.1), we consider the equation $5^m \Delta_m g = f$ on G_m.

Algorithm 2.3. If f is harmonic in G_m, $5^m \Delta_m g = f$, and T is a minimal triangle in G_{m-1}, then

$$\begin{aligned} g(v_{01}) &= \frac{2}{5}g(v_0) + \frac{2}{5}g(v_1) + \frac{1}{5}g(v_2) \\ &\quad - 5^{-m}\left(\frac{9}{50}f(v_0) + \frac{9}{50}f(v_1) + \frac{7}{50}f(v_2)\right) \end{aligned} \tag{2.7}$$

and similarly for $g(v_{12})$ and $g(v_{02})$. Conversely, if $5^{m-1}\Delta_{m-1} g = f$ on G_{m-1} for f harmonic on G_{m-1}, and we extend it to G_m using (2.7), then $5^m \Delta_m g = f$ on G_m, where f is extended to be harmonic on G_m.

Proof. The equation $5^m \Delta_m g = f$ at the midpoint v_{01} says

$$-4g(v_{01}) + g(v_0) + g(v_1) + g(v_{12}) + g(v_{02}) = 5^{-m} f(v_{01}) \ , \tag{2.8}$$

and similarly for the other midpoints. Adding these three equations, we obtain

$$\begin{aligned} &-2g(v_{01}) - 2g(v_{12}) - 2g(v_{02}) + 2g(v_0) + 2g(v_1) + 2g(v_2) \\ &\quad = 5^{-m}\left(f(v_{01}) + f(v_{12}) + f(v_{02})\right) \ . \end{aligned}$$

Using this to eliminate $g(v_{12})$ and $g(v_{02})$ from (2.8) we obtain

$$-5g(v_{01}) + 2g(v_0) + 2g(v_1) + g(v_2) = 5^{-m}\left(\frac{3}{2}f(v_{01}) + \frac{1}{2}f(v_{12}) + \frac{1}{2}f(v_{02})\right) \ .$$

Using (2.4) to replace the values of f at the midpoints by its values at the vertices yields (2.7).

Conversely, assume $5^{m-1}\Delta_{m-1} g = f$ on G_{m-1}, and use (2.7) to extend g to G_m. Then the previous argument shows that $5^m \Delta_m g = f$ holds at all the vertices in V_m but not in V_{m-1}. It

remains to show that this also holds at the vertices in V_{m-1}. This is essentially a consequence of the renormalization property proved in Kigami [11], but we give the proof for completeness.

Let T be any minimal triangle in G_{m-2}, and label the vertices as in Fig. 3. Then v_{01} is a vertex in V_{m-1}, and to show $5^m \Delta_m g(v_{01}) = f(v_{01})$, we need to establish

$$-4g(v_{01}) + g(v_{001}) + g(v_{012}) + g(v_{102}) + g(v_{101}) = 5^{-m} f(v_{01}) \ . \tag{2.9}$$

Now we have the analog of (2.7) holding at the points v_{001}, v_{012}, v_{102}, and v_{101}, and adding these four equations yields

$$\begin{aligned} &g(v_{001}) + g(v_{012}) + g(v_{102}) + g(v_{101}) \\ &\quad = \frac{3}{5} g(v_0) + \frac{3}{5} g(v_1) + \frac{8}{5} g(v_{01}) + \frac{3}{5} g(v_{02}) + \frac{3}{5} g(v_{12}) \\ &\qquad - 5^{-m-2} (8f(v_0) + 8f(v_1) + 18f(v_{01}) + 8f(v_{02}) + 8f(v_{12})) \ . \end{aligned}$$

We substitute this in the left side of (2.9) to obtain

$$\begin{aligned} &\frac{3}{5} g(v_0) + \frac{3}{5} g(v_1) - \frac{12}{5} g(v_{01}) + \frac{3}{5} g(v_{02}) + \frac{3}{5} g(v_{12}) \\ &\qquad -5^{-m-2} (8f(v_0) + 8f(v_1) + 18f(v_{01}) + 8f(v_{02}) + 8f(v_{12})) \ . \end{aligned} \tag{2.10}$$

Since we know $5^{m-1} \Delta_{m-1} g = f$ on G_{m-1}, we have

$$-4g(v_{01}) + g(v_0) + g(v_1) + g(v_{02}) + g(v_{12}) = 5^{1-m} f(v_{01}) \ .$$

Since f is harmonic on G_{m-1}, we have

$$f(v_0) + f(1) + f(v_{02}) + f(v_{12}) = 4f(v_{01}) \ .$$

We substitute these in (2.10) to obtain

$$3 \cdot 5^{-m} f(v_{01}) - 2 \cdot 5^{-m} f(v_{01}) \ ,$$

which proves (2.9).

More generally, the same argument works for any vertex in V_{m-1}, since we did not use the triangle v_2, v_{02}, v_{12} in Fig. 3 in any way. □

It is also possible to obtain the analog of Algorithm 2.2 for the restriction of biharmonic functions to a line, but we will not give the details.

We next consider the extension of solutions of $-\Delta_{m-1} f = \lambda_{m-1} f$ on G_{m-1} to solutions of $-\Delta_m f = \lambda_m f$ on G_m. According to Shima [21], this is possible for Dirichlet eigenfunctions if and only if

$$\lambda_m = \frac{1}{2} \left(5 + \varepsilon_m \sqrt{25 - 4\lambda_{m-1}} \right) \tag{2.11}$$

where $\varepsilon_m = \pm 1$, and $\lambda_m \neq 2, 5$. Note that this implies

$$\lambda_{m-1} = \lambda_m (5 - \lambda_m) \ . \tag{2.12}$$

Algorithm 2.4. If $-\Delta_m f = \lambda_m f$ on G_m, with $\lambda_m \neq 2, 5$, then for any T as in Algorithm 2.1, we have

$$f(v_{01}) = \frac{(4 - \lambda_m)}{(2 - \lambda_m)(5 - \lambda_m)} (f(v_0) + f(v_1)) + \frac{2}{(2 - \lambda_m)(5 - \lambda_m)} f(v_2) \ . \tag{2.13}$$

Conversely, suppose $-\Delta_{m-1} f = \lambda_{m-1} f$ on G_{m-1}, and λ_m satisfies (2.11) with $\lambda_m \neq 2, 5$. Then if we extend f to G_m using (2.13), we obtain a solution of $-\Delta_m f = \lambda_m f$.

Proof. If $-\Delta_m f = \lambda_m f$ on G_m, then instead of (2.5) we have

$$(4 - \lambda_m) f(v_{01}) = f(v_0) + f(v_1) + f(v_{12}) + f(v_{02}) \tag{2.14}$$

and similarly for v_{12} and v_{02}. When we solve this system of equations we obtain (2.13).

Conversely, if $-\Delta_{m-1} f = \lambda_{m-1} f$ and the other conditions hold, then Shima [21] proves that an extension exists. We will give a proof of this as well. We use (2.13) to define f at the midpoints. Then the eigenvalue equation at the midpoint v_{01} is (2.14), and similarly for v_{12} and v_{02}, and these are equivalent to (2.13). It remains to show that the eigenvalue equation also holds at the vertices of T. Let T be contained in the minimal G_{m-1} triangle shown in Fig. 3. The eigenvalue equation at v_{01} is

$$(4 - \lambda_m) f(v_{01}) = f(v_{001}) + f(v_{012}) + f(v_{102}) + f(v_{101}) \ .$$

To see that this is true we use (2.13) to express $f(v_{001})$, etc. in terms of $f(v_0)$, $f(v_1)$, $f(v_{01})$, $f(v_{12})$, and $f(v_{02})$. Thus, we need to show

$$\begin{aligned}(4 - \lambda_m) &\left(1 - \frac{4}{(2 - \lambda_m)(5 - \lambda_m)}\right) f(v_{01}) \\ &= \frac{6 - \lambda_m}{(2 - \lambda_m)(5 - \lambda_m)} \left(f(v_0) + f(v_1) + f(v_{02}) + f(v_{12})\right) \ .\end{aligned}$$

But this is just (2.14) (for λ_{m-1} in place of λ_m) in view of (2.12) (when $\lambda_m = 4$ we also have $\lambda_{m-1} = 4$). □

Notice that the coefficients in (2.13) do not add to 1. However, we do recover (2.4) in the limit as $\lambda_m \to 0$. Fukushima and Shima [8] show that any Dirichlet eigenfunction $-\Delta f = \lambda f$ on SG restricts to an eigenfunction $-\Delta_m f = \lambda_m f$ on G_m for all $m \geq m_0$, the eigenvalues λ_m satisfy (2.11), and

$$\lambda = \lim_{m \to \infty} 5^m \lambda_m \ . \tag{2.15}$$

In particular this shows that $\varepsilon_m = -1$ for all but a finite number of ms, and $\lambda_m \to 0$ as $m \to \infty$. In Section 4 we will show that the same holds for generic eigenfunctions.

Next we consider the analog of Algorithm 2.2. We refer again to Fig. 3 for the labeling of vertices in a minimal triangle in G_{m-2}.

Algorithm 2.5. Let f be as in Algorithm 2.4. Then

$$\begin{aligned} f(v_{001}) \ = \ & \frac{4 - \lambda_m}{5 - \lambda_m} f(v_{01}) \\ & + \left(\frac{3 - \lambda_m}{(2 - \lambda_m)(5 - \lambda_m)} + \frac{1}{(2 - \lambda_m)(5 - \lambda_m)(5 - \lambda_{m-1})}\right) f(v_0) \\ & - \left(\frac{1}{(2 - \lambda_m)(5 - \lambda_m)} + \frac{1}{(2 - \lambda_m)(5 - \lambda_m)(5 - \lambda_{m-1})}\right) f(v_1) \ . \end{aligned} \tag{2.16}$$

Proof. Using the analog of (2.13) we can solve for $f(v_2)$ in terms of $f(v_{01})$, $f(v_0)$, and $f(v_1)$, to obtain

$$f(v_2) = \frac{(2 - \lambda_{m-1})(5 - \lambda_{m-1})}{2} f(v_{01}) - \frac{(4 - \lambda_{m-1})}{2} \left(f(v_0) + f(v_2)\right) \ . \tag{2.17}$$

On the other hand, we have

$$f(v_{02}) = \frac{4-\lambda_{m-1}}{(2-\lambda_{m-1})(5-\lambda_{m-1})}(f(v_0)+f(v_2)) + \frac{2}{(2-\lambda_{m-1})(5-\lambda_{m-1})}f(v_1)\ , \tag{2.18}$$

and

$$f(v_{001}) = \frac{(4-\lambda_m)}{(2-\lambda_m)(5-\lambda_m)}(f(v_0)+f(v_{01})) + \frac{2}{(2-\lambda_m)(5-\lambda_m)}f(v_{02})\ . \tag{2.19}$$

So we substitute (2.17) in (2.18), and then substitute the result in (2.19), to obtain

$$f(v_{001}) = \left(\frac{8-\lambda_m-\lambda_{m-1}}{(2-\lambda_m)(5-\lambda_m)}\right)f(v_{01}) + \left(\frac{(4-\lambda_m)(5-\lambda_{m-1})-(4-\lambda_{m-1})}{(2-\lambda_m)(5-\lambda_m)(5-\lambda_{m-1})}\right)f(v_0) - \left(\frac{6-\lambda_{m-1}}{(2-\lambda_m)(5-\lambda_m)(5-\lambda_{m-1})}\right)f(v_1)\ .$$

Using (2.12), this simplifies to (2.16). □

Remark 1. The coefficients in (2.16) sum to 1. This will have important consequences. It is not at all clear why this should be so, in view of the fact that this is not the case in (2.13).

We conclude this section with a converse to Algorithm 2.1, which enables us to "blow up" the values of harmonic function on a small triangle to a larger triangle.

Algorithm 2.6. Let f and T be as in Algorithm 2.1. Then

$$\begin{cases} f(v_1) = \frac{10}{3}f(v_{01}) - \frac{5}{3}f(v_{02}) - \frac{2}{3}f(v_0) \text{ and} \\ f(v_2) = -\frac{5}{3}f(v_{01}) + \frac{10}{3}f(v_{02}) - \frac{2}{3}f(v_0)\ . \end{cases} \tag{2.20}$$

In particular,

$$f(v_1) - f(v_2) = 5(f(v_{01}) - f(v_{02}))\ . \tag{2.21}$$

Proof. Linear algebra from (2.4) and its analogous forms. □

It follows by induction that a harmonic function is uniquely determined by its values at the vertices of any triangle T. The same is not true for Dirichlet eigenfunctions.

3. Numerical Computations of Harmonic Functions and Eigenfunctions

The space of continuous harmonic functions on SG is three-dimensional, each harmonic function being uniquely determined by its values at the three boundary points. (Of course every harmonic function is continuous in the interior of SG, so it is the continuity at the boundary points that will be assumed throughout, except for a brief discussion at the end of Section 4.) Using Algorithm 2.1 we can recursively compute the values of the function at the vertices of the graphs G_m. This is an exact computation that could be performed in rational arithmetic, although we chose not to do this. In Figs. 4, 5, and 6, we display the graphs of some harmonic functions, with the computation

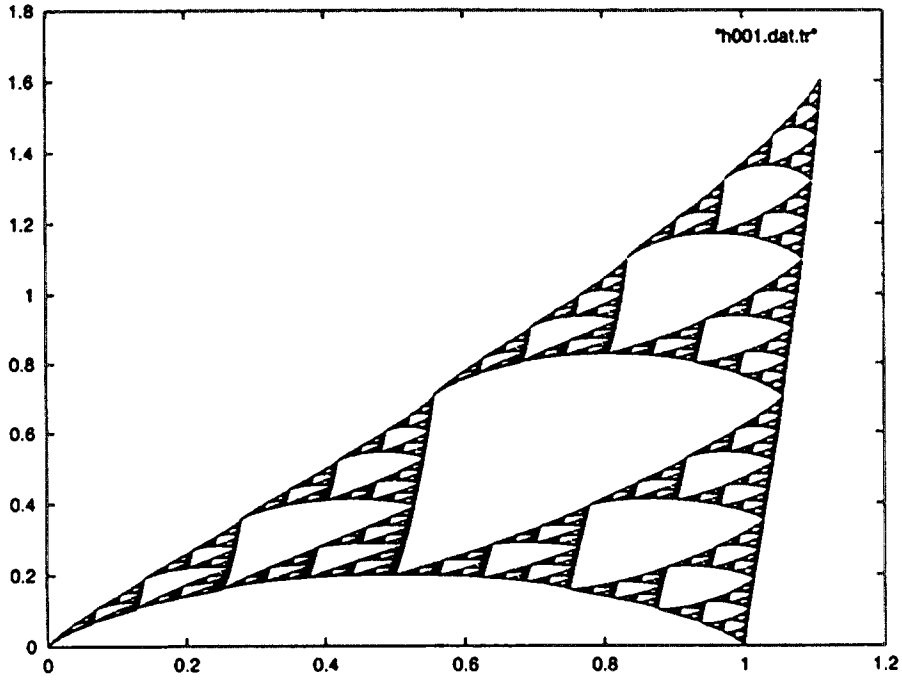

FIGURE 4 The harmonic function with boundary values (0, 0, 1).

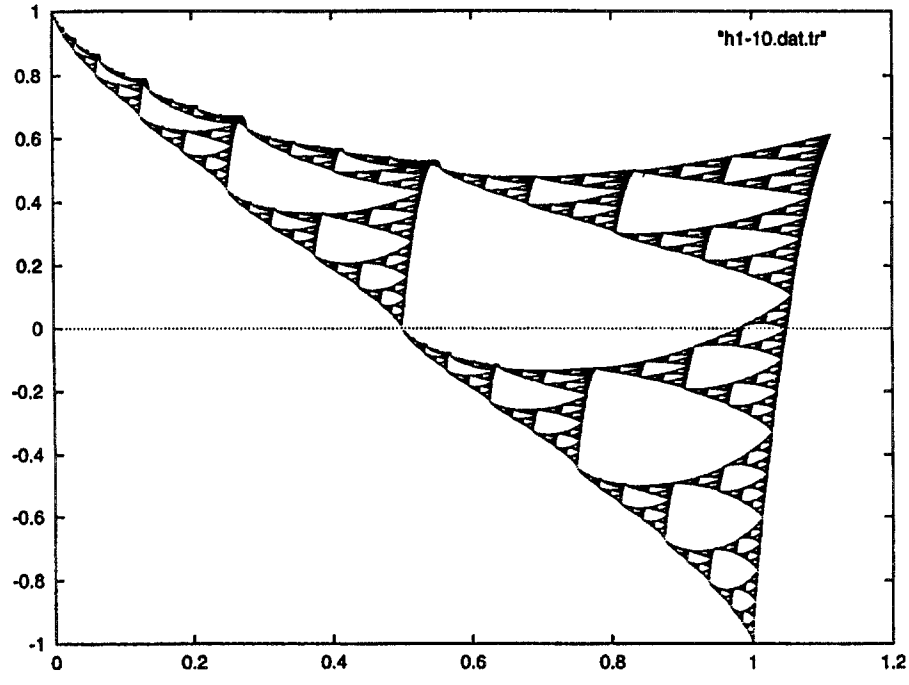

FIGURE 5 The harmonic function with boundary values $(1, -1, 0)$.

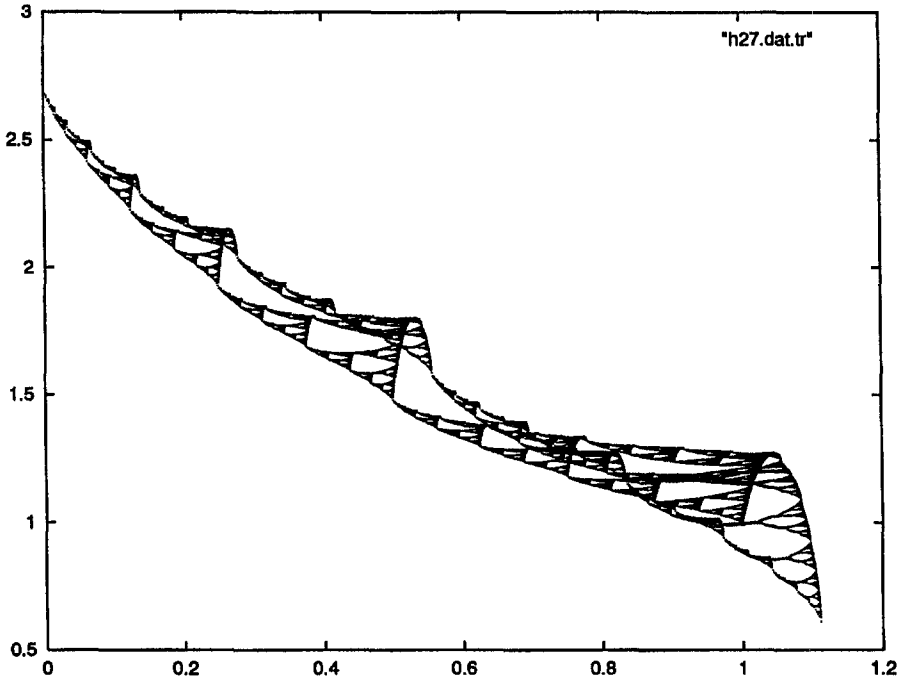

FIGURE 6 The harmonic function with boundary values (2.7, 1, 0).

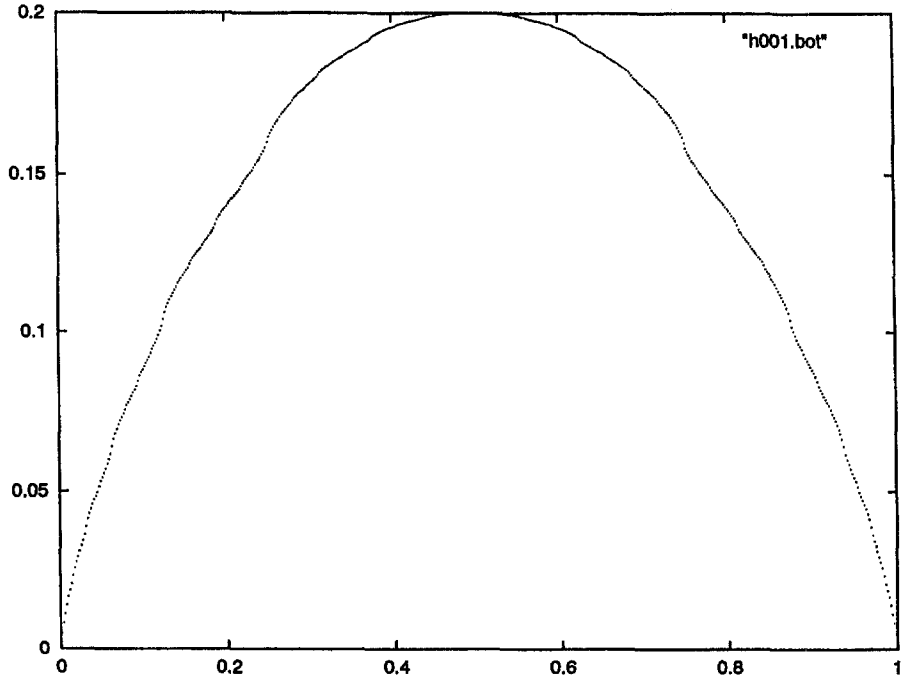

FIGURE 7 (a) Restriction of the function in Fig. 4 to the edge (a) joining the values (0, 0).

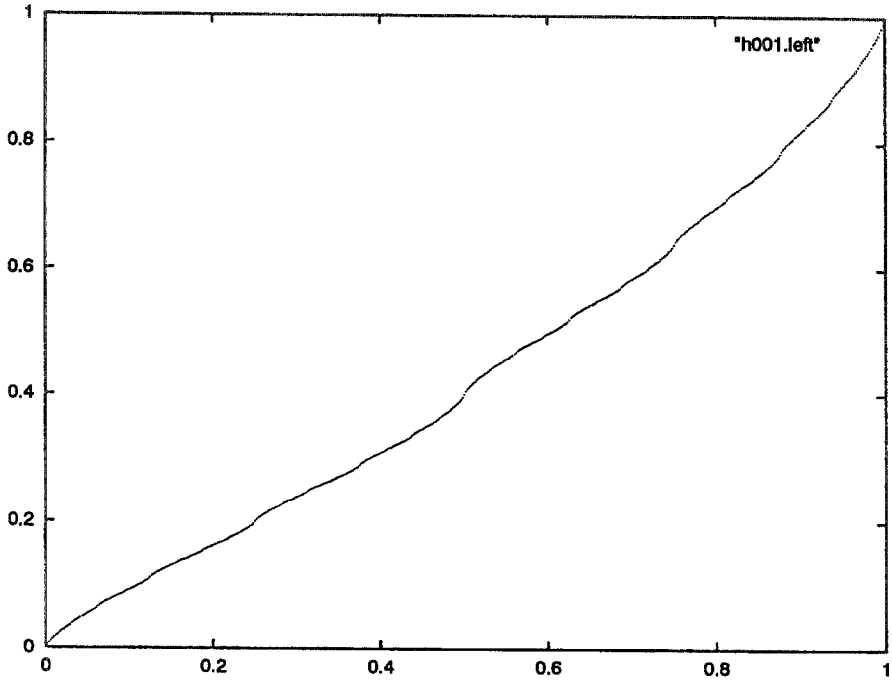

FIGURE 7 (b) Restriction of the function in Fig. 4 to the edge (b) joining the values (0, 1).

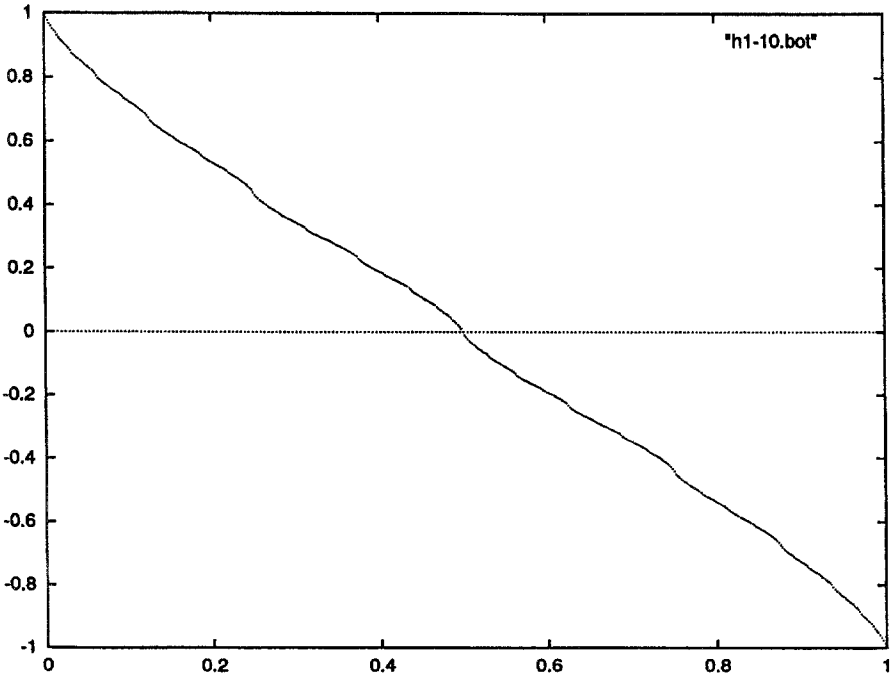

FIGURE 8 (a) Restriction of the function in Fig. 5 to the edge (a) joining the values $(1, -1)$.

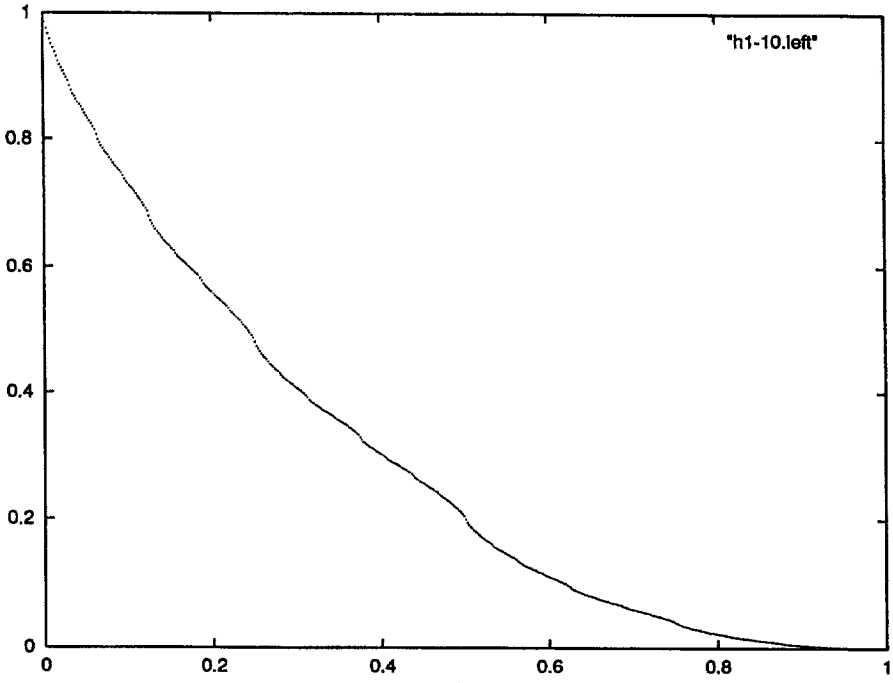

FIGURE 8 (b) Restriction of the function in Fig. 5 to the edge (b) joining the values (0, 1). Note that the boundary behavior at the antisymmetric vertex (value 0) is different.

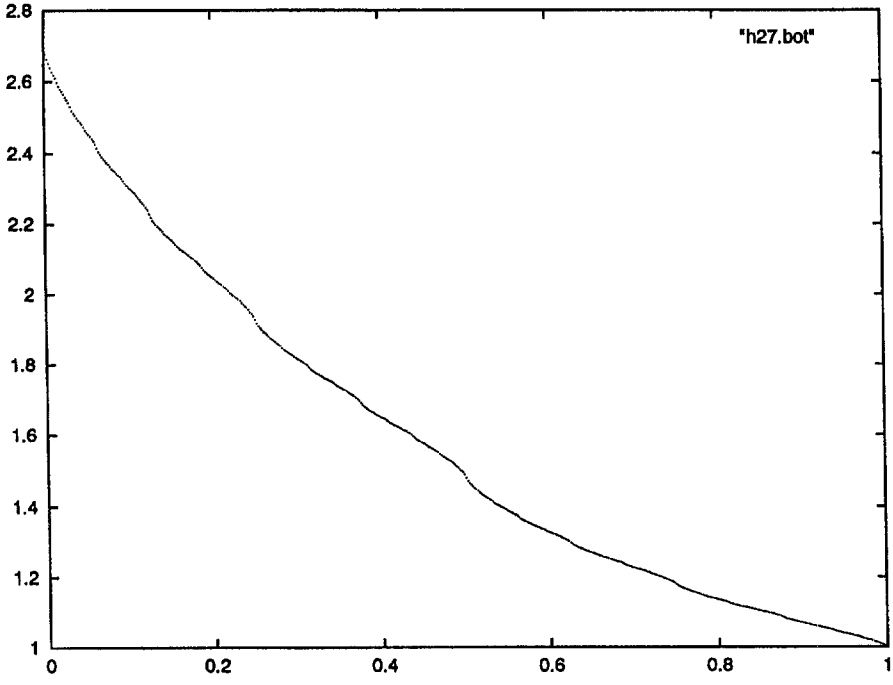

FIGURE 9 (a) Restriction of the function in Fig. 6 to the edge (a) joining the values (2.7, 1).

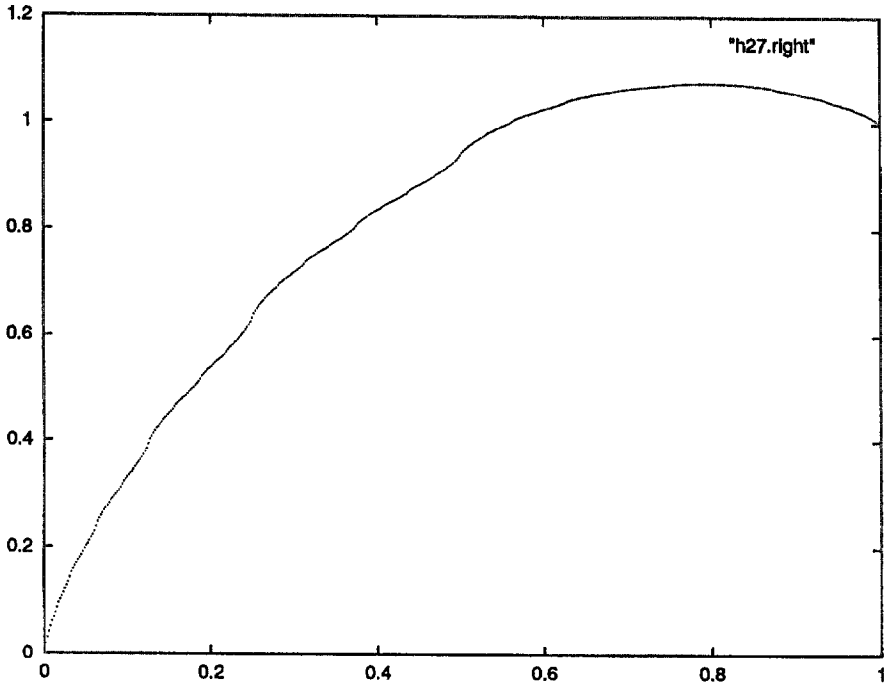

FIGURE 9 (b) Restriction of the function in Fig. 6 to the edge (b) joining the values (1, 0).

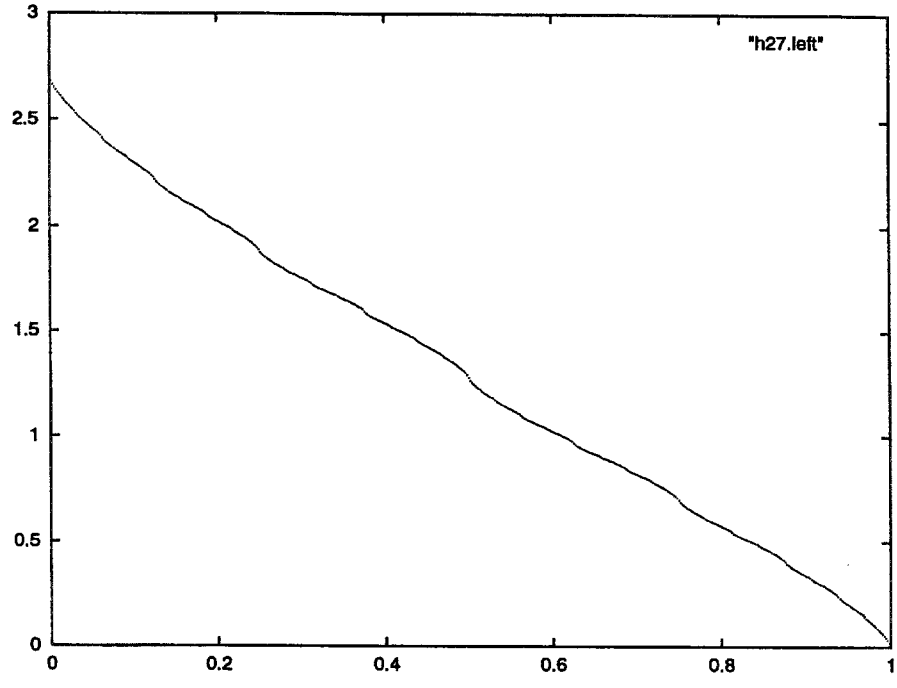

FIGURE 9 (c) Restriction of the function in Fig. 6 to the edge (c) joining the values (0, 2.7).

performed out to $m = 9$. The first example is symmetric with respect to the reflection that fixes p_0 and interchanges p_1 and p_2, while the second example is antisymmetric. The third example is generic, having no symmetries. In Figs. 7, 8, and 9, we display the graphs of the restrictions on these functions to some straight lines in the gasket. These computations could have been done using Algorithm 2.2, but in fact we just restricted the data obtained using Algorithm 2.1.

There are a number of interesting features observable in the graphs. It appears that the restriction of a harmonic function to a line is often a monotonic function. The behavior near the boundary point appears to be different in the case of an antisymmetric point, with the generic case resembling the symmetric case. All these observations will be verified in the next section.

The next set of figures shows the graphs of Dirichlet eigenfunctions, computed using Algorithm 2.4 (up to $m = 9$). According to Fukushima and Shima [8], there are three basic families of eigenfunctions, and all eigenfunctions are obtainable from these by a localization process that will be described in more detail in Section 4. We have chosen to index the eigenfunctions in each family by a natural number n, written in binary form

$$n = \sum_{j=0}^{\infty} \delta_j 2^j \quad \delta_j = 0 \text{ or } 1\,, \tag{3.1}$$

all but a finite number equal to 0. In the first family $\psi_n^{(2)}$, we take the initial conditions on G_1 with the value 1 at the three midpoints, as in Figure 10, and $\lambda_1 = 2$ and then take λ_m for $m \geq 2$ to be

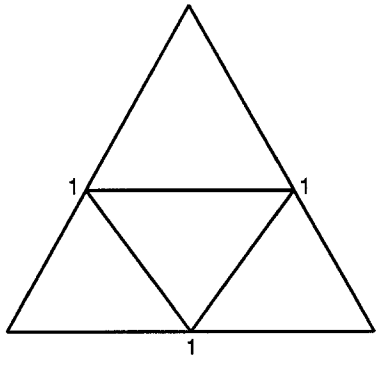

FIGURE 10 Initial values on G_1 for the family $\psi_n^{(2)}$.

given by (2.11) with

$$\varepsilon_m = (-1)^{1+\delta_{m-1}+\delta_{m-2}} \tag{3.2}$$

This ordering of eigenfunctions makes the eigenvalue an increasing function of n. This can be seen by a routine induction argument based on the observation that a choice of $\varepsilon_m = +1$ in (2.11) reverses order and $\varepsilon_m = -1$ preserves order, so if $\lambda_{m-1} \leq \lambda'_{m-1}$ then $\lambda_m \geq \lambda'_m$ for the choice $\varepsilon_m = \varepsilon'_m = +1$ and $\lambda_m \leq \lambda'_m$, for the choice $\varepsilon_m = \varepsilon'_m = -1$. On the other hand, $\lambda_m < \lambda'_m$ if $\varepsilon_m = -1$ and $\varepsilon'_m = +1$, regardless of the relative order of λ_{m-1} and λ'_{m-1}. We leave the details to the interested reader. Figure 11 shows the graphs of $\psi_n^{(2)}$ for $n = 0, 1, \ldots, 7$. In Fig. 12 we give a table of the values of λ_m and the limiting eigenvalue for each eigenfunction. In Fig. 13 we show the graphs of the restrictions to an edge of G_0. (All eigenfunctions in the $\psi_n^{(2)}$ family have complete dihedral D_3 symmetry, so the restrictions to all edges are the same, and are even functions.) The eigenfunction $\psi_0^{(2)}$ is the "ground state," with the lowest eigenvalue, and is strictly positive. All other eigenfunctions change sign, and it is interesting to study their *nodal sets*, the points where the

eigenfunction is zero. To visualize these nodal sets, we show in Fig. 14 the subset of SG where the eigenfunctions are positive; the nodal set is just the boundary of this set.

One of the most striking features of this data is that it appears that all these eigenfunctions are constant along the inner edges of G_1 (connecting the midpoints of the edges of G_0). We will prove that this is the case in the next section. Another obvious conjecture is that the restriction of $\psi_n^{(2)}$ to an edge of G_0 has exactly $2n+1$ local extrema; we do not have a proof of this.

The second family of eigenfunctions is denoted $\psi_n^{(5)}$, where we choose ε_m in (2.11) using (3.1) and (3.2) as before, but now $\lambda_1 = 5$ and we take initial conditions on G_1, shown in Figure 15, that are antisymmetric with respect to one vertex. (Under the action of the dihedral D_3 group, each such eigenfunction generates a two-dimensional representation space.) In Figs. 16 through 20 we display the same data for $\psi_n^{(5)}$ as we did for $\psi_n^{(2)}$. In the next section we will show how to chain together scaled-down copies of $\psi_n^{(5)}$ to obtain eigenfunctions that are localized along paths joining two boundary points.

The third family of eigenfunctions is $\psi_n^{(6)}$, where now n is required to be congruent to 1 or 2 mod 4. We give initial conditions on G_2, as shown in Figure 21, with $\lambda_2 = 6$, and then use (2.11) for $n \geq 3$, modifying (3.2) by replacing $m-2$ with $m-3$. Since $\delta_0 + \delta_1$ is odd, $\varepsilon_3 = +1$. We display the same data in Figs. 22 through 25, only for $n = 1, 2, 5, 6$. Again we observe certain edges along which these eigenfunctions appear to be constant; this will be established in the next section. The $\psi_n^{(6)}$ eigenfunctions can be scaled-down and localized to minimal triangles in G_m (this was already observed in [8]).

In the next section we will show that the three families and the scaled-down versions of $\psi_n^{(5)}$ and $\psi_n^{(6)}$ give a complete set of eigenfunctions. (Text continues on page 257.)

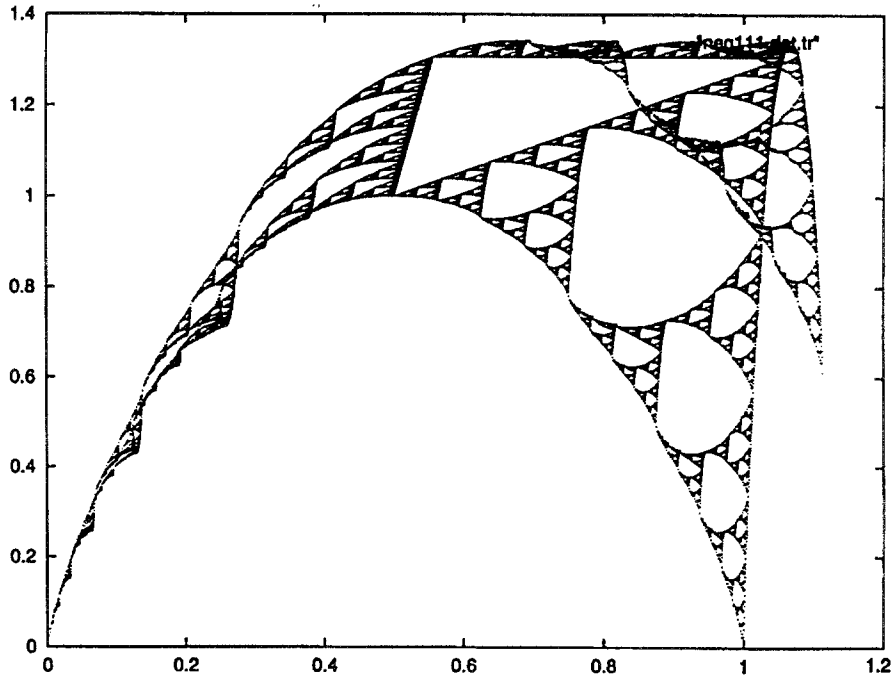

FIGURE 11 The graph of $\psi_n^{(2)}$ for $n = 0$.

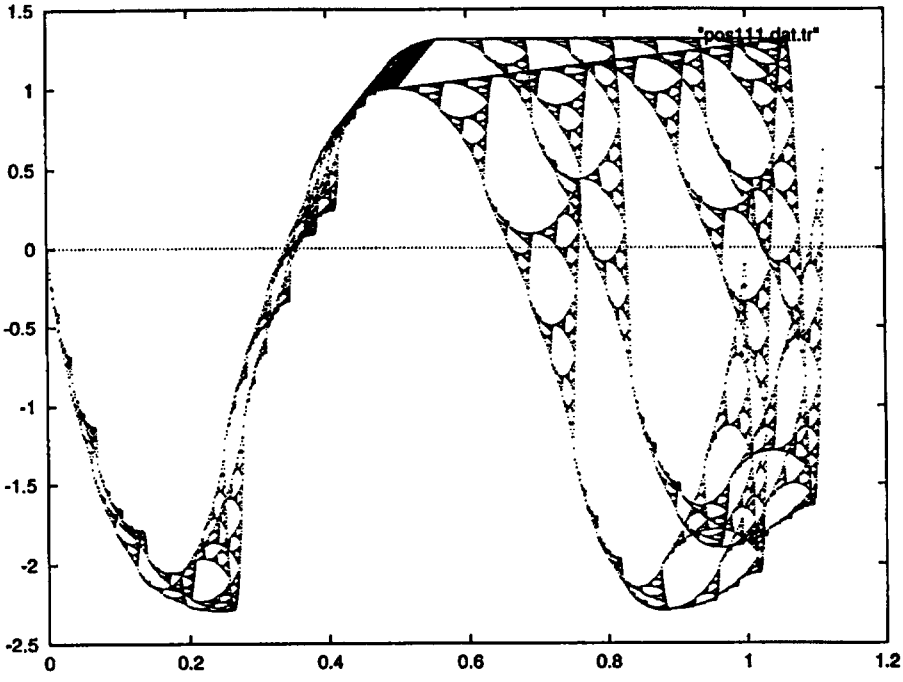

FIGURE 11 The graph of $\psi_n^{(2)}$ for $n = 1$.

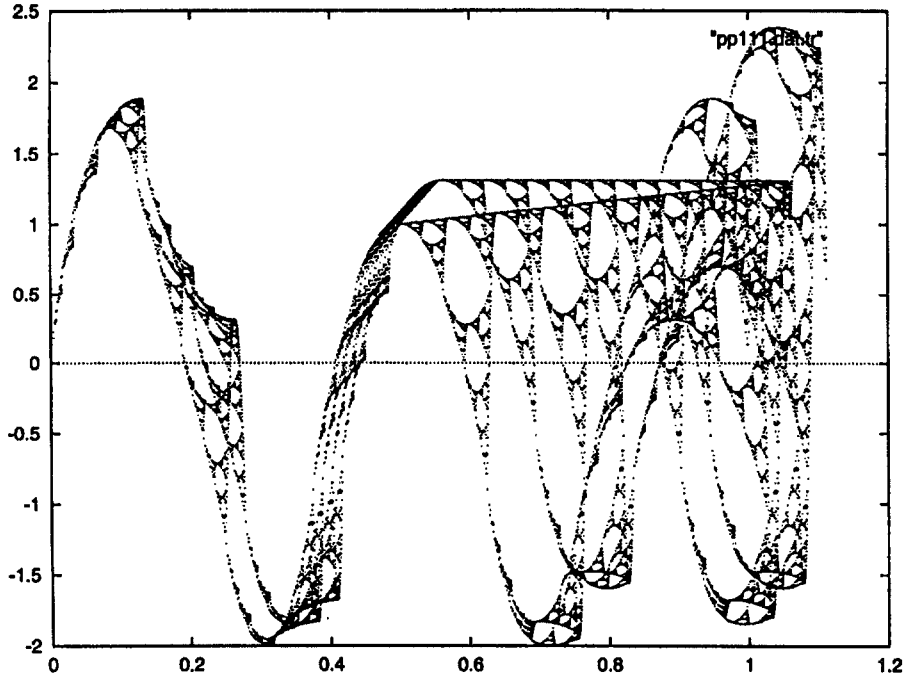

FIGURE 11 The graph of $\psi_n^{(2)}$ for $n = 2$.

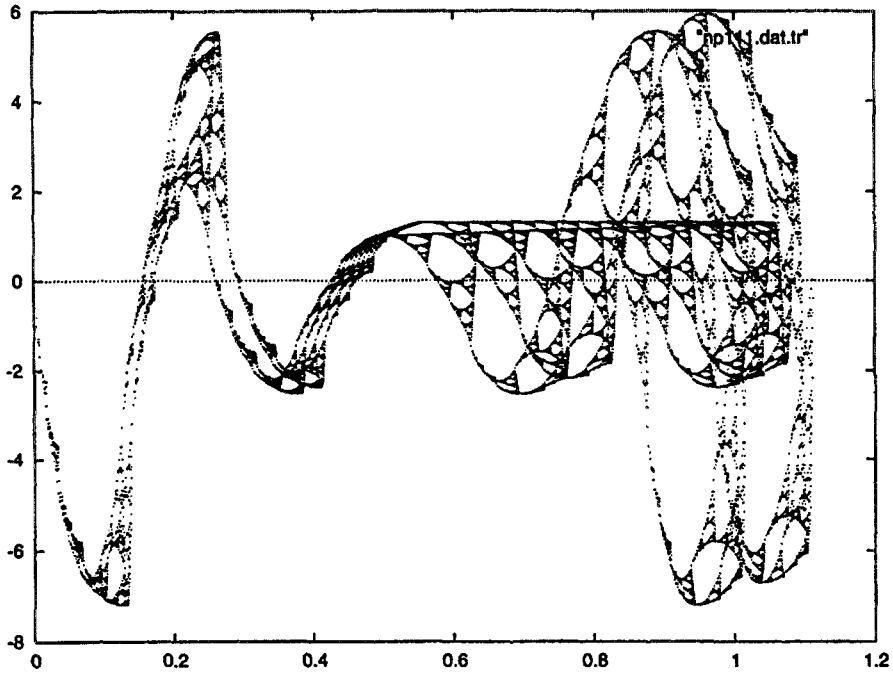

FIGURE 11 The graph of $\psi_n^{(2)}$ for $n = 3$.

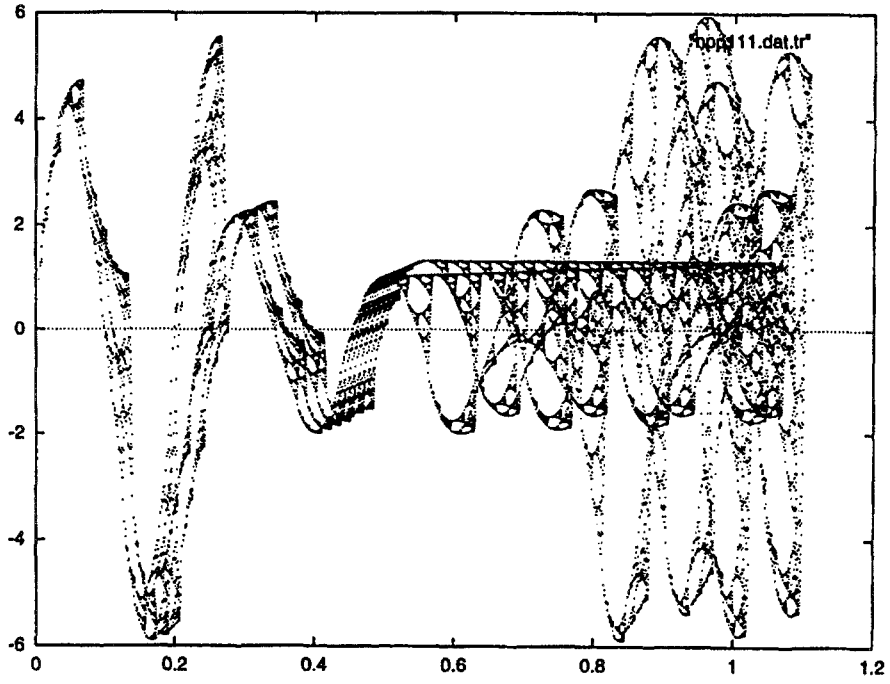

FIGURE 11 The graph of $\psi_n^{(2)}$ for $n = 4$.

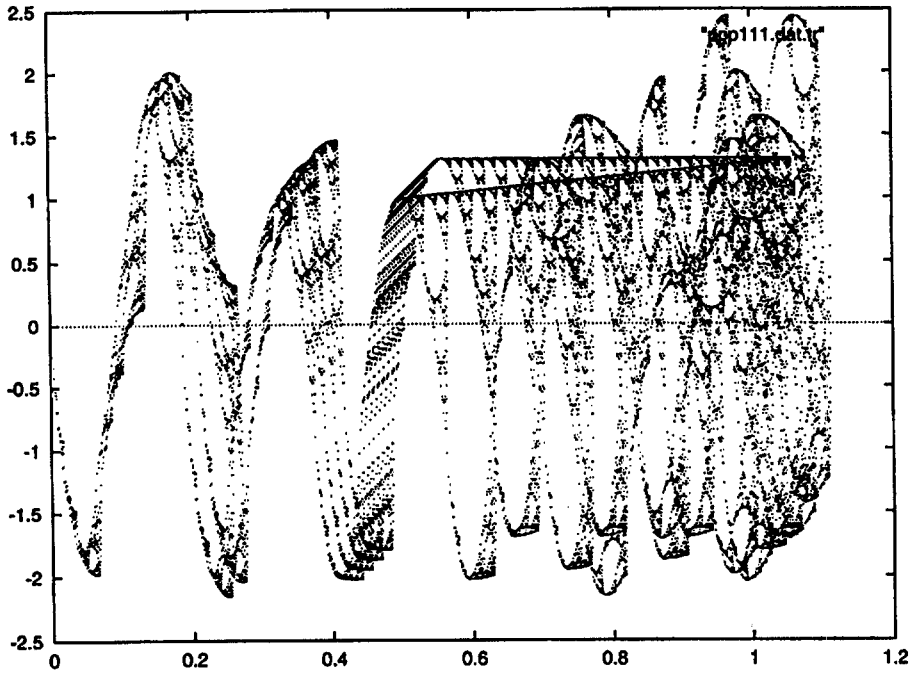

FIGURE 11 The graph of $\psi_n^{(2)}$ for $n = 5$.

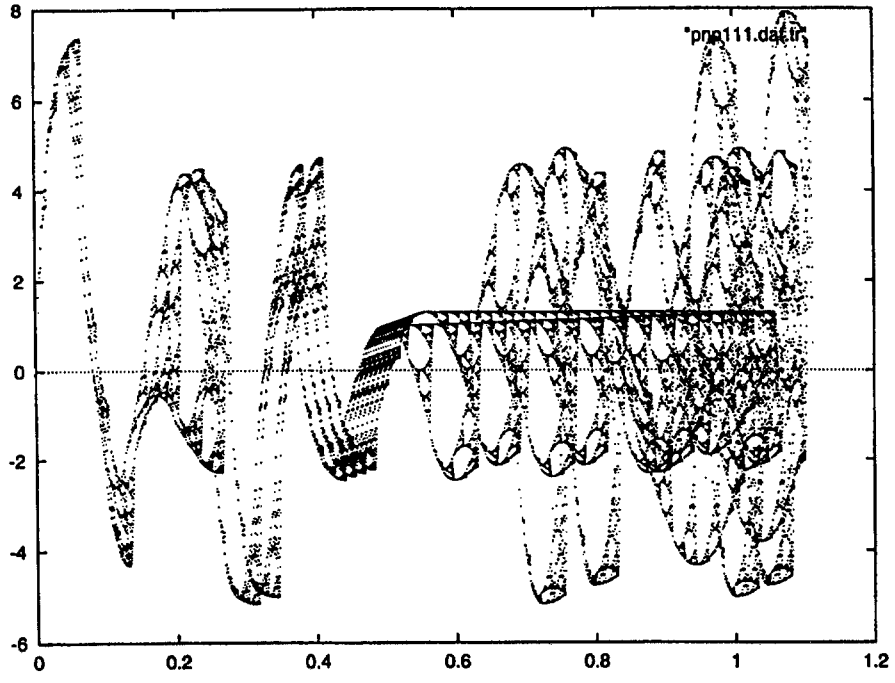

FIGURE 11 The graph of $\psi_n^{(2)}$ for $n = 6$.

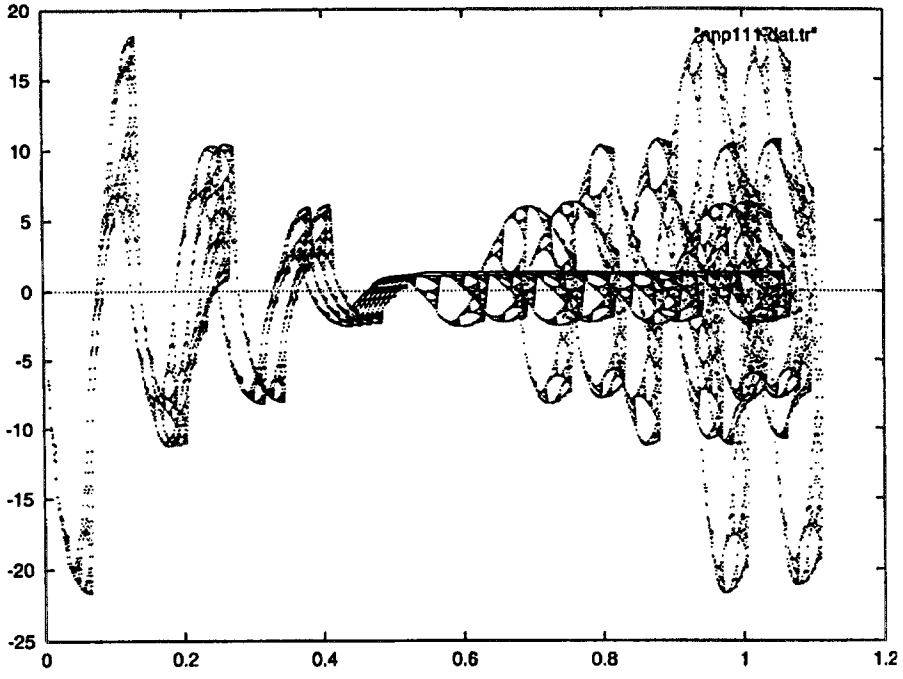

FIGURE 11 The graph of $\psi_n^{(2)}$ for $n = 7$.

2.000000000000000	2.000000000000000
0.438447187191170	2.192235935955850
0.089283755227748	2.232093880693689
0.017920983374572	2.240122921821492
0.003586769658231	2.241731036394142
0.000717456880521	2.242052751628976
0.000143495494296	2.242117098367850
0.000028699263589	2.242129967864985
0.000005739859307	2.242132541804311
0.000001147972125	2.242133056908763
0.000000229594435	2.242133158281666
0.000000045918888	2.242133182676215
0.000000009183778	2.242133209781269
0.000000001836755	2.242133142018633
0.000000000367351	2.242133480831812
0.000000000073470	2.242138563029496
0.000000000014694	2.242138563029496

$\psi_0^{(2)}$

2.000000000000000	2.000000000000000
4.561552812808830	22.807764064044150
1.200597372947411	30.014934323685271
0.252912412242774	31.614051530346742
0.051104823036064	31.940514397540280
0.010241944090965	32.006075284266892
0.002049228685835	32.019198216164284
0.000409879337381	32.021823232896047
0.000081977211529	32.022348253417896
0.000016395496068	32.022453258398301
0.000003279101364	32.022474258310183
0.000000655820359	32.022478459593600
0.000000131164075	32.022479286297752
0.000000026232815	32.022479354060394
0.000000005246563	32.022480370499927
0.000000001049313	32.022478676434034
0.000000000209863	32.022504087422455
0.000000000041973	32.022504087422455

$\psi_1^{(2)}$

FIGURE 12 A table of the values of λ_m and $5^{m-1}\lambda_m$. The limiting value λ for the eigenfunctions $\psi_n^{(2)}$ is the value at the bottom of the right hand column *(Cont.)*.

2.000000000000000	2.000000000000000
4.561552812808830	22.807764064044150
3.799402627052589	94.985065676314733
0.934561603592332	116.820200449041508
0.194476546116334	121.547841322708877
0.039202679235109	122.508372609715991
0.007852869358454	122.701083725843333
0.001571067522323	122.739650181458330
0.000314233252972	122.747364442220629
0.000062847440555	122.748907333035746
0.000012569519710	122.749215913237066
0.000002513905206	122.749277634156243
0.000000502781092	122.749289980508479
0.000000100556220	122.749292352200726
0.000000020111244	122.749292352200726

$\psi_2^{(2)}$

2.000000000000000	2.000000000000000
0.438447187191170	2.192235935955850
4.910716244772252	122.767906119306303
3.657274278305600	457.159284788200011
0.889805688218220	556.128555136387604
0.184790654869029	577.470796465715466
0.037235426369185	581.803537018513566
0.007458210253875	582.672676084010163
0.001492087315687	582.846607690042106
0.000298435275860	582.881398164146162
0.000059687767698	582.888356424069229
0.000011937582041	582.889748078872799
0.000002387517548	582.890026393570452
0.000000477503555	582.890082162219755
0.000000095500713	582.890093343054559
0.000000019100143	582.890093343054559

$\psi_4^{(2)}$

2.000000000000000	2.000000000000000
4.561552812808830	22.807764064044150
1.200597372947411	30.014934323685271
4.747087587757227	593.385948469653272
1.274066717866436	796.291698666522166
0.269319995576783	841.624986177446203
0.054457114581055	850.892415328991433
0.010915251459094	852.754020241723083
0.002184004266746	853.126666697733526
0.000436839019015	853.201209013412949
0.000087369330483	853.216117996749063
0.000017473927164	853.219099810221451
0.000003494787875	853.219696162073888
0.000000698957673	853.219815492075440
0.000000139791539	853.219840225437565
0.000000027958308	853.219845307635183
0.000000005591662	853.219845307635183

$\psi_6^{(2)}$

2.000000000000000	2.000000000000000
0.438447187191170	2.192235935955850
4.910716244772252	122.767906119306303
1.342725721694400	167.840715211799989
0.284763155257299	177.976972035811571
0.057616564758371	180.051764869908368
0.011549993421280	180.468647207505938
0.002311066890290	180.552100803935133
0.000462256114201	180.568794609843081
0.000092452932349	180.572133494675768
0.000018490654851	180.572801278104123
0.000003698133705	180.572934832838257
0.000000739626851	180.572961571974332
0.000000147925374	180.572966857459903
0.000000029585075	180.572968890338984
0.000000005917015	180.572973972536687
0.000000001183403	180.572982442866135
0.000000000236681	180.573024794513515
0.000000000047336	180.573660069223962
0.000000000009467	180.576836442776141
0.000000000001893	180.576836442776141

$\psi_3^{(2)}$

2.000000000000000	2.000000000000000
4.561552812808830	22.807764064044150
3.799402627052589	94.985065676314733
4.065438396407668	508.179799550958478
1.021973747326411	638.733592079006826
0.213512245238652	667.225766370788506
0.043073514579374	673.023665302722634
0.008629596904421	674.187258157925271
0.001726515552075	674.420137529137605
0.000345326960557	674.466719837677601
0.000069066346143	674.476036556081340
0.000013813307390	674.477899909303005
0.000002762663004	674.478272576694735
0.000000552532662	674.478346980068864
0.000000110506535	674.478361549035526
0.000000022101307	674.478359854969653
0.000000004420261	674.478359854969653

$\psi_5^{(2)}$

2.000000000000000	2.000000000000000
0.438447187191170	2.192235935955850
0.089283755227748	2.232093880693689
4.982079016625428	622.759877078178533
1.373980025321677	858.737515826047911
0.291828816717707	911.965052242833167
0.059063461848651	922.866591385167908
0.011840732961141	925.057262589172637
0.002369269279612	925.495812348462096
0.000473898771932	925.583538928910798
0.000094781551095	925.601084910939221
0.000018956382088	925.604594137268919
0.000003791279292	925.605295941335157
0.000000758255973	925.605436142228541
0.000000151651199	925.605464941348828
0.000000030330240	925.605468329480573
0.000000006066048	925.605459859151097
0.000000001213210	925.605417507503716
0.000000000242642	925.605841023977405
0.000000000048528	925.605841023977405

$\psi_7^{(2)}$

FIGURE 12 A table of the values of λ_m and $5^{m-1}\lambda_m$. The limiting value λ for the eigenfunctions $\psi_n^{(2)}$ is the value at the bottom of the right hand column *(Cont.)*.

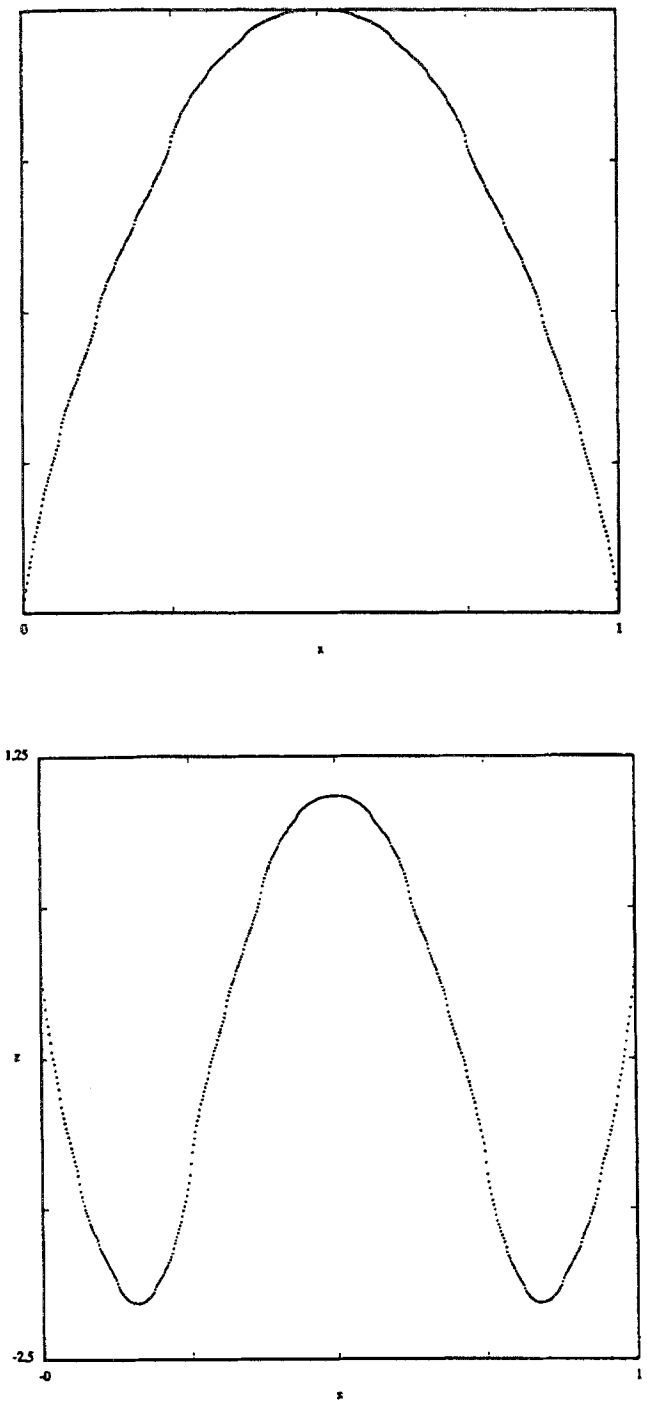

FIGURE 13 Restrictions to an edge of G_0 of the functions $\psi_n^{(2)}$ for $n = 0$ and $n = 1$. Note the pattern of $2n + 1$ relative extrema.

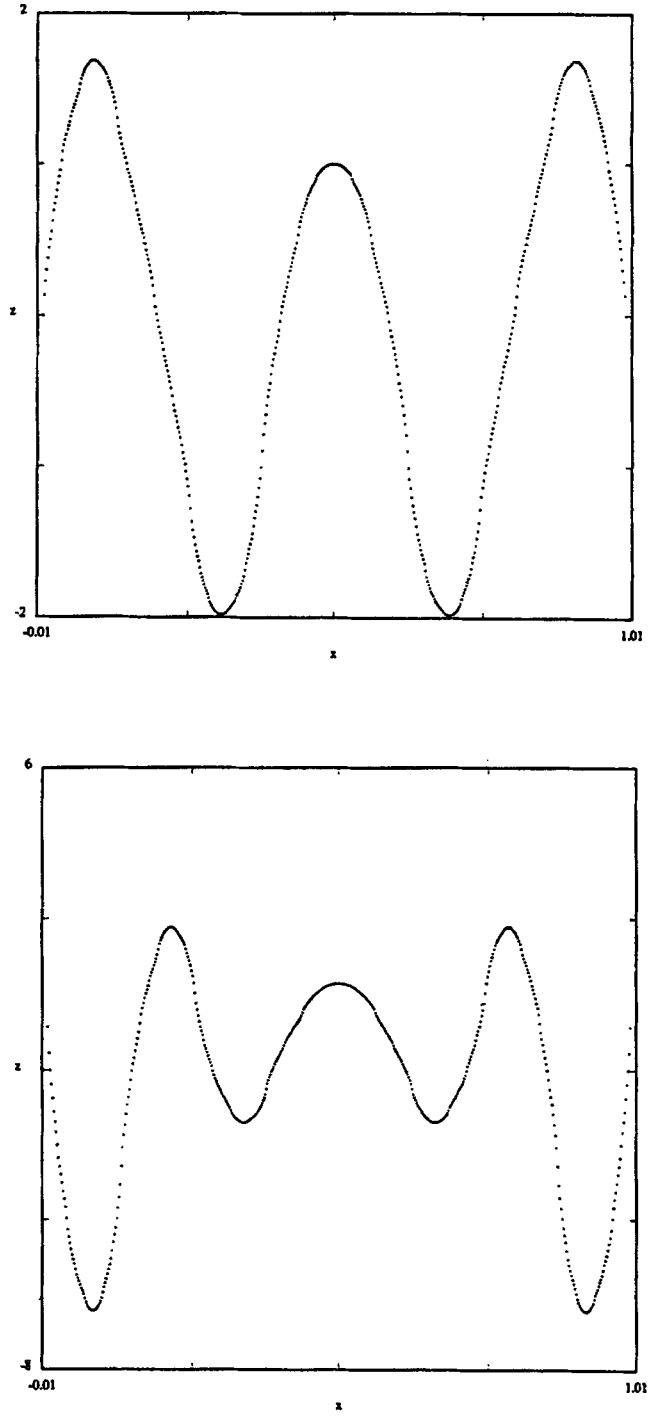

FIGURE 13 Restrictions to an edge of G_0 of the functions $\psi_n^{(2)}$ for $n = 2$ and $n = 3$. Note the pattern of $2n + 1$ relative extrema.

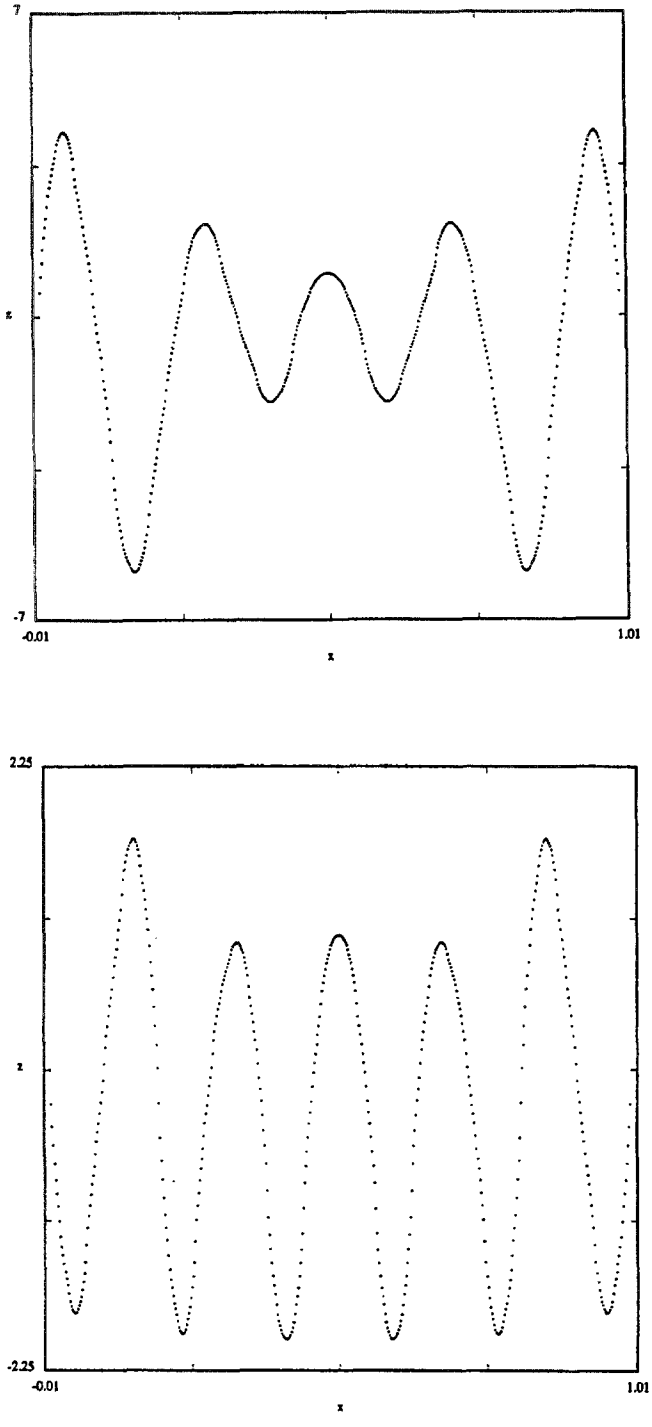

FIGURE 13 Restrictions to an edge of G_0 of the functions $\psi_n^{(2)}$ for $n = 4$ and $n = 5$. Note the pattern of $2n + 1$ relative extrema.

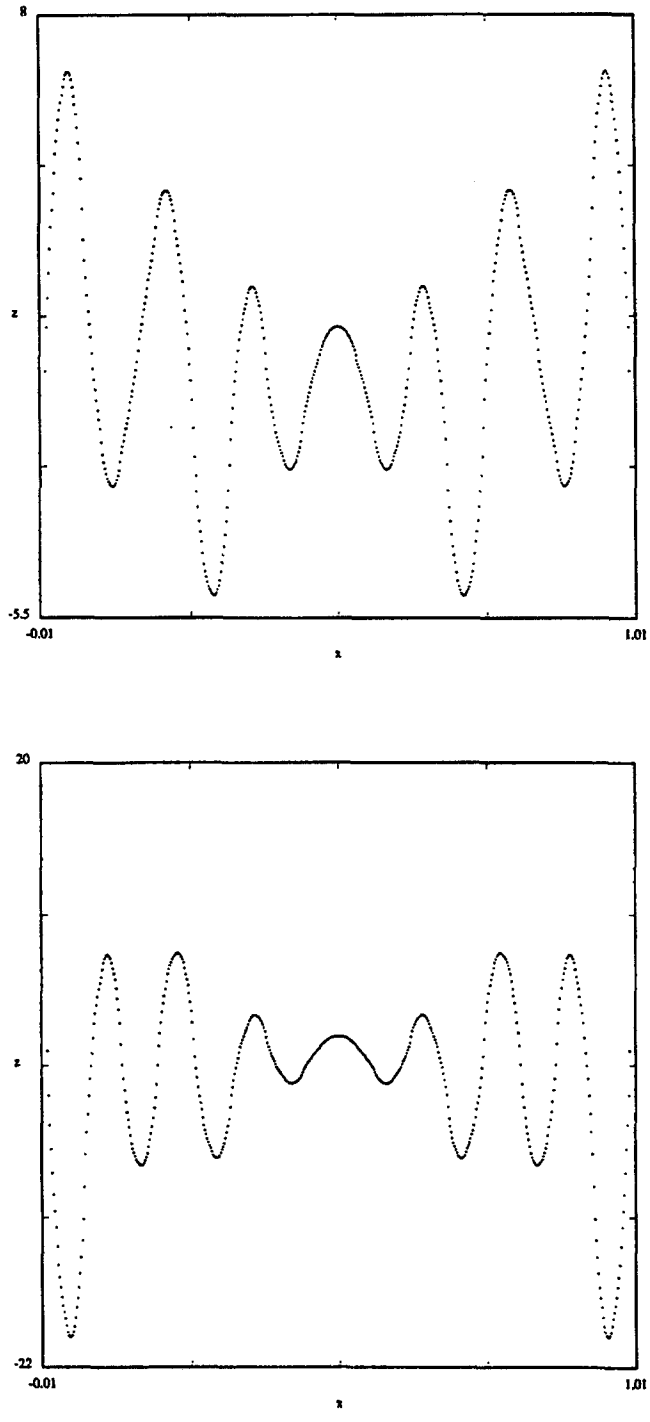

FIGURE 13 Restrictions to an edge of G_0 of the functions $\psi_n^{(2)}$ for $n = 6$ and $n = 7$. Note the pattern of $2n + 1$ relative extrema.

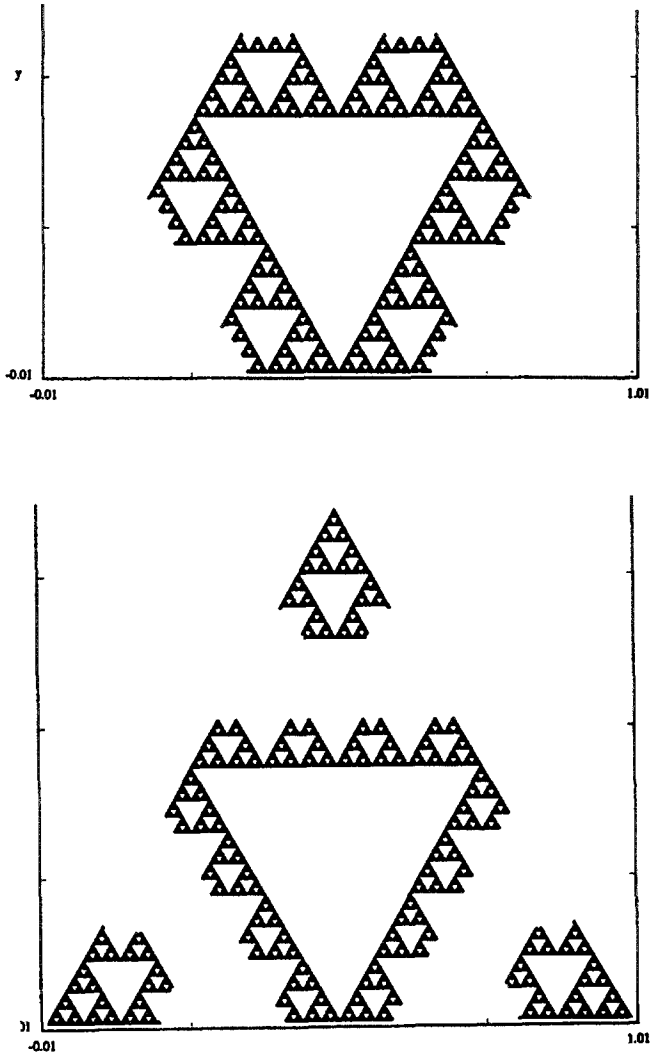

FIGURE 14 The subset of SG where $\psi_n^{(2)}$ is positive, for $n = 1$ and $n = 2$ (for $n = 0$ it is the whole SG). The boundary is the nodal set.

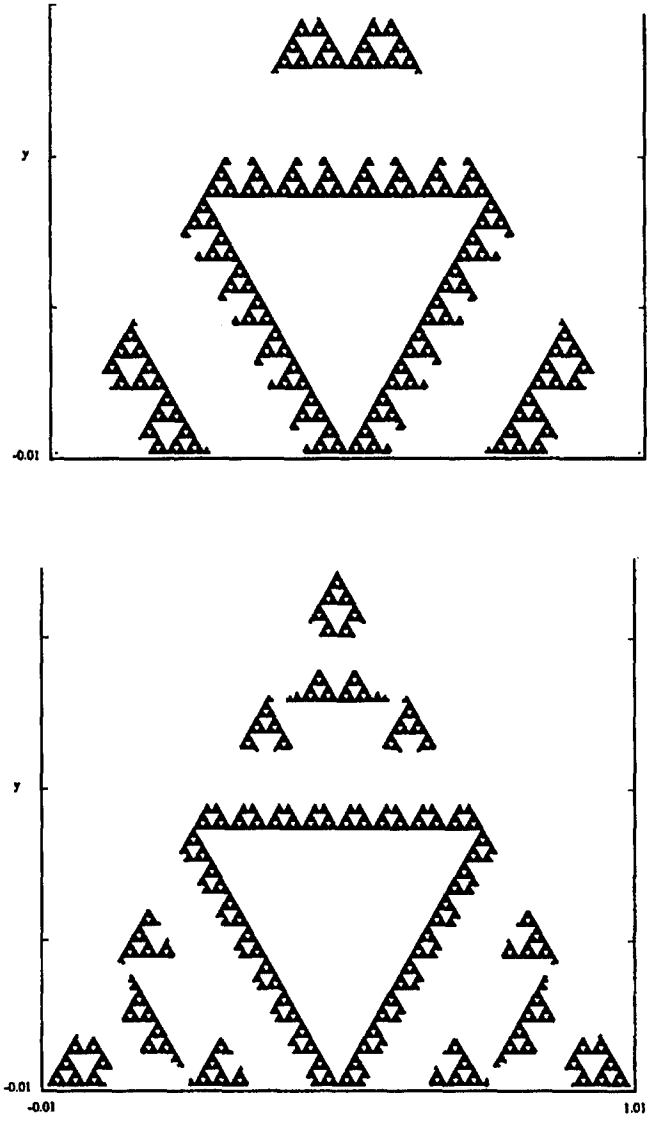

FIGURE 14 The subset of SG where $\psi_n^{(2)}$ is positive, for $n = 3$ and $n = 4$ (for $n = 0$ it is the whole SG). The boundary is the nodal set.

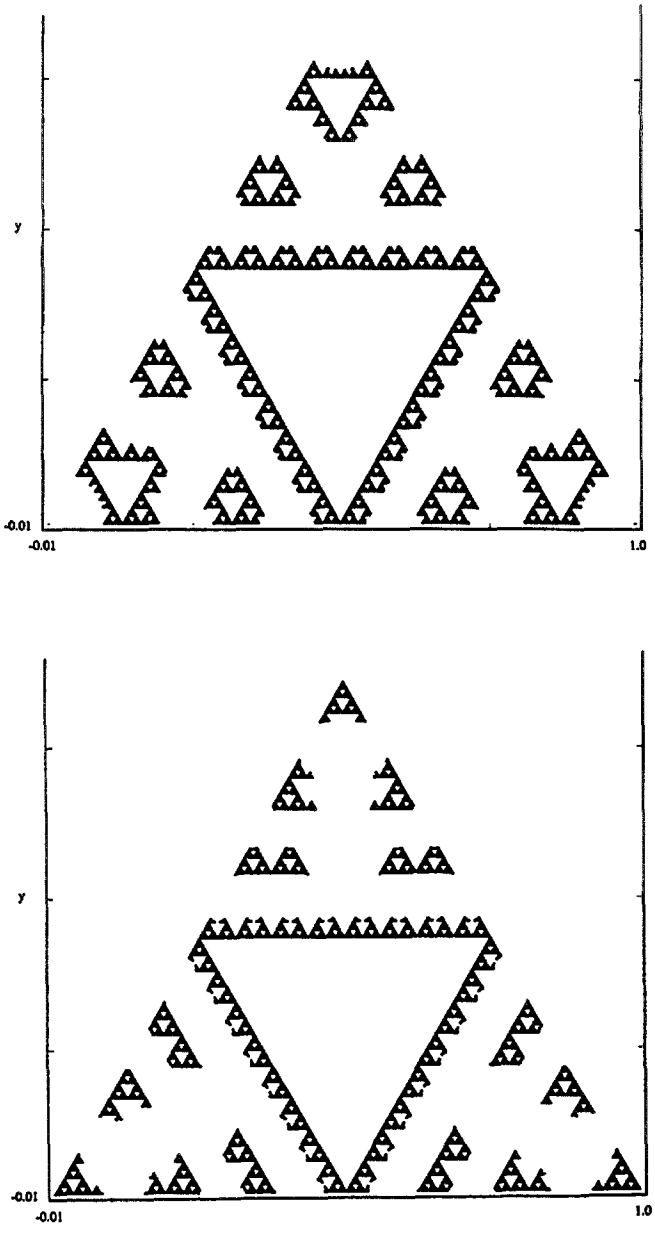

FIGURE 14 The subset of SG where $\psi_n^{(2)}$ is positive, for $n = 5$ and $n = 6$ (for $n = 0$ it is the whole SG). The boundary is the nodal set.

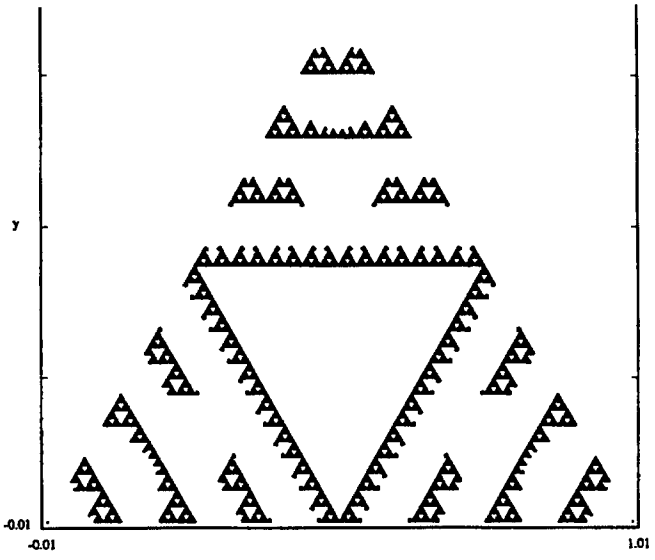

FIGURE 14 The subset of SG where $\psi_n^{(2)}$ is positive, for $n = 7$ (for $n = 0$ it is the whole SG). The boundary is the nodal set.

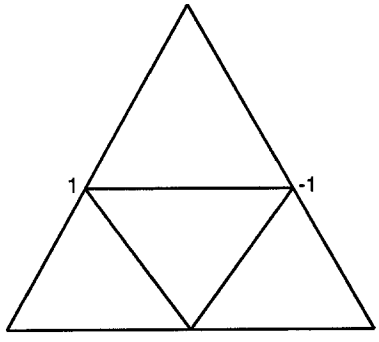

FIGURE 15 Initial value on G_1 for the family $\psi_n^{(5)}$. Under the action of the dihedral group D_3 this generates a two-dimensional representation space.

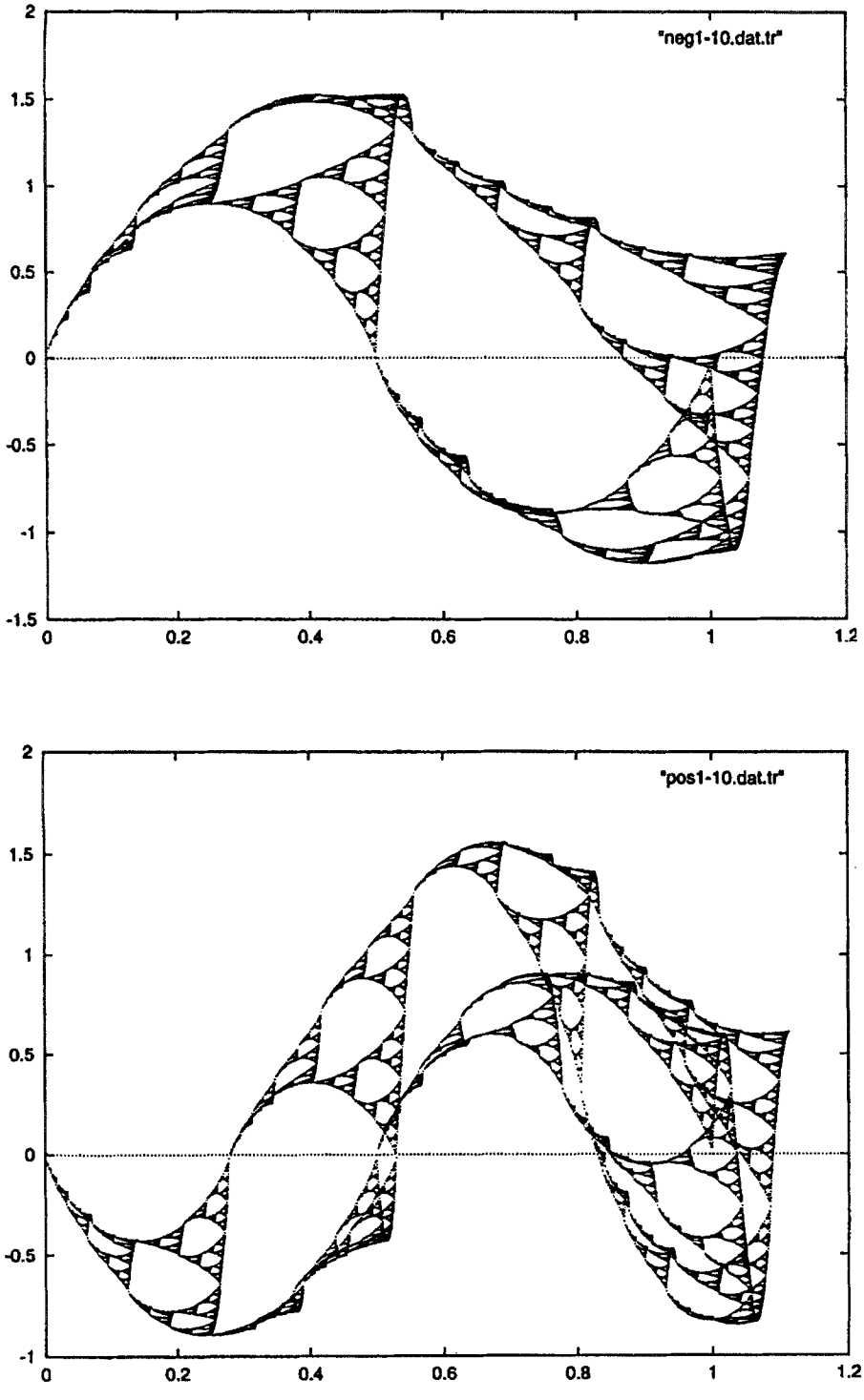

FIGURE 16 The graph of $\psi_n^{(5)}$ for $n = 0$ and $n = 1$.

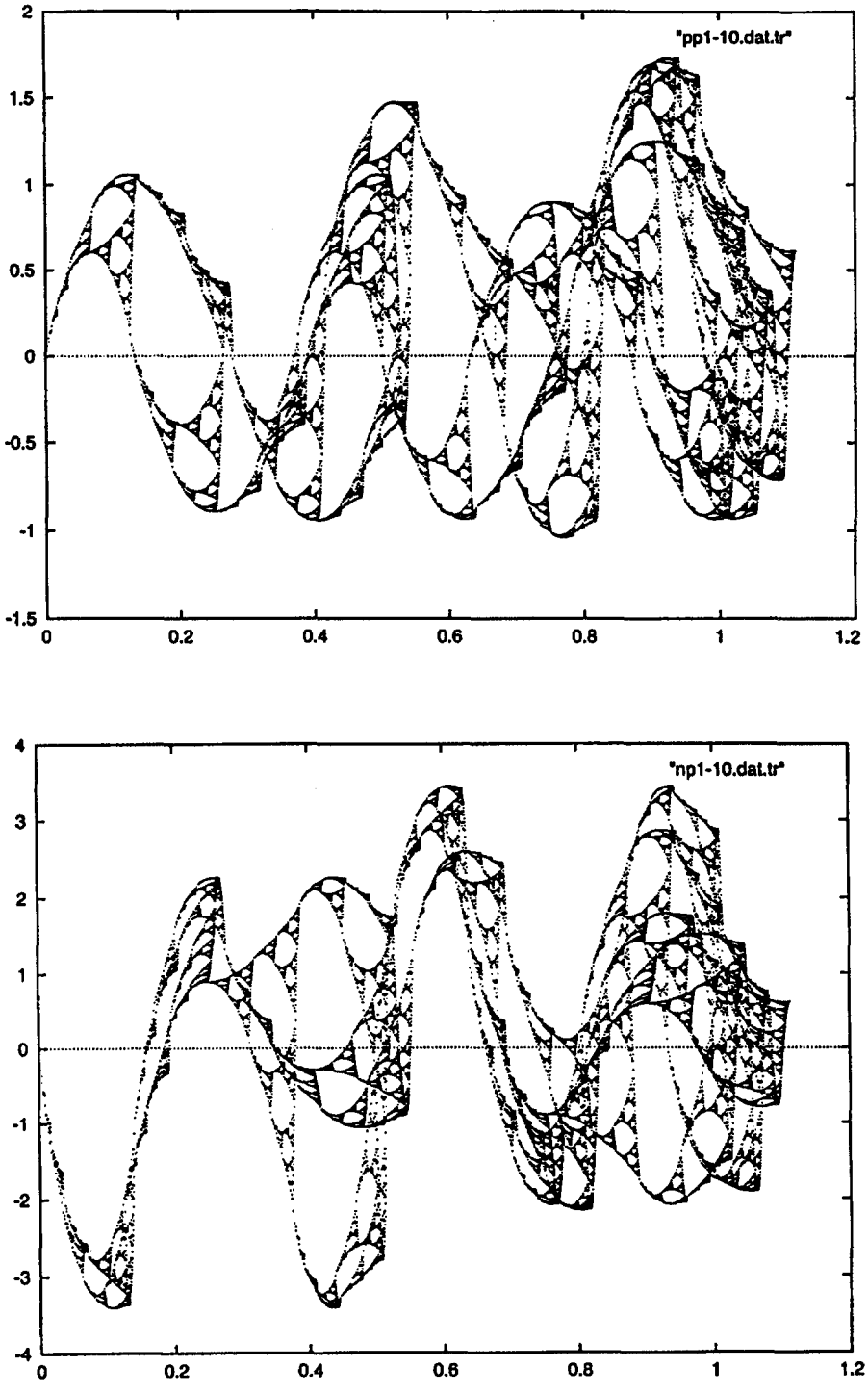

FIGURE 16 The graph of $\psi_n^{(5)}$ for $n = 2$ and $n = 3$.

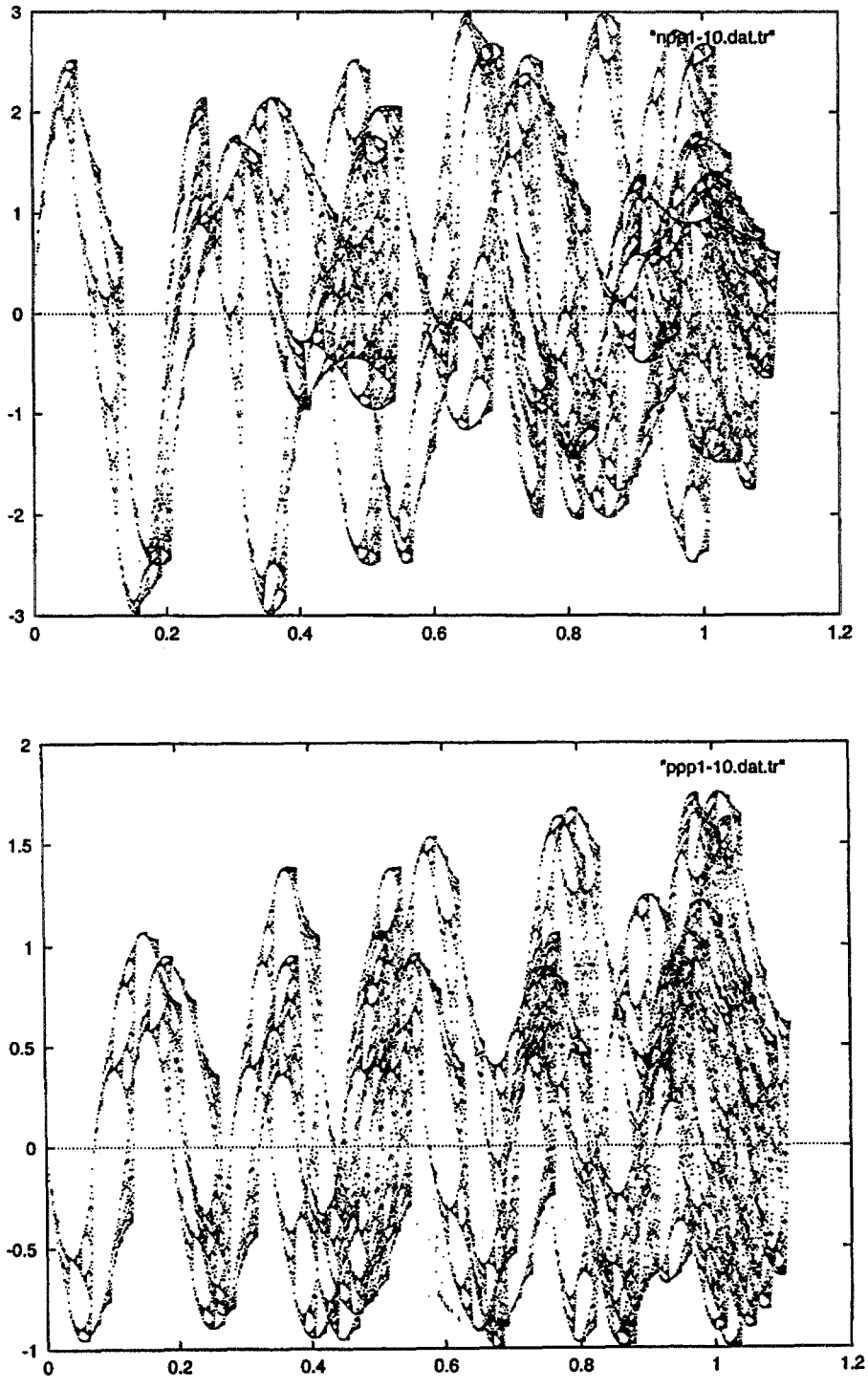

FIGURE 16 The graph of $\psi_n^{(5)}$ for $n = 4$ and $n = 5$.

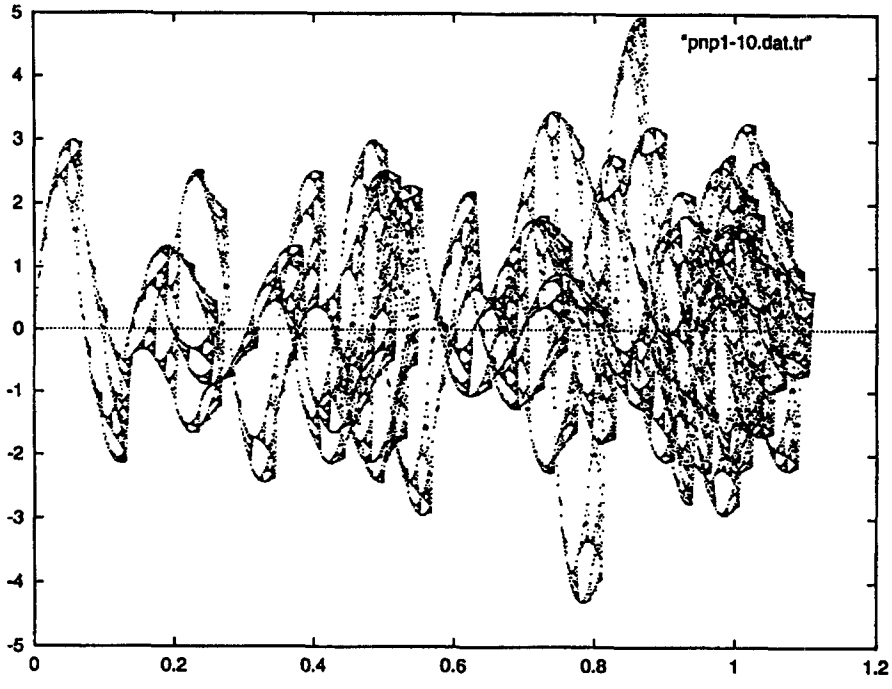

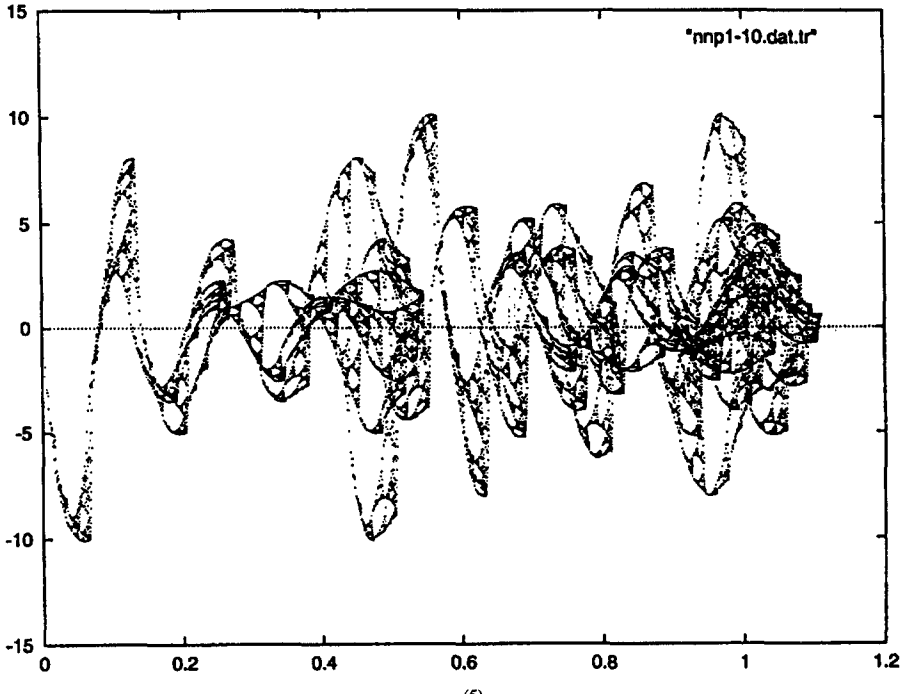

FIGURE 16 The graph of $\psi_n^{(5)}$ for $n = 6$ and $n = 7$.

5.000000000000000	5.000000000000000
1.381966011250105	6.909830056250526
0.293637838261838	7.340945956545955
0.059434048885759	7.429256110719831
0.011915204195355	7.447002622096993
0.002384177699732	7.450555311662097
0.000476881023048	7.451265985132689
0.000095378024003	7.451408125247472
0.000019075677577	7.451436553505483
0.000003815138427	7.451442239386936
0.000000763027802	7.451443376715015
0.000000152605565	7.451443609818482
0.000000030521113	7.451443636923536
0.000000006104223	7.451443704686173
0.000000001220845	7.451443704686173

$\psi_0^{(5)}$

5.000000000000000	5.000000000000000
3.618033988749895	18.090169943749473
0.877666491978266	21.941662299456656
0.182170517915148	22.771314739393478
0.036703533456671	22.939708410419161
0.007351515647798	22.973486399369484
0.001470735742284	22.980245973193771
0.000294164455002	22.981598047050294
0.000058833583279	22.981868468170685
0.000011766744347	22.981922552620279
0.000002353349977	22.981933370247454
0.000000470670040	22.981935541362304
0.000000094134010	22.981935975043172
0.000000018826802	22.981936110568444
0.000000003765361	22.981936788194801

$\psi_1^{(5)}$

5.000000000000000	5.000000000000000
3.618033988749895	18.090169943749473
4.122333508021734	103.058337700543362
1.041347713819957	130.168464227494610
0.217752799064036	136.095499415022317
0.043936645577732	137.302017430411894
0.008802827068426	137.544172944151057
0.001761185768747	137.592638183394769
0.000352261971449	137.602332597199478
0.000070453387026	137.604271534708289
0.000014090717115	137.604659324009816
0.000002818145011	137.604736876991211
0.000000563629066	137.604752353977233
0.000000112725816	137.604755403295854
0.000000022545163	137.604756080922215
0.000000004509033	137.604754386856314
0.000000000901807	137.604779797844714
0.000000000180361	137.604737446197362
0.000000000036072	137.604737446197362

$\psi_2^{(5)}$

5.000000000000000	5.000000000000000
1.381966011250105	6.909830056250526
4.706362161738162	117.659054043454049
1.257567773171575	157.195971646446878
0.265624868821615	166.015543013509415
0.053701749340775	167.817966689921491
0.010763520543051	168.180008485174767
0.002153631734540	168.252479260935445
0.000430763458339	168.266975913858658
0.000086154176176	168.269875344228922
0.000017230894616	168.270455235724000
0.000003446181298	168.270571210119869
0.000000689236355	168.270594398493841
0.000000137847275	168.270599006353081
0.000000027569455	168.270599683979441
0.000000005513891	168.270599683979441

$\psi_3^{(5)}$

FIGURE 17 A table of the values of λ_m and $5^{m-1}\lambda_m$. The limiting value λ for the eigenfunctions $\psi_n^{(5)}$ is the value at the bottom of the right hand column *(Cont.)*

5.000000000000000	5.000000000000000
1.381966011250105	6.909830056250526
4.706362161738162	117.659054043454049
3.742432226828425	467.804028353553122
0.916469838250128	572.793648906330077
0.190556309032439	595.488465726371487
0.038406270123447	600.097970678854040
0.007693090753758	601.022715137375144
0.001539091911534	601.207777942993289
0.000307837335072	601.244795062072512
0.000061568225144	601.252198668879942
0.000012313675354	601.253679399023554
0.000002462736284	601.253975535294444
0.000000492547305	601.254034624312794
0.000000098509463	601.254045466334560
0.000000019701893	601.254047160400432
0.000000003940379	601.254055630729908
0.000000000788076	601.254055630729908

$\psi_4^{(5)}$

5.000000000000000	5.000000000000000
3.618033988749895	18.090169943749473
0.877666491978266	21.941662299456656
4.817829482084852	602.228685260606426
1.303266730672558	814.541706670348617
0.275874718158295	862.108494244673238
0.055797618477205	871.837788706322726
0.011184542493599	873.792382312431641
0.002237910147085	874.183651205129536
0.000447622102526	874.261918996574423
0.000089526023487	874.277573115742939
0.000017905268817	874.280703958224876
0.000003581056328	874.281330112084561
0.000000716211368	874.281455405198130
0.000000143242278	874.281480477373407
0.000000028648456	874.281488947702883
0.000000005729691	874.281488947702883

$\psi_6^{(5)}$

5.000000000000000	5.000000000000000
3.618033988749895	18.090169943749473
4.122333508021734	103.058337700543362
3.958652286180043	494.831535772505390
0.986280173275135	616.425108296959024
0.205720194325708	642.875607267838632
0.041488294582616	648.254602853381812
0.008311475039992	649.333987499337695
0.001662848020706	649.550008088471373
0.000332591727593	649.593217954820375
0.000066519230480	649.601860158526506
0.000013303881495	649.603588612603403
0.000002660777715	649.603934283361127
0.000000532155600	649.604003401249543
0.000000106431122	649.604017631403053
0.000000021286224	649.604017631403053

$\psi_5^{(5)}$

5.000000000000000	5.000000000000000
1.381966011250105	6.909830056250526
0.293637838261838	7.340945956545955
4.940565951114241	617.570743889280152
1.355694949375055	847.309343359409240
0.287692369803660	899.038655636437966
0.058216301513105	909.629711142267865
0.011670500418625	911.757845205090803
0.002335190706853	912.183869864260942
0.000467081774447	912.269090717421705
0.000093418100278	912.286135526453791
0.000018683689872	912.289544512871544
0.000003736740767	912.290226340512845
0.000000747348265	912.290362475648067
0.000000149469657	912.290389919515519
0.000000029893932	912.290398389844995
0.000000005978786	912.290398389844995

$\psi_7^{(5)}$

FIGURE 17 A table of the values of λ_m and $5^{m-1}\lambda_m$.

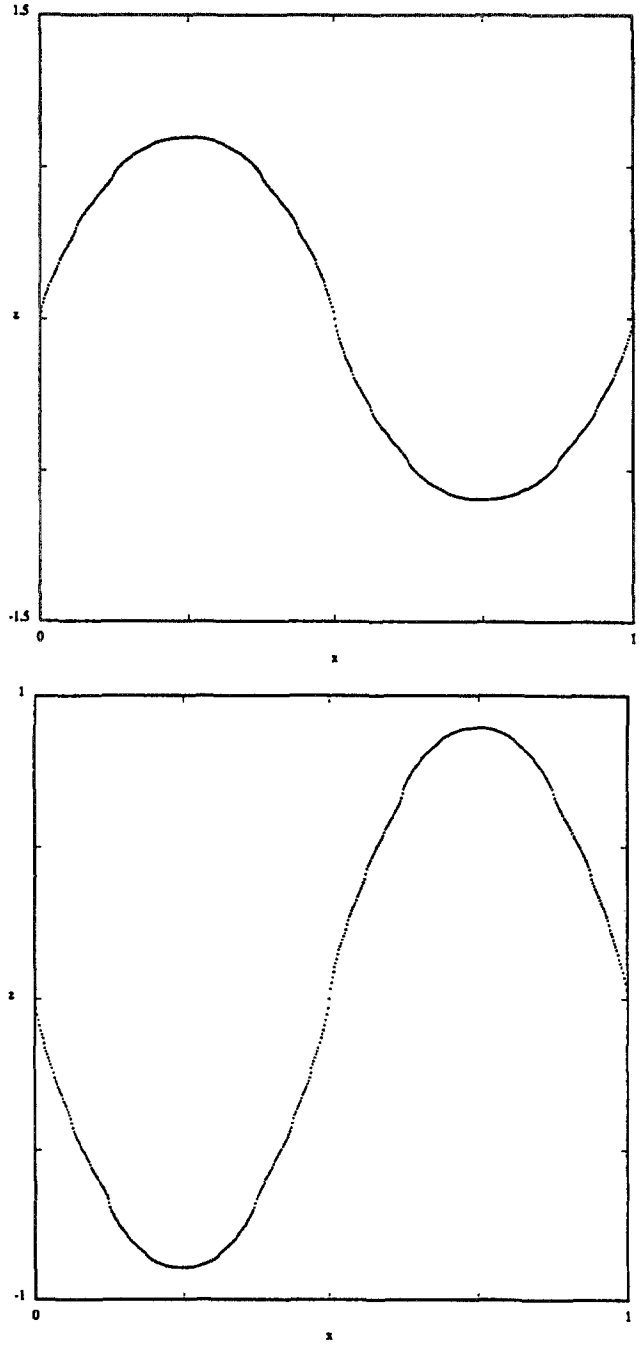

FIGURE 18 Restriction to the bottom edge in Fig. 15 of the functions $\psi_n^{(5)}$ for $n = 0$ and $n = 1$. Note the pattern 2, 2, 6, 6, 10, 10, 14, 14 for the number of local extrema.

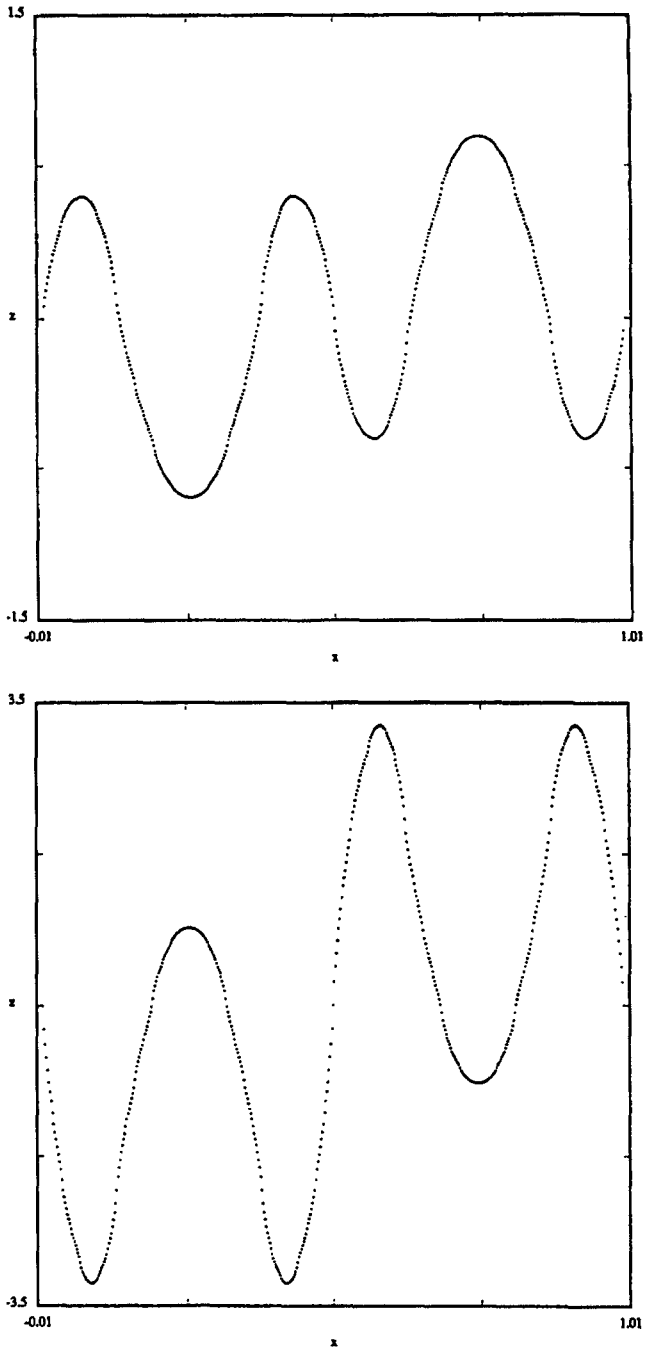

FIGURE 18 Restriction to the bottom edge in Fig. 15 of the functions $\psi_n^{(5)}$ for $n = 2$ and $n = 3$. Note the pattern 2, 2, 6, 6, 10, 10, 14, 14 for the number of local extrema.

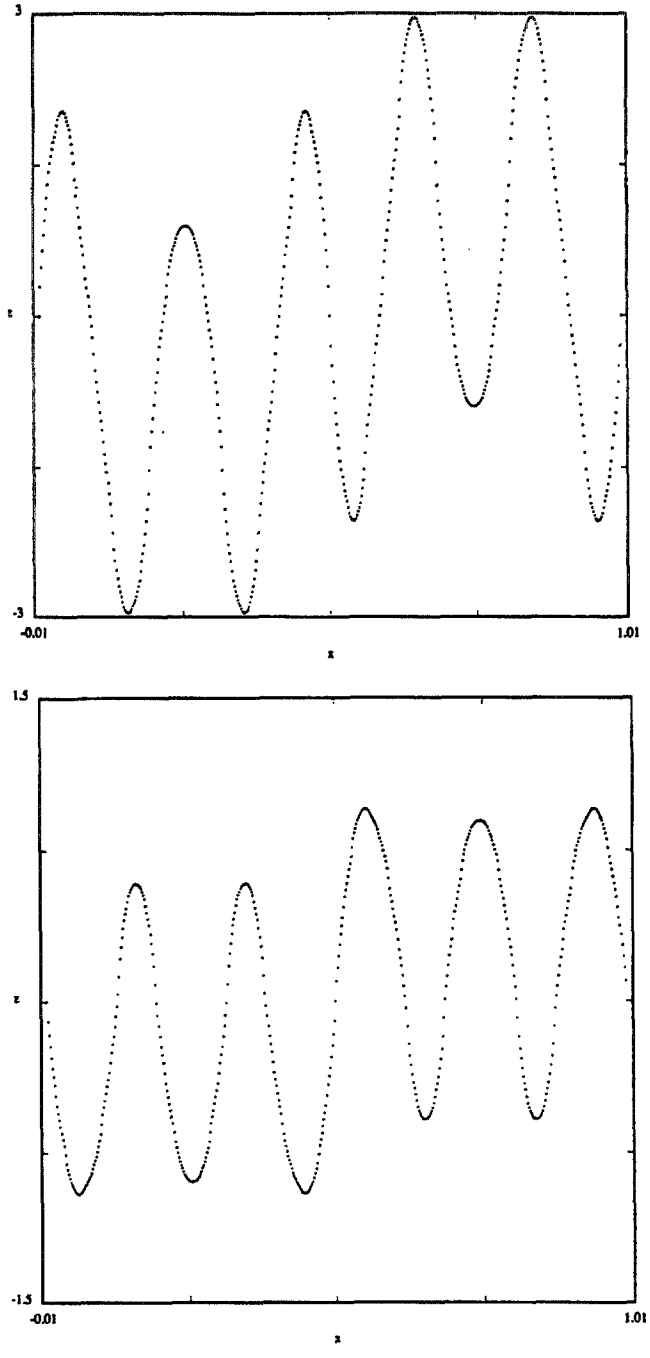

FIGURE 18 Restriction to the bottom edge in Fig. 15 of the functions $\psi_n^{(5)}$ for $n = 4$ and $n = 5$. Note the pattern 2, 2, 6, 6, 10, 10, 14, 14 for the number of local extrema.

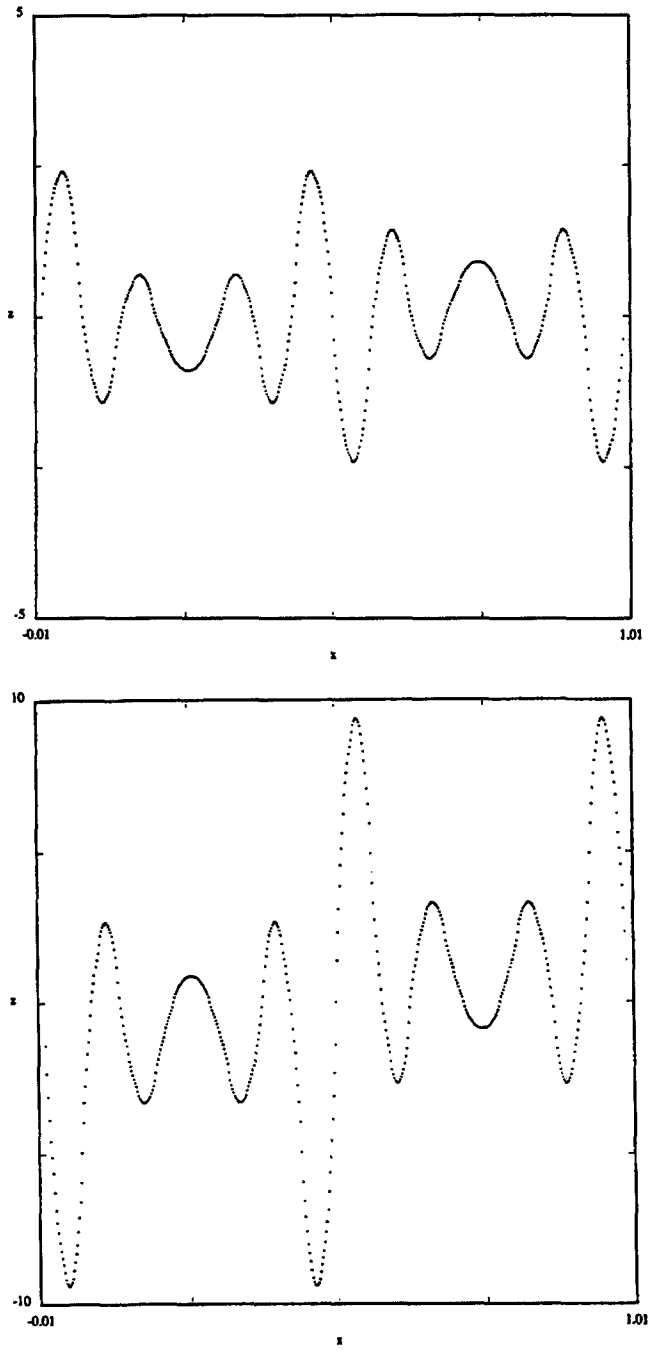

FIGURE 18 Restriction to the bottom edge in Fig. 15 of the functions $\psi_n^{(5)}$ for $n = 6$ and $n = 7$. Note the pattern 2, 2, 6, 6, 10, 10, 14, 14 for the number of local extrema.

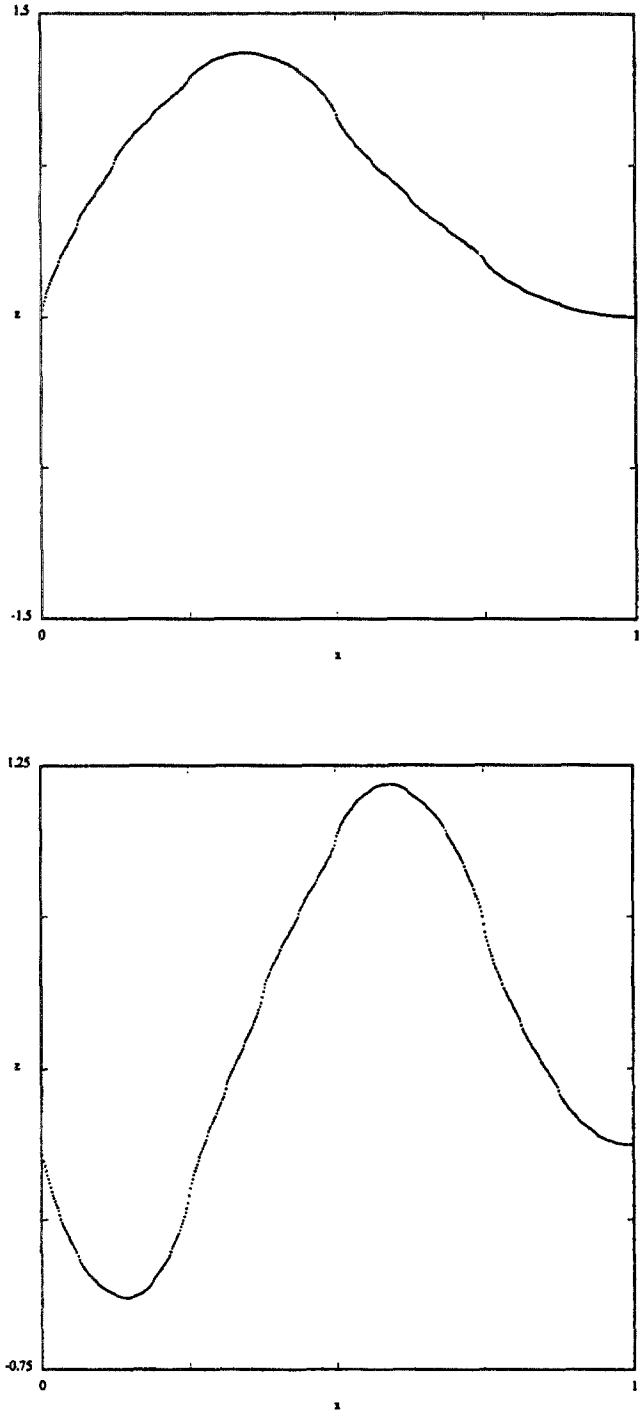

FIGURE 19 Restriction to the left edge in Fig. 15 of the functions $\psi_n^{(5)}$ for $n = 0$ and $n = 1$. Note the pattern 1, 2, 5, 6, 9, 10, 13, 14 for the number of local extrema.

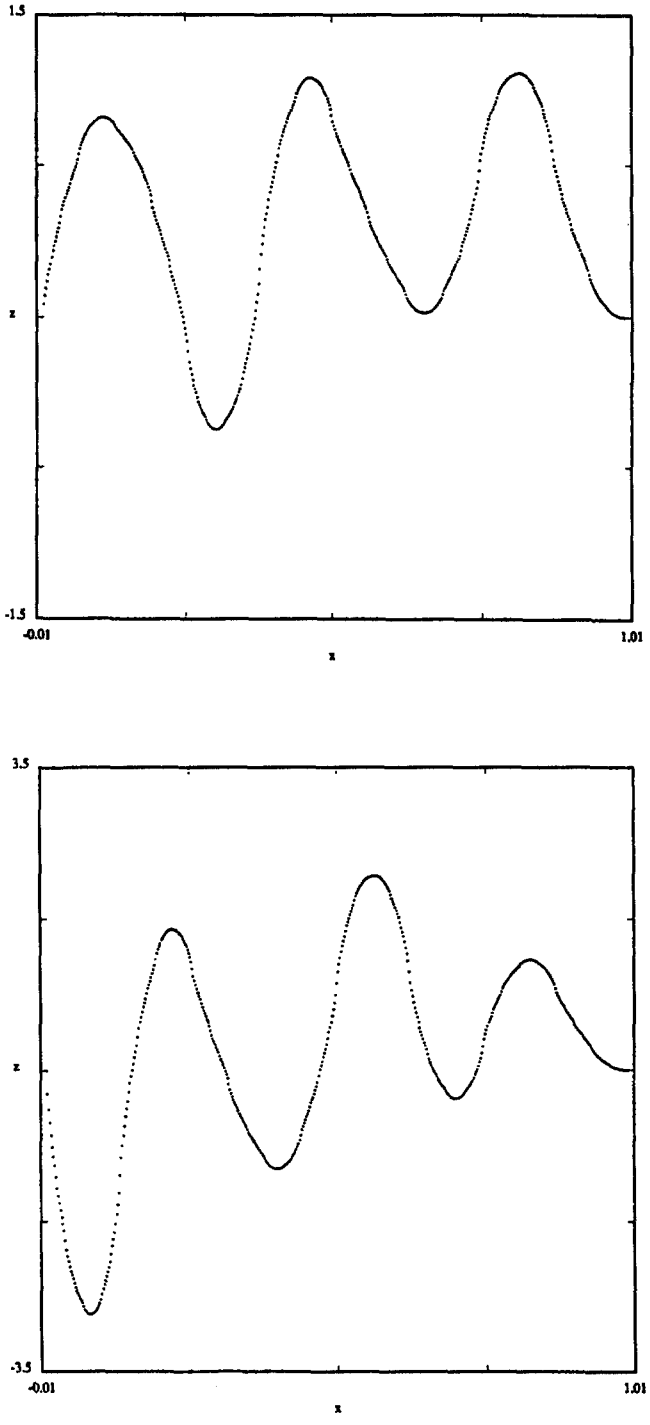

FIGURE 19 Restriction to the left edge in Fig. 15 of the functions $\psi_n^{(5)}$ for $n = 2$ and $n = 3$. Note the pattern 1, 2, 5, 6, 9, 10, 13, 14 for the number of local extrema.

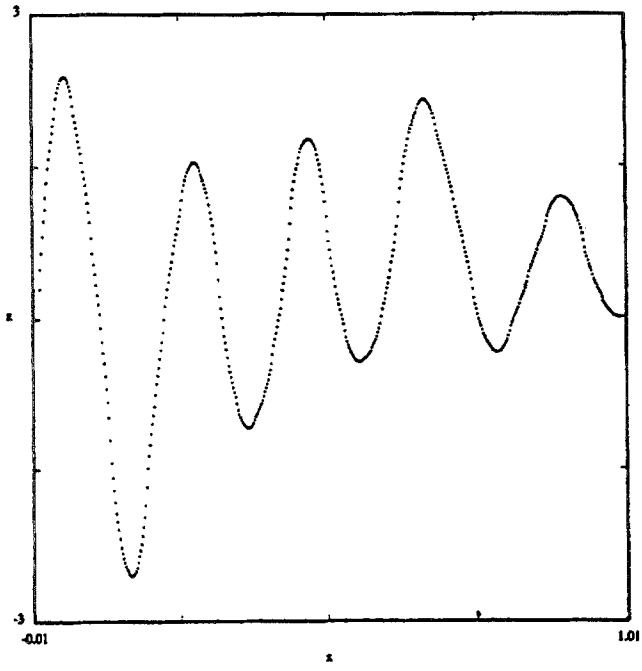

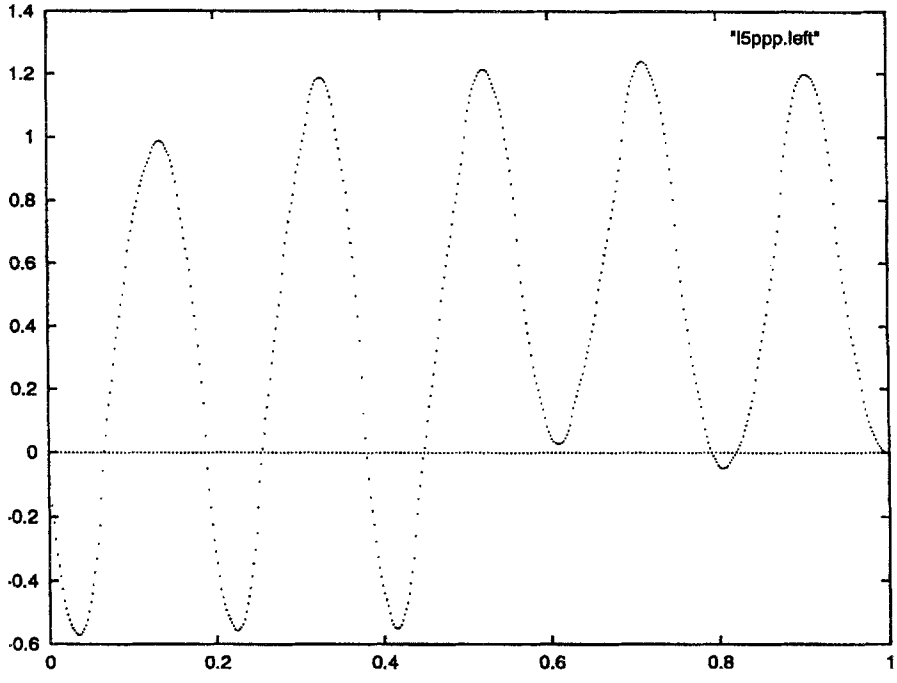

FIGURE 19 Restriction to the left edge in Fig. 15 of the functions $\psi_n^{(5)}$ for $n = 4$ and $n = 5$. Note the pattern 1, 2, 5, 6, 9, 10, 13, 14 for the number of local extrema.

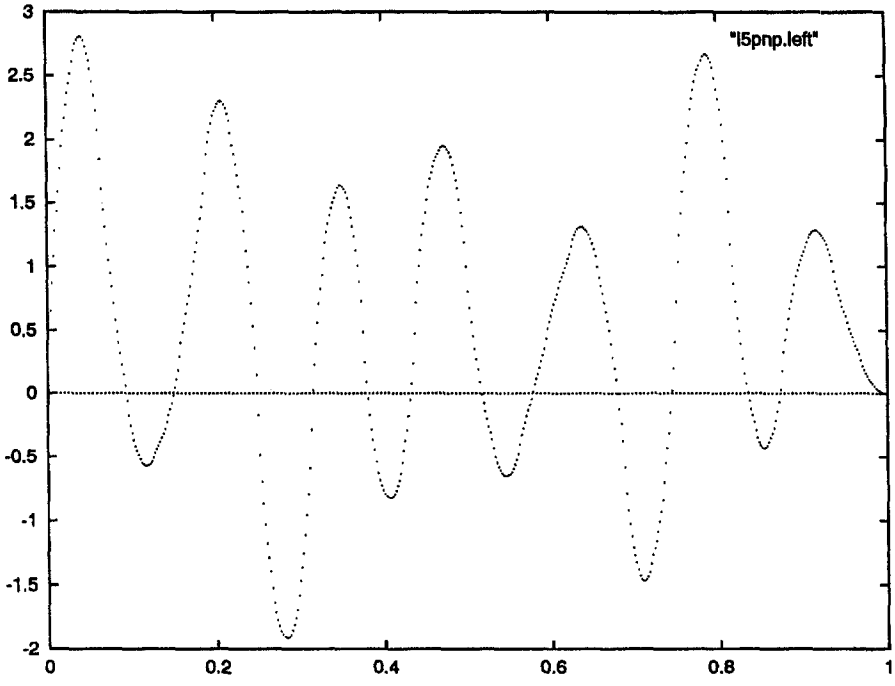

FIGURE 19 Restriction to the left edge in Fig. 15 of the functions $\psi_n^{(5)}$ for $n = 6$. Note the pattern 1, 2, 5, 6, 9, 10, 13, 14 for the number of local extrema.

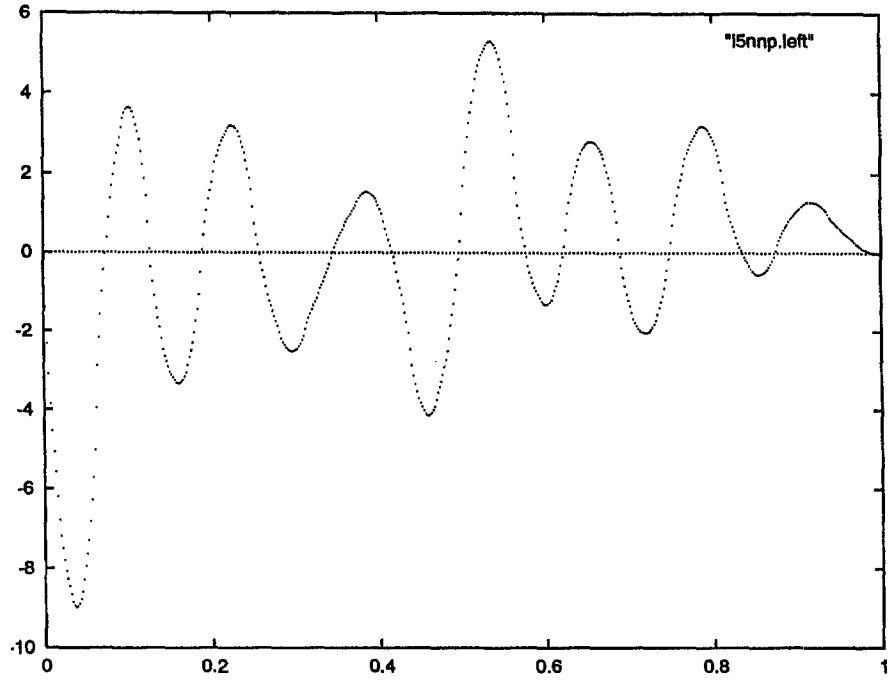

FIGURE 19 Restriction to the left edge in Fig. 15 of the functions $\psi_n^{(5)}$ for $n = 7$. Note the pattern 1, 2, 5, 6, 9, 10, 13, 14 for the number of local extrema.

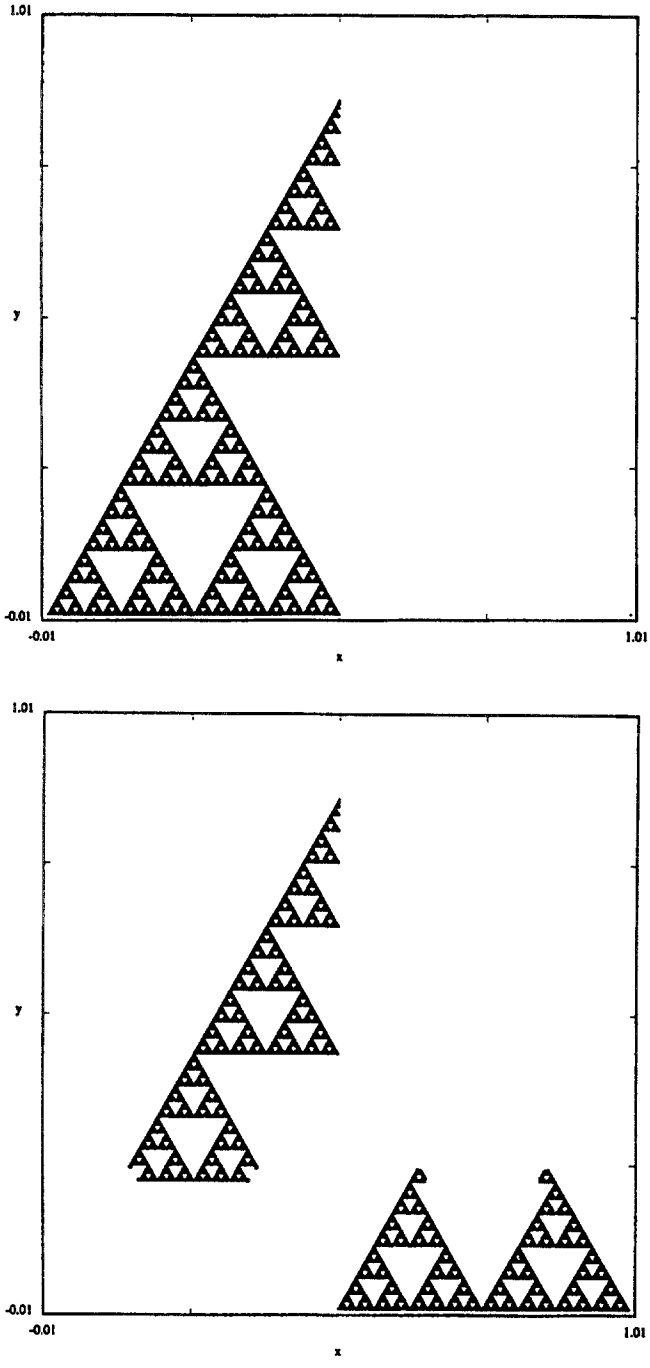

FIGURE 20 The subset of SG where $\psi_n^{(5)}$ is positive, for $n = 0$ and $n = 1$. The boundary is the nodal set.

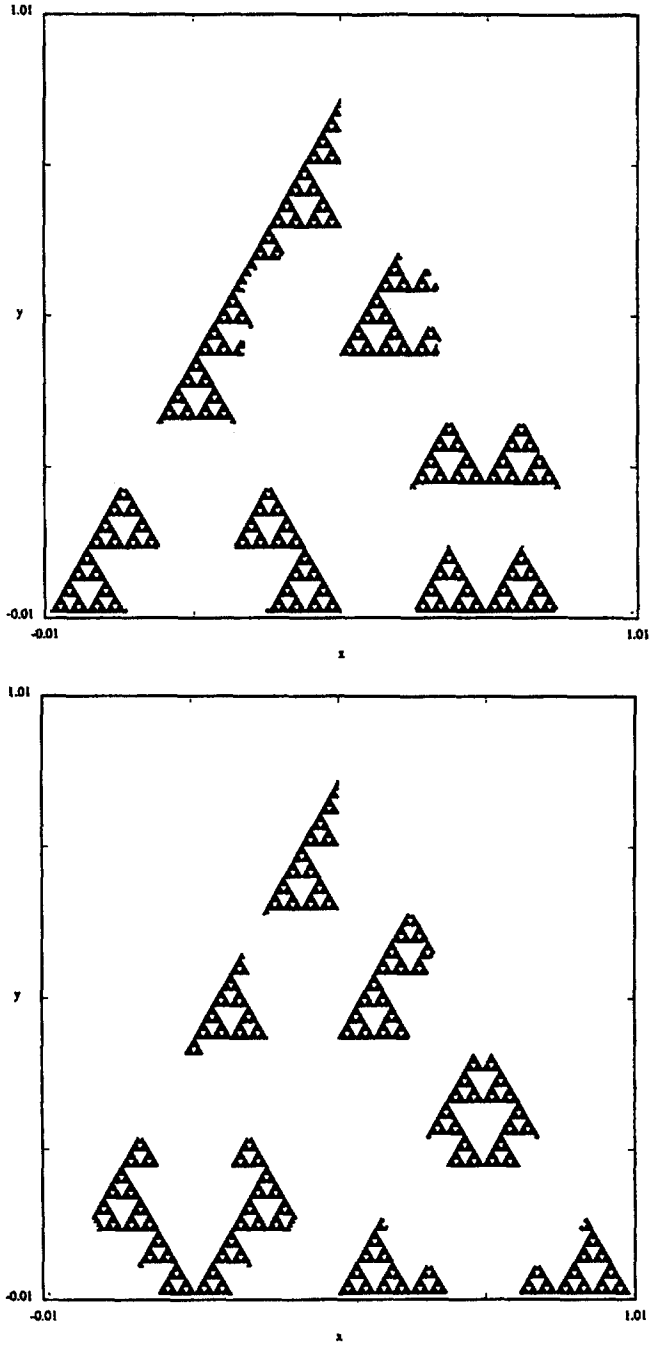

FIGURE 20 The subset of SG where $\psi_n^{(5)}$ is positive, for $n = 2$ and $n = 3$. The boundary is the nodal set.

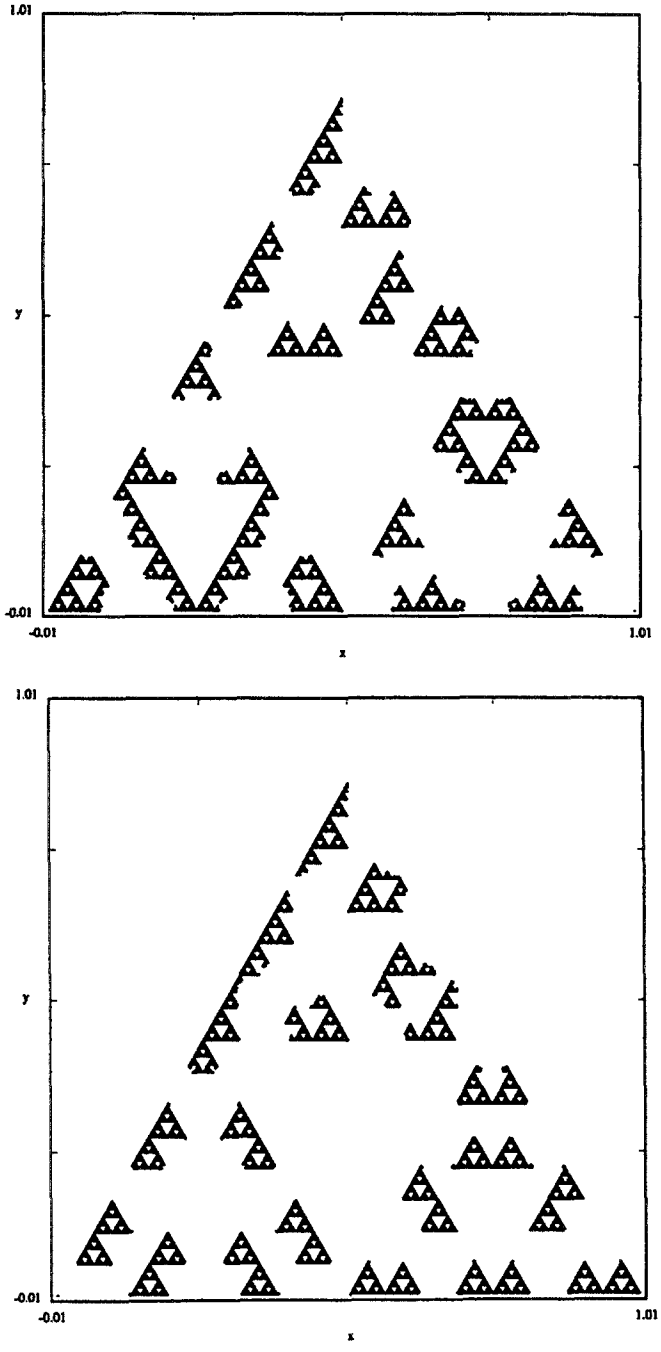

FIGURE 20 The subset of SG where $\psi_n^{(5)}$ is positive, for $n = 4$ and $n = 5$. The boundary is the nodal set.

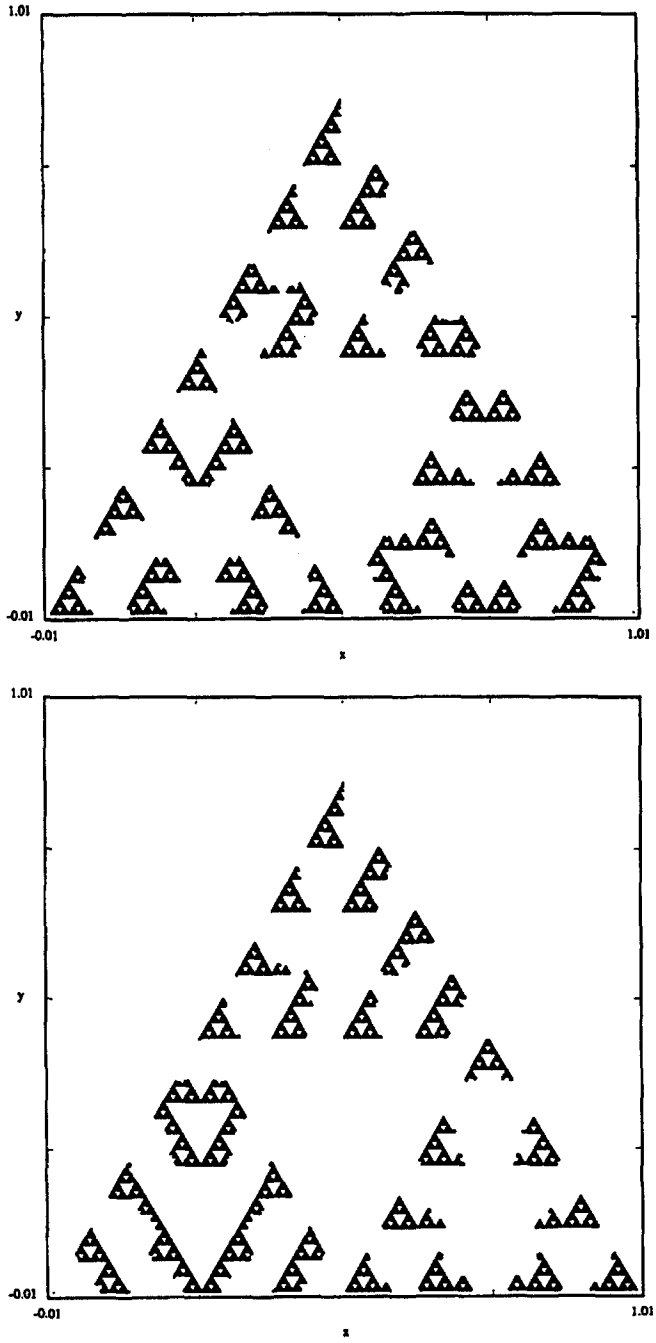

FIGURE 20 The subset of SG where $\psi_n^{(5)}$ is positive, for $n = 6$ and $n = 7$. The boundary is the nodal set.

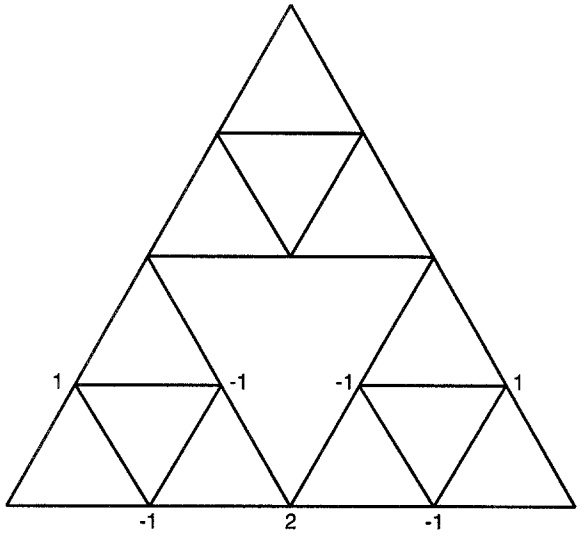

FIGURE 21 Initial values on G_2 for the family $\psi_n^{(6)}$.

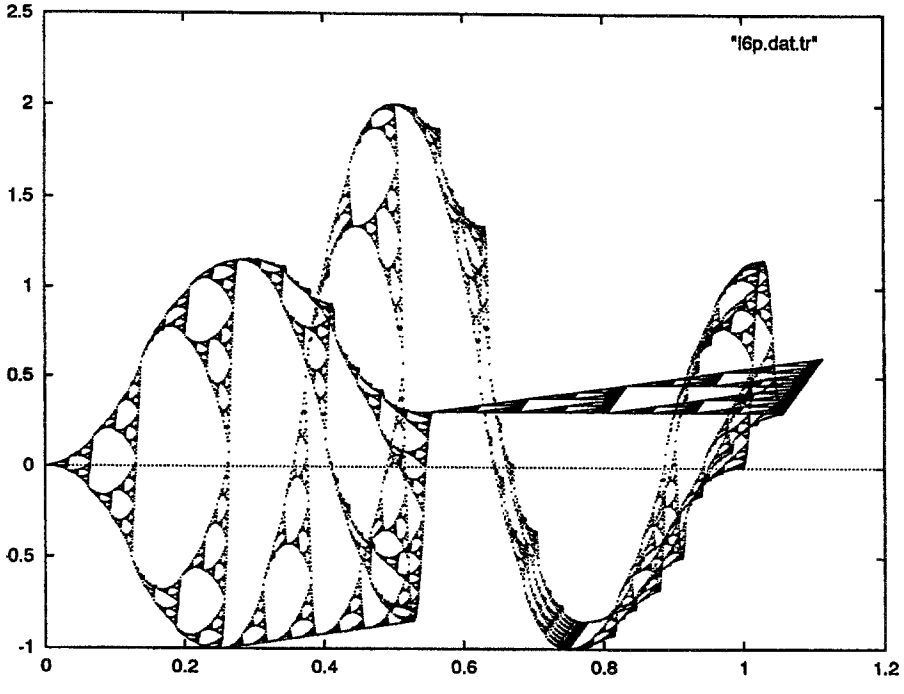

FIGURE 22 The graph of $\psi_n^{(6)}$ for $n = 1$.

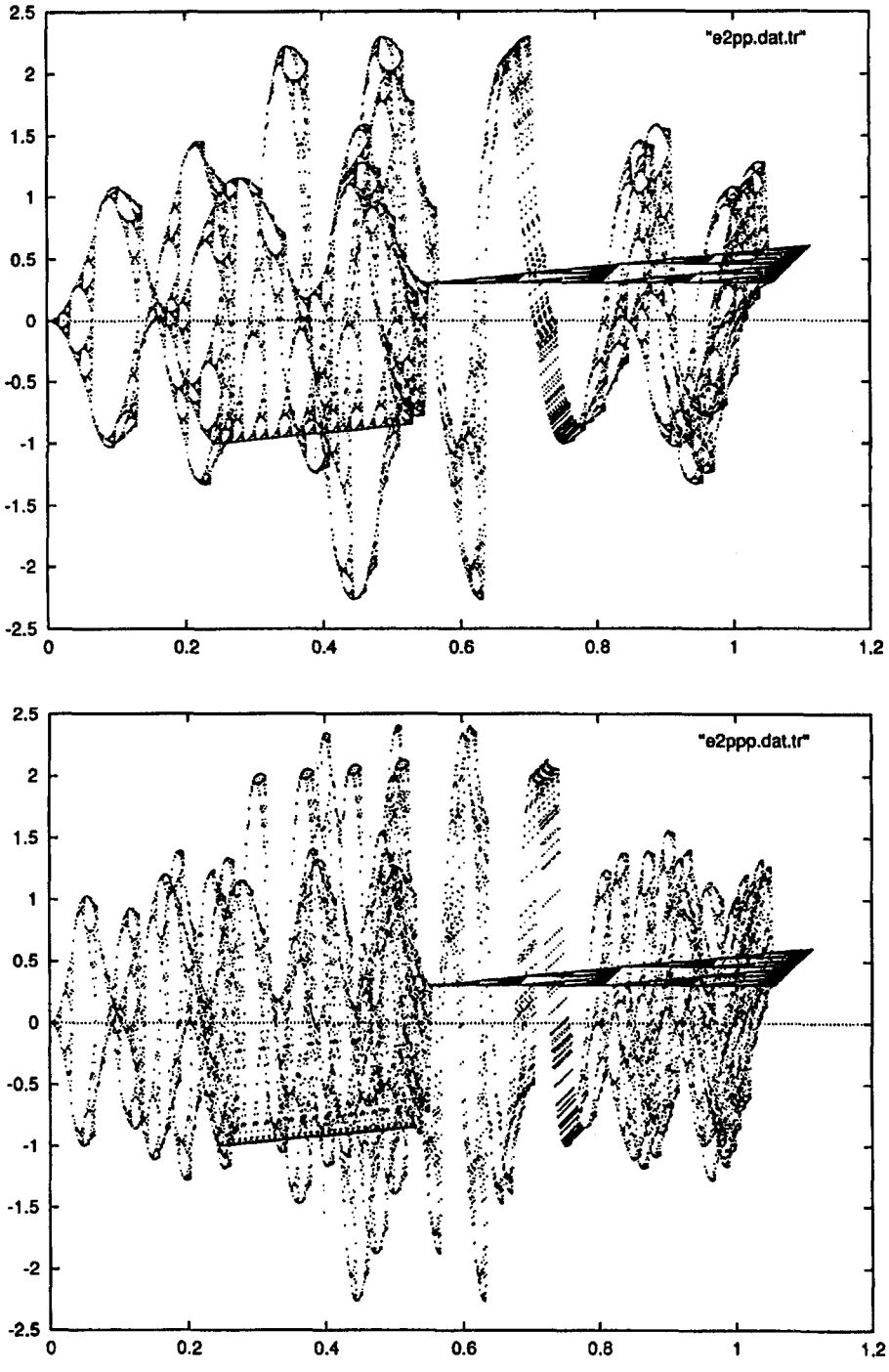

FIGURE 22 The graph of $\psi_n^{(6)}$ for $n = 2$ and $n = 5$.

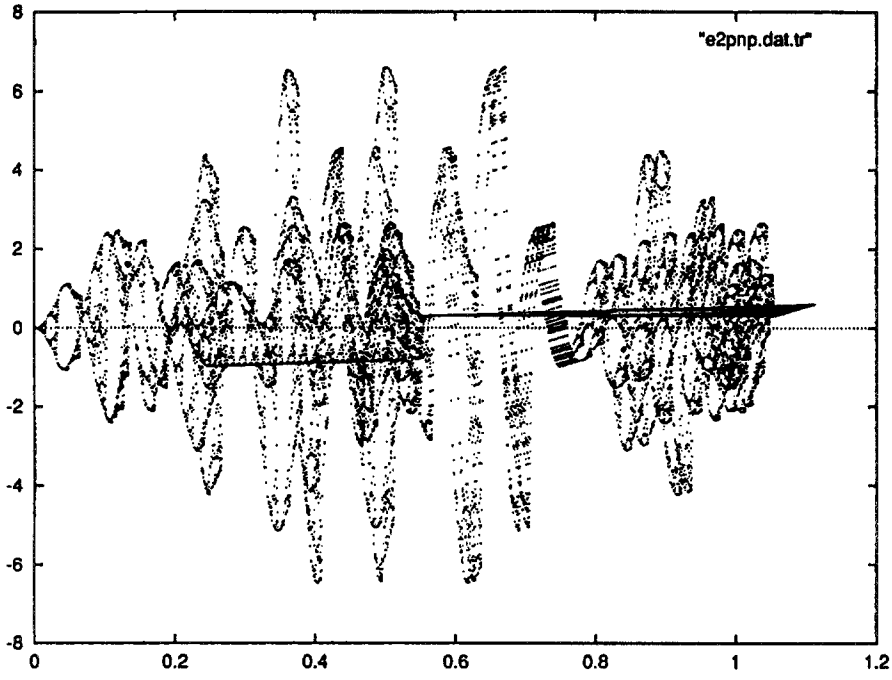

FIGURE 22 The graph of $\psi_n^{(6)}$ for $n = 6$.

	$\psi_1^{(6)}$ sign choice: $+--$		$\psi_2^{(6)}$ sign choice: $++-$		$\psi_5^{(6)}$ sign choice: $+++$		$\psi_6^{(6)}$ sign choice: $+-+$	
m	λ_m	$5^{m-1}\lambda_m$	λ_m	$5^{m-1}\lambda_m$	λ_m	$5^{m-1}\lambda_m$	λ_m	$5^{m-1}\lambda_m$
2	6	30	6	30	6	30	6	30
3	3.	75.	3.	75.	3.	75.	3.	75.
4	0.697224	87.153	4.30278	537.847	4.30278	537.847	0.697224	87.153
5	0.143567	89.7295	1.10457	690.356	3.89543	2434.64	4.85643	3035.27
6	0.0288802	90.2508	0.231646	723.894	0.965539	3017.31	1.31951	4123.45
7	0.00578274	90.3553	0.0467666	730.729	0.201204	3143.82	0.279528	4367.63
8	0.00115682	90.3762	0.00937089	732.101	0.0405701	3169.54	0.0565451	4417.59
9	0.000231374	90.3804	0.00187488	732.375	0.00812723	3174.7	0.0113347	4427.63
10	0.0000462752	90.3812	0.000375004	732.43	0.00162597	3175.73	0.00226797	4429.64

FIGURE 23 A table of the values of λ_m and $5^{m-1}\lambda_m$ for the eigenfunctions $\psi_n^{(6)}$.

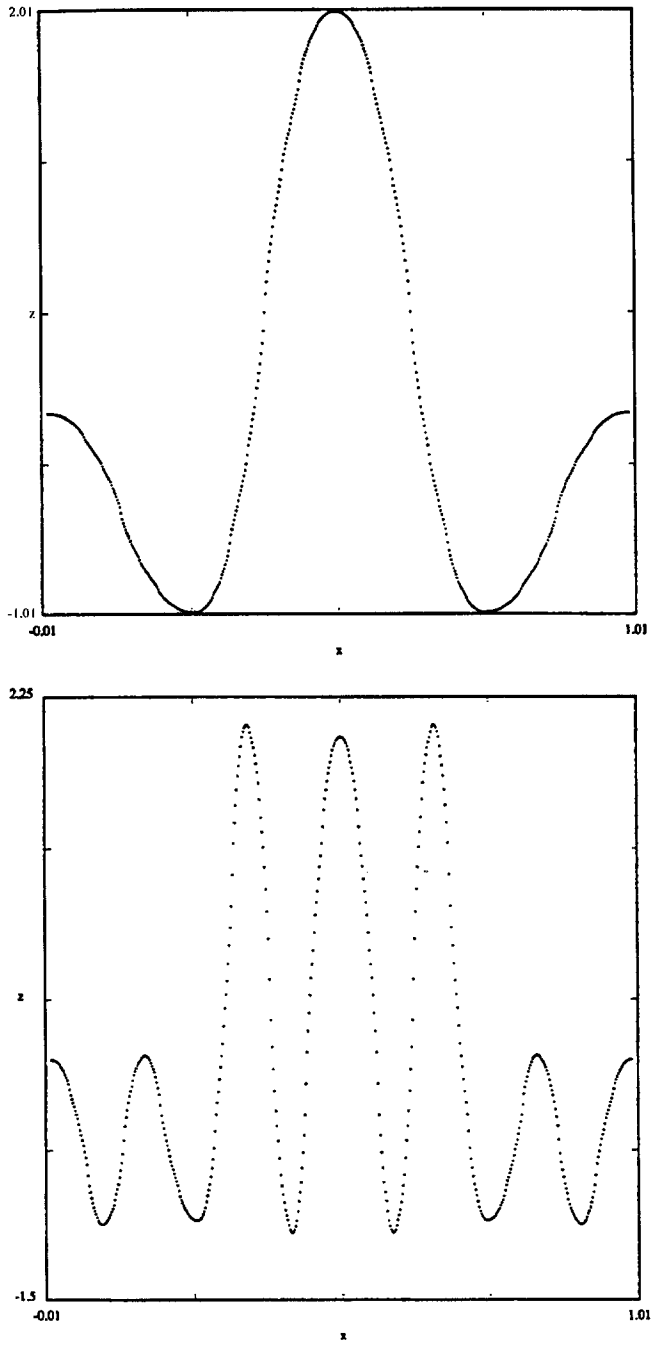

FIGURE 24 Restrictions to the bottom edge in Fig. 20 of the functions $\psi_n^{(6)}$ for $n = 1$ and $n = 2$. Note the pattern 3, 11, 19, 27 for the number of local extrema.

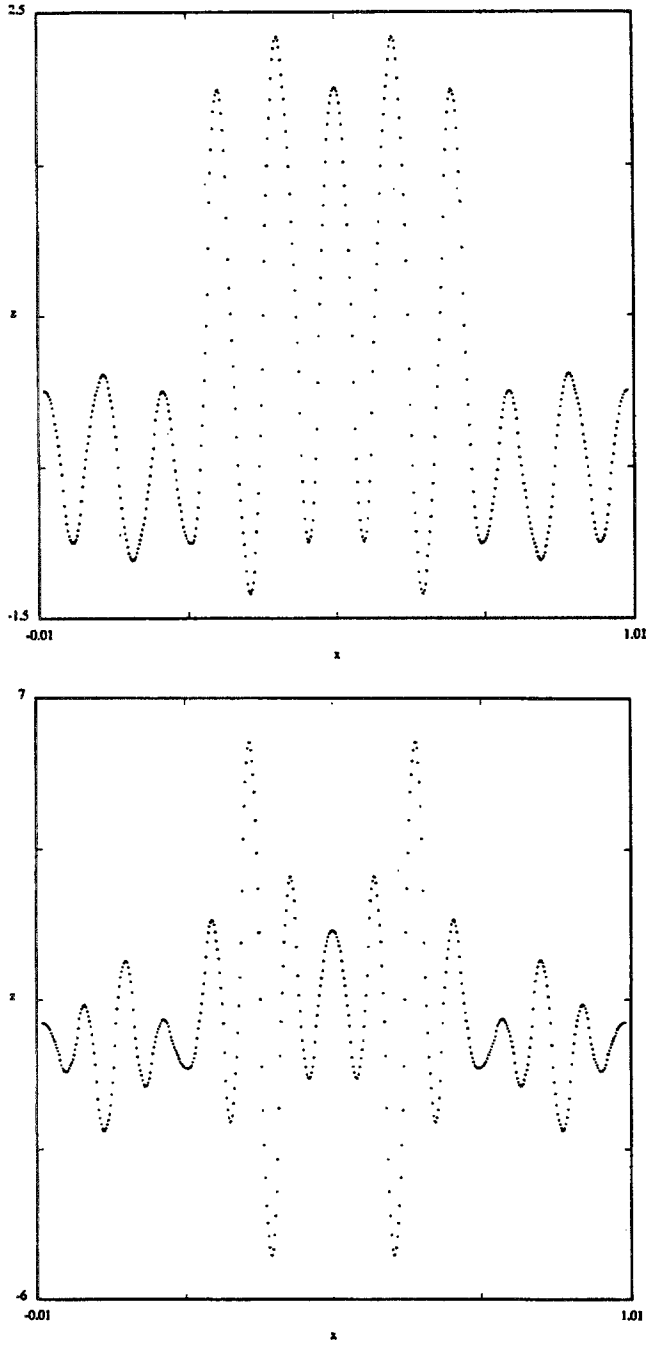

FIGURE 24 Restrictions to the bottom edge in Fig. 20 of the functions $\psi_n^{(6)}$ for $n = 5$ and $n = 6$. Note the pattern 3, 11, 19, 27 for the number of local extrema.

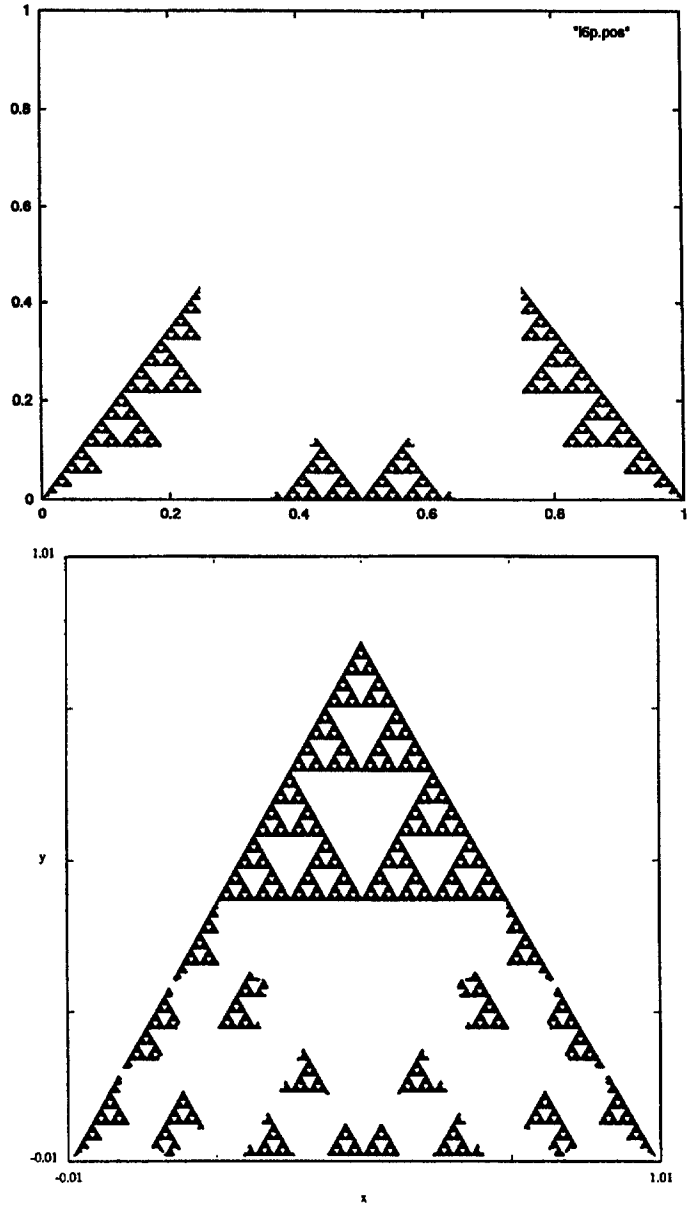

FIGURE 25 The subset of SG where $\psi_n^{(6)}$ is positive, for $n = 1$ and $n = 2$. The boundary is the nodal set.

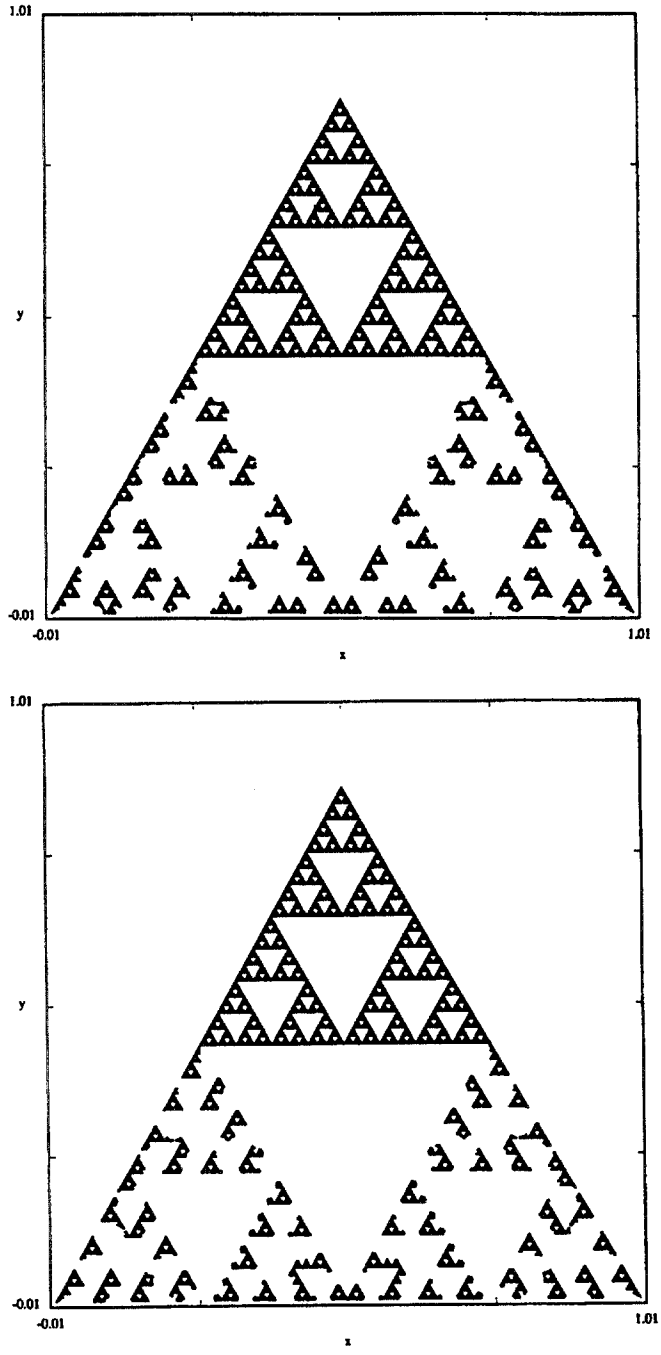

FIGURE 25 The subset of SG where $\psi_n^{(6)}$ is positive, for $n = 5$ and $n = 6$. The boundary is the nodal set.

4. Properties of Harmonic Functions and Eigenfunctions

It appears from our numerical computations that some harmonic functions have restrictions to lines that are monotonic. We will now demonstrate that this is in fact the case.

Theorem 1.

Let f be a harmonic function on SG, E an edge in G_m with endpoints v_0, v_1 and midpoint v_{01}. Suppose $f(v_0) < f(v_{01}) < f(v_1)$ and

$$\frac{1}{4} \leq \frac{f(v_1) - f(v_{01})}{f(v_{01}) - f(v_0)} \leq 4 . \tag{4.1}$$

Then the restriction of f to E is strictly increasing.

Proof. Let

$$\frac{f(v_1) - f(v_{01})}{f(v_{01}) - f(v_0)} = x$$

and

$$\frac{f(v_{01}) - f(v_{001})}{f(v_{001}) - f(v_0)} = y ,$$

using the notation in Fig. 3. Now by (2.6) we have

$$f(v_{01}) - f(v_{001}) = \frac{8}{25}(f(v_{01}) - f(v_0)) + \frac{3}{25}(f(v_1) - f(v_{01})) \tag{4.2}$$

and

$$f(v_{001}) - f(v_0) = \frac{17}{25}(f(v_{01}) - f(v_0)) - \frac{3}{25}(f(v_1) - f(v_{01})) . \tag{4.3}$$

Using $x \leq 4$ from (4.1) we obtain

$$f(v_{001}) - f(v_0) \geq \left(\frac{17}{25} - \frac{12}{25}\right)(f(v_1) - f(v_{01})) ,$$

and so $f(v_0) < f(v_{001}) < f(v_{01})$. From (4.2) and (4.3) we obtain

$$y = \frac{8 + 3x}{17 - 3x} . \tag{4.4}$$

Since the right side of (4.4) is an increasing function of x on the interval $\frac{1}{4} \leq x \leq 4$, we obtain $\frac{7}{13} \leq y \leq 4$, hence $\frac{1}{4} \leq y \leq 4$. Thus, the hypotheses of the theorem also hold for the half of the edge from v_0 to v_{01}. A similar argument, using $x \geq \frac{1}{4}$ from (4.1), shows that the hypotheses hold for the other half of the edge.

It follows by induction that the same is true for any dyadic subinterval in E. Thus, in particular, we have $f(a) < f(b)$ if $a < b$ and a and b are dyadic points in E. Since the dyadic points are dense in E, and f is continuous, it follows that f is strictly increasing on E. □

Now let T be any minimal triangle in G_m, with vertices v_0, v_1, v_2. Assuming that the harmonic function f is not constant, we order the edges according to the relative sizes of $|f(v_j) - f(v_k)|$ along the edge.

Theorem 2.

If there is a tie for smallest edge, then f is monotone along all three edges. If not, then f is monotone along the two largest edges, and has a single extremum along the smallest edge. Furthermore, if E denotes the largest edge, then we have the following stronger monotone property:

if T' is any minimal triangle in G_m with $m' > m$ which has an edge E' contained in E, then the absolute maximum and minimum values of f on T' are assumed at the endpoints of E'.

Proof. We may assume without loss of generality that $f(v_0) \le f(v_1) \le f(v_2)$ and $f(v_0) \ne f(v_2)$, so the largest edge joins v_0 to v_2. It follows easily from Algorithm 2.1 that the two halves of this edge (v_0 to v_{20} and v_{20} to v_2 in Fig. 2) are the largest edges in the two minimal G_{m+1} triangles containing them. An inductive argument shows that the same is true for any smaller triangle bordering on the edge. In particular, f is increasing along this edge.

Next consider the second largest edge. Suppose $f(v_2) - f(v_1) \ge f(v_1) - f(v_0)$ (a similar argument works in the contrary case). Then $f(v_{12}) = \frac{2}{5}(f(v_2) + f(v_1)) + \frac{1}{5}f(v_0)$, so $f(v_1) \le f(v_{12}) \le f(v_2)$ (because $f(v_{12}) - f(v_1) = \frac{2}{5}(f(v_2) - f(v_1)) - \frac{1}{5}(f(v_1) - f(v_0))$ and $f(v_2) - f(v_{12}) = \frac{3}{5}(f(v_2) - f(v_1)) + \frac{1}{5}(f(v_1) - f(v_0))$). Thus, we may apply Theorem 1 once we have verified the analog of (4.1), namely

$$\frac{1}{4} \le \frac{f(v_2) - f(v_{12})}{f(v_{12}) - f(v_1)} \le 4 .$$

But since

$$\frac{f(v_2) - f(v_{12})}{f(v_{12}) - f(v_1)} = \frac{3(f(v_2) - f(v_1)) + (f(v_1) - f(v_0))}{2(f(v_2) - f(v_1)) - (f(v_1) - f(v_0))}$$

the left inequality is trivial and the right inequality is exactly $f(v_2) - f(v_1) \ge f(v_1) - f(v_0)$.

Finally, we consider the smallest edge, assuming $f(v_2) - f(v_1) > f(v_1) - f(v_0)$ (a similar argument works in the contrary case). Without loss of generality we may take $f(v_0) = 0$, $f(v_1) = 1$ and $f(v_2) = a > 2$. (In the case that $f(v_0) = f(v_1)$, it is easy to see that v_{01} is the unique local maximum; this would correspond to the limiting case $a = \infty$.) Now the top triangle in Fig. 2 has $f(v_0) = 0$, $f(v_{01}) = \frac{a+2}{5}$ and $f(v_{20}) = \frac{2a+1}{5}$, so the edge from v_0 to v_{01} is the second largest ($\frac{a+2}{5} - 0 > \frac{2a+1}{5} - \frac{a+2}{5}$) and by what we have already proven we know that f is increasing on the edge from v_0 to v_{01}. On the other hand, the lower right triangle has $f(v_{01}) = \frac{a+2}{5}$, $f(v_1) = 1$ and $f(v_{12}) = \frac{2a+2}{5}$, and we need to distinguish two cases: 1) if $a \ge 3$, then $f(v_{12}) > f(v_{01}) \ge f(v_1)$ and the edge joining v_1 to v_{01} is the smallest edge, 2) if $2 < a \le 3$, then $f(v_{12}) > f(v_1) \ge f(v_{01})$ and the edge joining v_{01} to v_1 is the smallest edge. By repeating the argument we obtain that f is increasing on half of this edge, namely from v_1 to v_{011} in the first case, and from v_{01} to v_{011} in the second (see Fig. 3 for notation). By induction, we continue to add half of the remaining piece of the edge either to one side or the other, and in the limit there is a unique point x on this edge such that f is increasing from v_0 to x and from v_1 to x, so x is the unique (maximum) extremum. (In the contrary case $f(v_2) - f(v_1) < f(v_1) - f(v_0)$ and the unique extremum is a minimum.) □

Remark 2. The proof actually yields a formula for the extreme point $M(a)$ on the smallest edge as a function of the parameter a ($= \frac{f(v_2)-f(v_0)}{f(v_1)-f(v_0)}$ in general). If we parametrize points on the edge by $x \in [0, 1]$ with 0 corresponding to v_0 and 1 corresponding to v_1, then our argument shows $\frac{1}{2} \le M(a) < 1$ ($M(\infty) = \frac{1}{2}$ corresponds to the degenerate case $f(v_1) = f(v_0)$), with $\frac{3}{4} \le M(a) < 1$ if $2 < a \le 3$ and $\frac{1}{2} < M(a) \le \frac{3}{4}$ if $3 \le a < \infty$. More precisely, the induction argument gives us the recursion identity

$$M(a) = \begin{cases} \frac{1}{2}\left(1 + M\left(\frac{a}{3-a}\right)\right) & 2 < a < 3 \\ \frac{3}{4} & a = 3 \\ 1 - \frac{1}{2}M\left(\frac{2a-3}{a-3}\right) & a > 3 . \end{cases}$$

By iterating this identity we can compute $M(a)$ to any desired accuracy. It also follows that $M(a)$ is continuous, decreasing in a, and assumes all values in $\left(\frac{1}{2}, 1\right)$. Figure 26 shows a portion of the graph of $M(a)$.

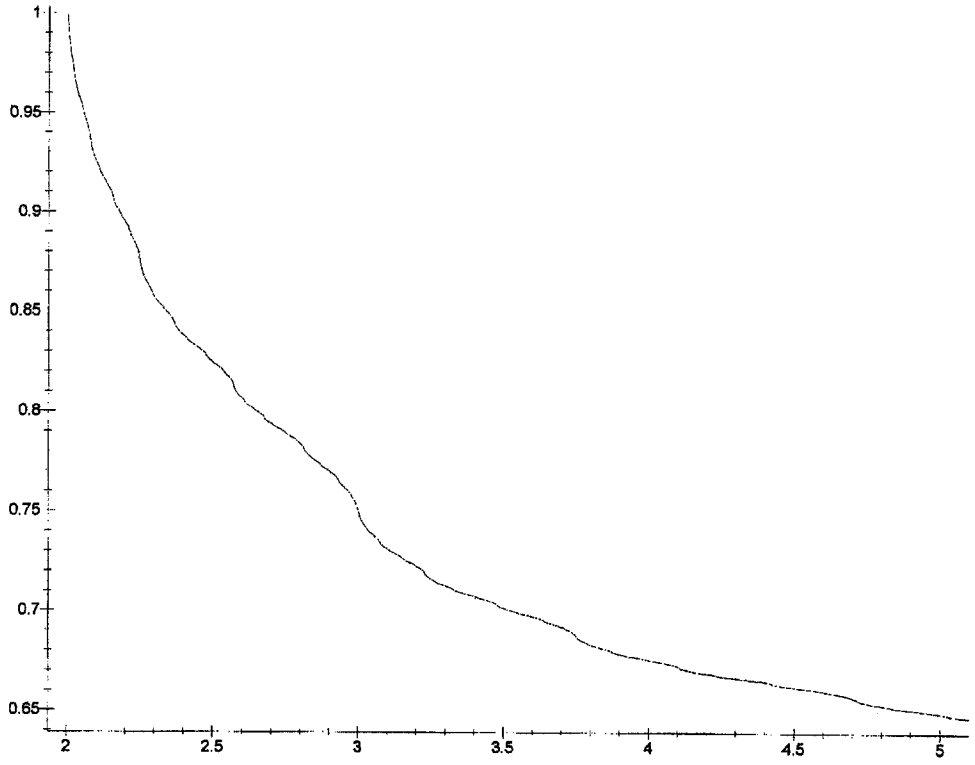

FIGURE 26 A portion of the graph of $M(a)$.

We have the analog of Theorem 1 for Dirichlet eigenfunctions and biharmonic functions (we omit the details for this case).

Theorem 3.

Let f be a Dirichlet eigenfunction on SG, $-\Delta f = \lambda f$. There exists m_0 depending on λ such that if $m \geq m_0$ and E is an edge in G_m with $f(v_0) < f(v_{01}) < f(v_1)$ and

$$\frac{1}{4-\delta_m} \leq \frac{f(v_1) - f(v_{01})}{f(v_{01}) - f(v_0)} \leq 4 - \delta_m \tag{4.5}$$

then the restriction of f to E is strictly monotone (δ_m is a constant depending on λ with $\delta_m \to 0$ as $m \to \infty$).

Proof. By (2.15) we can choose m_0 so that λ_m is close to 0 for all $m \geq m_0$. Then using Algorithm 2.5 and the remark following it, we obtain the analog of (4.2) and (4.3) with the coefficients changed slightly, say

$$f(v_{01}) - f(v_{001}) = a_m (f(v_{01}) - f(v_0)) + b_m (f(v_1) - f(v_{01})) \tag{4.6}$$

$$f(v_{001}) - f(v_0) = c_m (f(v_{01}) - f(v_0)) - b_m (f(v_1) - f(v_{01})) \tag{4.7}$$

with $a_m > \frac{8}{25}$, $b_m > \frac{3}{25}$, $c_m = 1 - a_m$. By taking m_0 large we can make a_m close to 8/25 and b_m close to 3/25. We need

$$1 - a_m - (4 - \delta_m) b_m > 0 \tag{4.8}$$

in order to show $f(v_{001}) > f(v_0)$ as before. The analog of (4.4) is

$$y = \frac{a_m + b_m x}{1 - a_m - b_m x}, \tag{4.9}$$

so we choose $4 - \delta_m$ to be the larger fixed point of the transformation (4.9). Then we can complete the induction step as before. □

Next we consider the behavior of harmonic functions in a neighborhood of a vertex. We fix a triangle T, and let R denote the reflection that has v_0 as fixed point and interchanges v_1 and v_2.

Theorem 4.

Let f be a nonconstant harmonic function on T. Then there exist positive constants c_j such that

$$|f(x) - f(v_0)| \leq c_1 |x - v_0|^\beta \tag{4.10}$$

$$|f(x) - f(Rx)| \leq c_2 |x - v_0|^\gamma \tag{4.11}$$

for all x in T, where $\beta = \frac{\log(\frac{5}{3})}{\log 2} \approx .7369655$ and $\gamma = \frac{\log 5}{\log 2} \approx 2.3219281$. Further, we have the following dichotomy: (i) either

$$f(v_1) - f(v_0) = f(v_0) - f(v_2) , \tag{4.12}$$

in which case

$$|f(x) - f(v_0)| \leq c_3 |x - v_0|^\gamma , \tag{4.13}$$

or (ii) for every other nonconstant harmonic function,

$$c_4 |x - v_0|^\beta \leq |f(x) - f(v_0)| \tag{4.14}$$

for all x sufficiently close to v_0.

Proof. Without loss of generality, we may assume $f(v_0) = 0$. Then $f(Rx)$ is also a harmonic function, so we can write f as a sum of a symmetric $\frac{1}{2}(f(x) + f(Rx))$ and an antisymmetric $\frac{1}{2}(f(x) - f(Rx))$ harmonic function. To prove the theorem it suffices to show that a nonconstant symmetric harmonic function satisfies (4.10) and (4.14), while an antisymmetric harmonic function satisfies (4.13), since $\beta < \gamma$.

Suppose f is symmetric, with $f(v_0) = 0$, $f(v_1) = f(v_2) = a \neq 0$. Then by Algorithm 2.1, we have $f(v_{01}) = f(v_{02}) = \frac{3}{5}a$, while $f(v_{12}) = \frac{4}{5}a$. By the maximum principle for harmonic functions, the values of f on the two smaller triangles at the vertices v_1 and v_2 must lie between $\frac{3}{5}a$ and $\frac{4}{5}a$, so with the appropriate choice of constants we have (4.10) and (4.14) holding on these two triangles. On the third small triangle at the vertex v_0, we again have that f is symmetric. Since we scale lengths by a factor of $1/2$ and the values of f by a factor of $3/5$, we see that (4.10) and (4.14) scale exactly to this smaller triangle, and we continue by induction to prove (4.10) and (4.14).

Suppose f is antisymmetric, with $f(v_0) = 0$, $f(v_1) = -f(v_2) = a$. Then by Algorithm 2.1 we have $f(v_{01}) = -f(v_{20}) = \frac{1}{5}a$, so now it is (4.13) that scales exactly to the small triangle at vertex v_0. The rest of the argument is the same. There is no lower bound in this case because f vanishes on the line of symmetry. □

Essentially the same result is true for Dirichlet eigenfunctions, except that we need an extra hypothesis for the lower bound (4.14).

Corollary 1.

Let f be a Dirichlet eigenfunction. Then (4.10) and (4.11) hold. If (4.12) holds, then (4.13) holds. On the other hand, if $f(v_0) = 0$ but (4.12) does not hold, then (4.14) holds.

Proof. We are no longer able to assume $f(v_0) = 0$, but we can still write f as a sum of a symmetric and an antisymmetric eigenfunction (the Dirichlet boundary conditions need not hold for these eigenfunctions, but that is irrelevant to the argument). We use Algorithm 2.4, together with the observation from (2.15) that

$$\lambda_m \approx c5^{-m} \text{ for large } m . \tag{4.15}$$

Consider first the symmetric case. If we write $f(v_1) = f(v_2) = f(v_0) + a_m$ then $f(v_{01}) = f(v_{02}) = f(v_0) + a_{m+1}$ for

$$a_{m+1} \approx c_1 \lambda_m f(v_0) + \frac{3}{5}(1 + c_2 \lambda_m) a_m . \tag{4.16}$$

Using (4.15) we obtain by induction the upper bound $a_m \leq c_3 (\frac{3}{5})^m$, and this yields (4.10) (although we do not have a strictly maximum principle for Dirichlet eigenfunctions, it follows from Algorithm 2.4 and (4.15) that $|f(x)|$ on T is bounded by a constant times the maximum of $|f(v_j)|$). Also if $f(v_0) = 0$ but $f(v_1) = f(v_2) \neq 0$, then we obtain the lower bound (4.14). On the other hand, if $f(v_0) = f(v_1) = f(v_2)$, then since the sum of the coefficients in (2.13) differs from 1 by a term of order λ_m, we obtain the estimate (4.13).

Next consider the antisymmetric case, with $f(v_0) = 0$ and $f(v_1) = -f(v_2) = a$. Then by Algorithm 2.4 we have $f(v_{01}) = -f(v_{02}) = \frac{1}{5-\lambda_m} a$, and again by induction we obtain (4.13). □

Next we consider the phenomenon of lines along which certain Dirichlet eigenfunctions are constant.

Theorem 5.

Let f be a Dirichlet eigenfunction, and let E be an edge in G_m such that $f(v_0) = f(v_1) = f(v_{01})$. Then the restriction of f to E is constant.

Proof. Algorithm 2.5 and the remark that the coefficients sum to 1 implies $f(v_{001})$ and $f(v_{011})$ are both equal to the common value. By induction it follows that f takes on the same value at all dyadic points on E. Since f is continuous, f is constant on E. □

Corollary 2.

The eigenfunctions $\psi_n^{(2)}$ are constant on the inner edges of G_1.

Proof. In order to apply the theorem we need to check that $\psi_n^{(2)}$ takes on the value 1 at the midpoints of these edges. According to Algorithm 2.4, this value is equal to

$$\frac{2(4 - \lambda_2)}{(2 - \lambda_2)(5 - \lambda_2)} .$$

However, in view of (2.12) and $\lambda_1 = 2$, this does equal 1. □

Corollary 3.

The eigenfunctions $\psi_n^{(6)}$ are constant on the edges of G_2 joining endpoints where $\psi_n^{(6)}$ is set equal to -1.

Proof. According to Algorithm 2.4, the value at the midpoint of one of these edges is equal to

$$\frac{-2(4 - \lambda_3) + 4}{(1 - \lambda_3)(5 - \lambda_3)} = \frac{-2}{5 - \lambda_3} .$$

But we have $\varepsilon_3 = +1$ so $\lambda_3 = 3$, and so $\psi_n^{(6)}$ takes the same value -1 at the midpoint. Then we can apply the theorem. □

In the next three results, we derive specific properties of Dirichlet eigenfunctions based on our algorithms. These results actually hold more generally (Theorem 6 for all functions in the domain of Δ, and Theorem 7 and Corollary 4 for subharmonic functions) using methods in [11].

Theorem 6.

Let f be a Dirichlet eigenfunction. Then there exists m_0 such that if $m \geq m_0$ and T is any minimal triangle in G_m, then

$$|f(x) - h(x)| \leq c\lambda \|f\|_\infty 5^{-m} \quad \text{on} \quad T, \text{ with } c = 5/4\,, \tag{4.17}$$

where h is the harmonic function that is equal to f on the vertices of T.

Proof. We choose m_0 so that

$$\lambda_m < 1 \quad \text{for} \quad m \geq m_0\,. \tag{4.18}$$

Comparing Algorithms 2.1 and 2.4, we see that for $\lambda_m < 1$ the coefficients differ in L^1 norm by at most λ_m, and so (4.17) holds at the midpoints of the edges of T. At the next level, the left side of (4.17) can be bounded by a sum of two terms: the error $\|f\|_\infty \lambda_m$ from level m and the error $\|f\|_\infty \lambda_{m+1}$ from level $m+1$. Since $\lambda_m \leq 5^{-m}\lambda$ for all m, these errors form a convergent geometric series. The result follows by induction and a density argument. □

Since the size of T in G_m is on the order of 2^{-m}, the estimate (4.17) is very strong.

Theorem 7.

Let f be a Dirichlet eigenfunction with λ given by (2.11) with $\varepsilon_m = -1$ for all $m \geq k$. Let T be any minimal triangle in G_{m_0} with $m_0 \geq k$ with f taking on nonnegative values on the vertices v_0, v_1, v_2 of T. Then

$$f(x) \geq \min\left(f(v_0), f(v_1), f(v_2)\right) \quad \text{for} \quad x \quad \text{in} \quad T\,, \tag{4.19}$$

with strictly inequality unless x is a vertex or f is identically zero on T.

Proof. The condition that $\varepsilon_m = -1$ for $m \geq k$ implies that $\lambda_m < 2$, in fact $\lambda_m \leq \frac{1}{2}(5 - \sqrt{5}) \approx 1.381966$ for $m \geq k$. Now in Algorithm 2.4 the coefficients of (2.13) are positive and sum to $\frac{2}{2-\lambda_m}$, which is greater than 1. Thus, (4.19) holds at the points of the edges of T, in fact with strict inequality unless $f(v_0) = f(v_1) = f(v_2) = 0$. We may then use an induction argument to show that (4.19) holds at all vertices of any $G_{m'}$ for $m' > m_0$ that lie in T. By density this proves (4.19) for any point in T, and it is routine to see that strict inequality holds except in trivial cases. □

Corollary 4.

A Dirichlet eigenfunction cannot have a local minimum at a point where it is positive.

Proof. Suppose first that the point x where f has a local minimum is not a vertex in any G_m. If $f(x) > 0$ then by continuity we can find an infinite sequence of triangles T_j containing x and shrinking to x on which f is positive. The theorem then shows that $f(x)$ cannot be the minimum value of f in T_j. On the other hand, if x is a vertex in G_k, hence in G_m for all $m \geq k$, we can argue directly from the eigenvalue equation (2.14) that $f(x)$ is strictly greater than the average of 4 neighboring values, hence cannot be a local minimum. □

In particular, these results hold for the ground state $\psi_0^{(2)}$, since this function is nonnegative. We can actually say more about it. First we need a computation that is valid for all the $\psi_n^{(2)}$ eigenfunctions.

Lemma 1.

Let x parametrize an edge of G_0, with $x = 0, 1$ corresponding to the endpoints and $x = 1/2$ the midpoint. Then

$$\psi_n^{(2)}\left(\frac{1}{2} \pm \frac{1}{2^m}\right) = 1 - \frac{\lambda_m}{2}\,, \tag{4.20}$$

where λ_m are given by (2.11) and ε_m are determined from n by (3.1) and (3.2).

Proof. Since $\lambda_1 = 2$ we see that (4.20) is consistent with $\psi_n^{(2)}(0) = \psi_n^{(2)}(1) = 0$. We prove the result by induction. By Corollary 2, we have the point corresponding to $\frac{1}{2} \pm \frac{1}{2^{m+1}}$ as the midpoint of a minimal triangle T in G_m with $\psi_n^{(2)}$ equal to 1 at 2 vertices of T, and $1 - \frac{\lambda_m}{2}$ at the third vertex by the induction hypothesis. Thus, Algorithm 2.4 gives us

$$f\left(\frac{1}{2} \pm \frac{1}{2^{m+1}}\right) = \frac{(4 - \lambda_{m+1})\left(2 - \frac{\lambda_m}{2}\right) + 2}{(2 - \lambda_{m+1})(5 - \lambda_{m+1})} .$$

Note that the numerator is equal to $2(5 - \lambda_{m+1}) - (4 - \lambda_{m+1})\frac{\lambda_m}{2}$, and if we substitute (2.12) to eliminate λ_m this becomes

$$(5 - \lambda_{m+1})\left(2 - (4 - \lambda_{m+1})\frac{\lambda_{m+1}}{2}\right) = (5 - \lambda_{m+1})(2 - \lambda_{m+1})\left(1 - \frac{\lambda_{m+1}}{2}\right) . \qquad \square$$

Theorem 8.

The groundstate $\psi_0^{(2)}$ satisfies

$$0 \le \psi_0^{(2)}(x) \le 1 , \tag{4.22}$$

attaining the minimum value 0 exactly at the 3 boundary points, and the maximum value 1 exactly along the 3 inner edges of G_1. Furthermore, it is increasing along the other edges of G_1 (joining a boundary point to a midpoint of an edge of G_0).

Proof. For the groundstate we have $\lambda_m < 2$ for $m \ge 2$, so all the coefficients in (2.13) are positive. It follows easily that $\psi_0^{(2)}$ is positive except at the boundary points (nonnegativity is of course a generic property of goundstates). To prove the upper bound we prove by induction that $\psi_0^{(2)}$ does not attain its maximum value on any minimal triangle T in G_m except one that borders on one of the three edges where $\psi_0^{(2)}$ is identically 1. The reason is that for each point x in T there are positive coefficients $a_0(x)$, $a_1(x)$, $a_2(x)$ such that

$$\psi_0^{(2)}(x) = a_0(x)\psi_0^{(2)}(v_0) + a_1(x)\psi_0^{(2)}(v_1) + a_2(x)\psi_0^{(2)}(v_2) ,$$

and these coefficients are the same for corresponding points x in all the minimal triangles in G_m (Algorithm 2.4 gives the coefficients explicitly for the midpoints of the edges of T). So if $\psi_0^{(2)}$ is larger at the vertices of one triangle T' as opposed to another T'', then $\psi_0^{(2)}(x') > \psi_0^{(2)}(x'')$ for corresponding points x' and x'' in T' and T''. In particular, $\psi_0^{(2)}$ cannot achieve its maximum on T''. Now in G_2 there are two types of minimal triangles, six inner triangles where $\psi_0^{(2)}$ takes values 1, 1, $1 - \frac{\lambda_2}{2}$ on the vertices, and three outer triangles where the corresponding values are $1 - \frac{\lambda_2}{2}$, $1 - \frac{\lambda_2}{2}$, 0. This eliminates the outer triangles. In the induction step we need to compare minimal triangles where the vertex values for $\psi_0^{(2)}$ are 1, 1, $1 - \frac{\lambda_{m+1}}{2}$ for the inner one and $1 - \frac{\lambda_{m+1}}{2}$, $1 - \frac{\lambda_{m+1}}{2}$, $1 - \frac{\lambda_m}{2}$ for the outer (see Fig. 27). Since λ_m is decreasing in m for the groundstate, we can eliminate the outer triangles.

To show that $\psi_0^{(2)}$ is increasing along the outer edges of G_1 we could in principle invoke Theorem 3, but the details are rather delicate, so instead we give a direct argument. We need one additional observation: we can compare the values of $\psi_0^{(2)}$ at corresponding points of triangles of different sizes, as long as the larger vertex values are taken on the larger triangle. The reason is that the coefficients in (2.13) decrease with λ_m, and λ_m decreases with m, so the larger triangle (smaller m) has larger coefficients. So, for example, since

$$\psi_0^{(2)}\left(\frac{1}{2}\right) = 1 > \psi_0^{(2)}\left(\frac{3}{8}\right) = 1 - \frac{\lambda_3}{2} > \psi_0^{(2)}\left(\frac{1}{4}\right) = 1 - \frac{\lambda_2}{2} > \psi_0^{(2)}(0) = 0$$

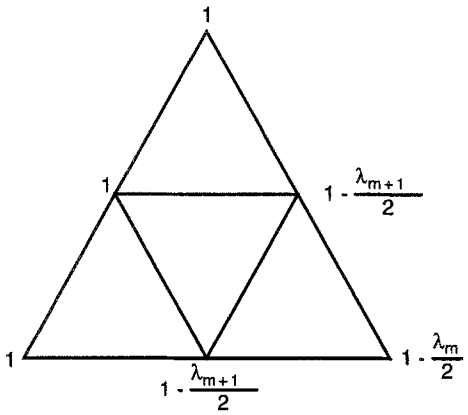

FIGURE 27 Groundstate values on a minimal triangle in G_{m-1} bordering on the edge where it is identically 1.

we can now conclude that

$$\psi_0^{(2)}\left(\frac{1}{4}\right) > \psi_0^{(2)}\left(\frac{1}{8}\right)$$

(using the notation in Lemma 1) by comparing the G_1 triangle in Fig. 28 with the G_2 triangle in the lower right. An induction argument based on these types of comparisons shows that $\psi_0^{(2)}$ is increasing on dyadic points, and hence by continuity that it is increasing along the whole edge. □

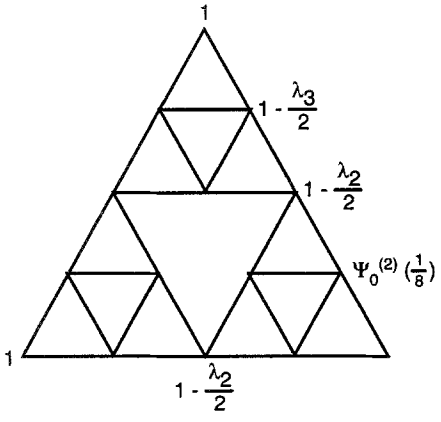

FIGURE 28 Groundstate values on a minimal triangle in G_1.

It seems likely that $\psi_0^{(2)}$ is increasing along every edge that is in the direction joining the vertex to a midpoint in the G_1 minimal triangle containing that edge. This is supported by the numerical results, and can probably be established by a similar argument. The numerical evidence suggests that on lines parallel to the inner edge on which $\psi_0^{(2)}$ is constant, there is a single minimum, and $\psi_0^{(2)}$ assumes its maximum on the endpoint closest to the outer edge. It is not clear exactly where the minimum lies, or how one could prove this.

We turn next to a description of a basis for the space of Dirichlet eigenfunctions. Since Fukushima and Shima [8] have computed all the eigenvalues with their multiplicities, it suffices to construct a linearly independent set of eigenfunctions of the correct size for each eigenvalue. Let $\lambda_n^{(2)}$, $\lambda_n^{(5)}$, and $\lambda_n^{(6)}$ denote the eigenvalues associated with the three families of eigenfunctions described

in Section 3. Then [8] shows that the spectrum consists of all $\lambda_n^{(2)}$ with multiplicity 1, all $5^k\lambda_n^{(5)}$ with multiplicity

$$b_k = \frac{1}{2}\left(3^k + 3\right)$$

for $k = 0, 1, 2, \ldots$, and all $5^k\lambda_n^{(6)}$ with multiplicity

$$a_k = \frac{1}{2}\left(3^{k+2} - 3\right)$$

for $k = 0, 1, 2, \ldots$ and n odd. Clearly, the eigenfunctions $\psi_n^{(2)}$ account for the simple eigenvalues $\lambda_n^{(2)}$. Also, the eigenfunctions $\psi_n^{(5)}$ and their rotations account for the multiplicity $b_0 = 2$ eigenvalues $\lambda_n^{(5)}$.

We now show how to construct the $5^k\lambda_n^{(5)}$ eigenspace by chaining together scaled-down copies of $\psi_n^{(5)}$. Let $T_1, \ldots, T_N$ be a sequence of distinct minimal triangles in G_k such that T_1 and T_N have a boundary point vertex, and each consecutive pair of triangles has a vertex in common. We call this sequence a *chain* of level k. To each such chain we associate an eigenfunction with eigenvalue $5^k\lambda_n^{(5)}$ by placing a scaled-down and rotated copy of $\psi_n^{(5)}$ in each triangle, aligned according to the rule that each vertex should have total charge zero, where we assign a charge of 0, $+1$, and -1 to the vertices of each triangle equal to the sum of the values of the eigenfunction at the two neighboring midpoints. The eigenfunction so constructed is supported in the union of the triangles in the chain, and satisfies both $\Delta f = 0$ and $f = 0$ at all the vertices of the triangles in the chain because of the total charge zero alignment. An example of a chain of level 1 with $N = 3$ and the (non-zero) values of the eigenfunction at all vertices of G_2 is shown in Fig. 29. It is easy to see that we have an eigenfunction since the eigenvalue equation holds in the interior of each triangle in the chain because each contraction multiplies the eigenvalue by 5, and it holds by default (both sides are 0) at the vertices and in all other triangles.

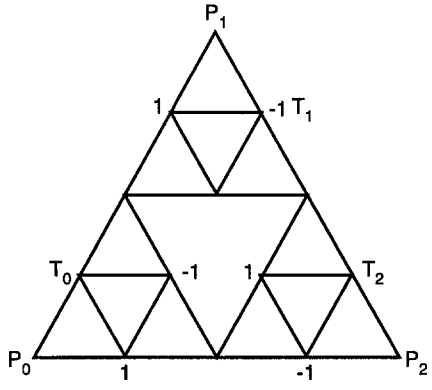

FIGURE 29 The values on G_2 of an eigenfunction obtained from a chain of level 1 with $N = 3$.

We now describe an inductive procedure for obtaining b_k chains of level k. When $k = 1, b_1 = 3$. We take the chains (T_0, T_1), (T_0, T_2), and (T_0, T_1, T_2) for the triangles marked in Fig. 29, we call them the *high road*, the *low road*, and the *middle road* of level 1. Note that $b_{k+1} = 3(b_k - 2) + 3$. For the induction step we create a high road, a low road and a middle road of level $k + 1$ in the obvious way:

i) For the high road we take two scaled copies of the high road at level k in triangles T_0 and T_1.

ii) For the low road we take two scaled copies of the low road of level k in triangles T_0 and T_2.

iii) For the middle road we take a scaled copy of the high road of level k in T_0, a scaled copy of the low road of level k in T_1, and a scaled and rotated (so it goes down) copy of the high road of level k in T_2.

In addition, for each chain of level k that is not the high road or the low road (note that this includes the middle road), we create three offspring chains as follows:

iv) Take a scaled copy of the chain in T_0 and a scaled copy of the low road of level k in T_2.

v) Take a scaled copy of the low road of level k in T_0 and a scaled copy of the chain in T_2.

vi) Take a scaled copy of the high road of level k in T_0, a scaled copy of the chain in T_1, and a scaled and rotated (so it goes down) copy of the high road of level k at T_2.

Note that an easy induction argument shows that all the offspring chains are indeed chains and join p_0 to p_2, as is true of the middle road and the low road. Only the high road joins p_0 to p_1. Note that our induction step creates $3 + 3(b_k - 2) = b_{k+1}$ chains, as required. As an example, referring to Fig. 30 for notation, the level 2 chains are the following:

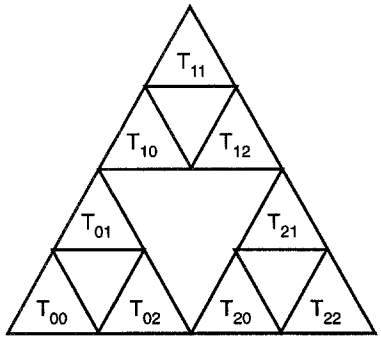

FIGURE 30 The minimal triangles in G_2.

i) $T_{00}, T_{01}, T_{10}, T_{11}$ (high road)
ii) $T_{00}, T_{02}, T_{20}, T_{22}$ (low road)
iii) $T_{00}, T_{01}, T_{10}, T_{12}, T_{21}, T_{22}$ (middle road)
iv) $T_{00}, T_{01}, T_{02}, T_{20}, T_{22}$
v) $T_{00}, T_{02}, T_{20}, T_{21}, T_{22}$
vi) $T_{00}, T_{01}, T_{10}, T_{11}, T_{12}, T_{21}, T_{22}$

(The last three are the offsprings of the middle road T_0, T_1, T_2 of level 1.)

Theorem 9.

The b_k eigenfunctions obtained by chaining scaled-down copies of $\psi_n^{(5)}$ for each of the level k chains constructed in i) through vi) above are linearly independent; hence, they span the $5^k\lambda^{(5)}$ eigenspace.

Proof. We prove this by induction. The case $k = 1$ is straightforward since the high road, low road, and middle road eigenvectors are already linearly independent when restricted to the vertices of G_2. For the inductive step, assume the result is true at level k and consider any linear combination of the b_{k+1} eigenvectors associated with the chains of level $k + 1$. If this vanishes, we must show all the coefficients vanish. First we restrict attention to the triangle T_1. The only chains that pass through T_1 are the high road, the middle road, and the offsprings of type vi). The restrictions to T_1 of these b_k chains give us exactly a scaled version of all the b_k chains of level k (the high road of level $k + 1$ gives the high road of level k, while the middle road of level $k + 1$ gives the low road of level k). By the induction argument these are linearly independent, so their coefficients vanish.

Next we restrict attention to T_0. The low road of level $k + 1$ and all the offsprings of type v) restricted to T_0 are equal to a scaled copy of the low road of level k. By the induction hypothesis all

the coefficients of the offsprings of type iv) vanish.

Finally, we are left with a linear combination of the low road and offsprings of type v). The restriction of these to T_2 and the induction hypothesis kills all the remaining coefficients. □

Remark 3. A different construction of a basis for the $\lambda_n^{(5)}$ eigenfunctions has been given by Kigami [10]. It has the advantage that some of the basic functions are localized. It is also based on chaining scaled copies of $\psi_n^{(5)}$, but with the chains forming loops around the perimeters of triangles. All but two of the basis functions are pre-localized in the sense of [2].

To complete the eigenfunction story, we show how to construct a basis for the $5^k\lambda_n^{(6)}$ eigenspace out of scaled-down and rotated copies of $\psi_n^{(6)}$. Let T_1, T_2 be any pair of adjacent minimal triangles in G_{k+1} (note that we do not require that they both belong to the same minimal triangle in G_k). Note that $\psi_n^{(6)}$ is supported in two of the three minimal triangles in G_1. By scaling and rotating $\psi_n^{(6)}$ we can map these two triangles to the pair T_1, T_2, and this is the localized eigenfunction supported on the pair of triangles. Because $\psi_n^{(6)}$ vanishes on all vertices, except the common vertex, of the two minimal G_1 triangles and is antisymmetric at these vertices, the localized eigenfunction satisfies the eigenvalue equation by default at all the vertices, except the common vertex of T_1 and T_2. The existence of these localized eigenfunctions is already pointed out in [8].

There are 3^{k+1} minimal triangles in G_{k+1}, and each one, with the exception of the three corners, is adjacent to three other triangles. The corner triangles are adjoint to two others. Thus, there are exactly $\frac{1}{2}(3^{k+2} - 3) = a_k$ pairs. It remains to see that they are linearly independent. But this is trivial, since on the common vertex of the two triangles T_1, T_2, only the eigenfunction associated with this pair is nonzero.

They are not orthogonal, however. Consider the eigenfunctions supported on pairs with one triangle T in common. On T the two functions are shown in Fig. 31.

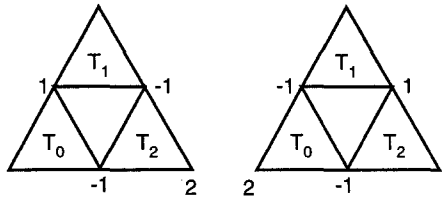

FIGURE 31 The values of two different localized $\psi_n^{(6)}$ eigenfunctions on a triangle where they overlap.

The inner product on T_0 and T_2 must vanish because we have the product of an odd and an even function. However, on T_1 the two functions are identical up to the constant factor -1, so the inner product is strictly negative.

Finally, we discuss the case of continuous eigenfunctions, solutions of $-\Delta f = \lambda f$ for λ any real or complex value, that are continuous up to the boundary. We will show that Algorithm 2.4 actually constructs a three-dimensional space of eigenfunctions, hence, all of them, in the case that λ is not a Dirichlet eigenvalue, starting from any given boundary conditions. In the case of a Dirichlet eigenvalue, if we let $m(\lambda)$ denote its multiplicity, the space of all solutions may have dimension up to $3 + m(\lambda)$. We will see that Algorithm 2.4 will also construct the extra solutions in all cases.

Given any complex value λ, there exists a unique sequence λ_m, and $\varepsilon_m = \pm 1$ with all but a finite number equal to -1, such that (2.11), (2.12), and (2.15) hold. Indeed, we consider the function $\Phi(z) = \lim_{n\to\infty} \varphi_n(5^{-n}z)$ where $\varphi_n(z)$ denotes the n-fold iterate of the polynomial $\varphi_1(z) = z(5-z)$. The existence of the limit follows from Koenigs' Linearization Theorem (see [18, p. 37]) and depends

only on the fact that φ_1 is entire and $\varphi_1'(0) = 5$. The theorem also gives $\Phi'(0) = 1$. Now set

$$\lambda_k = \Phi\left(5^{-k}\lambda\right) .$$

Then (2.15) follows from the fact that $\Phi'(0) = 0$, and (2.12) follows easily from the definition. Solving (2.12) yields (2.11) for $\varepsilon_m = \pm 1$ uniquely determined except when $\lambda_{m-1} = 25/4$. But the requirement that $5^m\lambda_m$ remains bounded requires that all but a finite number of choices must be $\varepsilon_m = -1$.

We say λ is *generic* if no λ_m equals 2 or 5. It is easy to see that the only nongeneric λs are of the form $5^k\lambda_n^{(2)}$ and $5^k\lambda_n^{(5)}$.

Theorem 10.

If λ is generic, then Algorithm 2.4 starting with $m = 1$ constructs a solution to $-\Delta f = \lambda f$ with any given boundary conditions $f(p_j) = c_j$.

Proof. Since we never encounter $\lambda_m = 2, 5$, we can use Algorithm 2.4 starting with $m = 1$ to produce a function on $\bigcup_{m=1}^{\infty} V_m$. Because $\lambda_m \to 0$ it is easy to see that this function is continuous, and hence, extends to a continuous function on SG. Since $-\Delta_m f = \lambda_m f$ on V_m and (2.15) holds we obtain $-\Delta f = \lambda f$ in the limit on all points in $\bigcup_{m=1}^{\infty} V_m$. Since both f and λf are continuous, this is the definition of $-\Delta f = \lambda f$ on SG. □

The generic case includes the Dirichlet eigenvalues $5^k\lambda_n^{(6)}$, where Theorem 10 constructs a three-dimensional space of eigenfunctions linearly independent from the Dirichlet eigenfunctions (constructed by Algorithm 2.4 but starting with $m = k + 2$, not $m = 1$). In the other cases of generic eigenvalues, which are not Dirichlet eigenvalues, the three-dimensional space constructed in the theorem gives all continuous eigenfunctions.

What happens in the nongeneric case, which includes the values $5^k\lambda_n^{(2)}$ for $k \geq 1$ that are not Dirichlet eigenfunctions? First consider the case $\lambda = \lambda_n^{(2)}$. Then the function shown in Fig. 32 is seen to satisfy $-\Delta_1 f = 2f$ on G_1, and then Algorithm 2.4 for $m \geq 2$ extends this to an eigenfunction. Together with its rotation, we obtain a two-dimensional eigenspace that is linearly independent of the Dirichlet eigenfunction for this eigenvalue. Note that all eigenfunctions constructed for these eigenvalues satisfy

$$f(p_0) + f(p_1) + f(p_2) = 0 , \tag{4.23}$$

and (4.23) is a consequence of $-\Delta_1 f = 2f$ on G_1. If we knew that all continuous eigenfunctions on SG for these eigenvalues satisfied (4.23), then we would have constructed all of them.

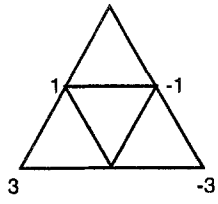

FIGURE 32 Another eigenfunction on G_1 with eigenvalues $\lambda_1 = 2$.

Next consider the case $\lambda = 5^k\lambda_n^{(2)}$ for $k \geq 1$. These are not Dirichlet eigenvalues, so it suffices to construct a solution for arbitrary boundary conditions. Algorithm 2.4 will take over for $m \geq k+2$ if we can find a solution of $-\Delta_{k+1} f = 2f$ on G_{k+1}. A solution for $k = 1$ is shown in Fig. 33, and under rotation this generates the desired space of solutions. Similarly, for $k > 1$, we can find analogous solutions. (The eigenvalue equation imposes $N - 3$ homogeneous linear conditions on

the N-dimensional space of functions on V_{k+1}, for $N = \#(V_k)$. So linear algebra guarantees a three-dimensional space of solutions.)

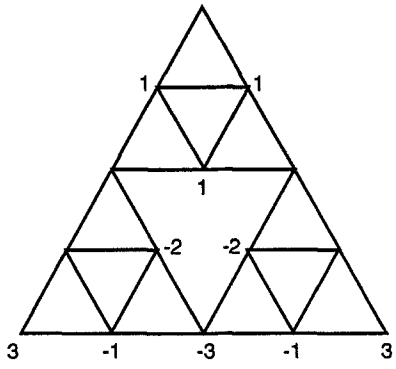

FIGURE 33 Another eigenfunction on G_2 with eigenvalue $\lambda_2 = 2$.

Finally, consider the case $\lambda = 5^k \lambda_n^{(5)}$. Here we need to find solutions of $-\Delta_{k+1} f = 5f$ on G_{k+1}. There are already b_k linearly independent solutions given by Theorem 9. We can find one more, namely the one shown in Fig. 34 when $k = 0$, and the same solution in each minimal G_k triangle when $k \geq 1$. Note that all solutions constructed satisfy

$$f(p_0) = f(p_1) = f(p_3) , \tag{4.24}$$

and (4.24) is indeed a consequence of $-\Delta_{k+1} f = 5f$ on G_{k+1}.

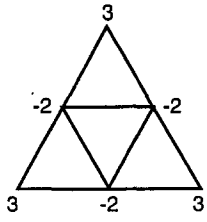

FIGURE 34 Another eigenfunction on G_1 with eigenvalue $\lambda_1 = 5$.

Conjecture 1.

Any solution of $-\Delta f = \lambda_n^{(2)} f$ on SG continuous up to the boundary satisfies (4.23), and any solution of $-\Delta f = 5^k \lambda_n^{(5)} f$ on SG continuous up to the boundary satisfies (4.24).

This conjecture was recently proved by Kigami [10].

Corollary 5.

Any solution of $-\Delta f = \lambda f$ on SG continuous up to the boundary for $\lambda \neq \lambda_n^{(2)}$, $5^k \lambda_n^{(5)}$ is constructed by Algorithm 2.4 starting with $m = m_0$ for some m_0. In particular, Theorems 3, 5, 6, and 7 and Corollaries 1, and 4 hold. Furthermore, the dimension of the spaces of solutions is $m(\lambda)+3$, where $m(\lambda)$ is the multiplicity of the Dirichlet eigenvalue λ ($m(\lambda) = 0$ if it is not a Dirichlet eigenvalue). Essentially the same is true for the exceptional values, except now the dimension is $m(\lambda) + 2 = 3$ for $\lambda = \lambda_n^{(2)}$, and $m(\lambda) + 1 = b_k + 1$ for $\lambda = 5^k \lambda_n^{(5)}$.

If we drop the requirement that the eigenfunction be continuous up to the boundary, then we

add (generically) another three dimensions to the space of solutions. For simplicity we discuss only the case of harmonic functions. Figure 35 shows a function that is harmonic on SG with a singularity at a single vertex (it is skew-symmetric about the axis through this vertex). By taking rotations of this example, together with the continuous harmonic functions, we obtain a six-dimensional space of harmonic functions on SG. On the other hand, it is easy to see that the dimension is at most 6, so we have constructed them all. (The idea of the proof is that the function is uniquely determined by its values at the six vertices shown in Fig. 36. These values easily determine the values at the other six nonboundary vertices of G_2, hence, the values in the shaded region in Fig. 36 by using Algorithm 2.1 on each of the six triangles. To show that there is a unique harmonic continuation into the remaining triangles, it is convenient to consider separately the symmetric and skew-symmetric harmonic functions with respect to one axis; the argument is outlined in Fig. 37.)

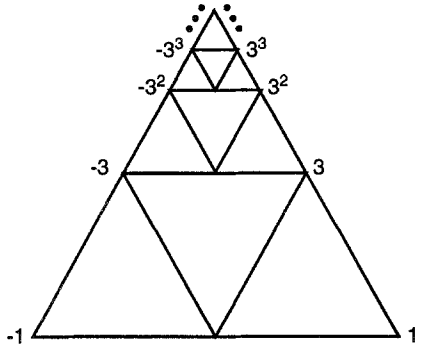

FIGURE 35 A function harmonic in the interior of SG with a singularity at the top vertex. This function is skew-symmetric about the vertical axis and grows by a factor of 3 as you move up the ladder of triangles toward the upper vertex.

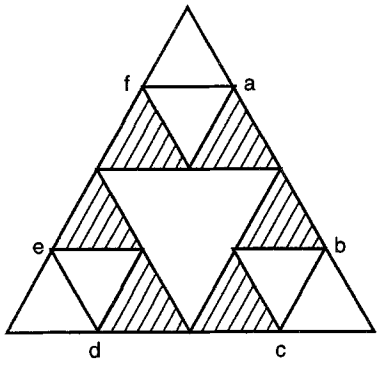

FIGURE 36 Six vertices in G_2. Any harmonic function is uniquely determined by its values at these points.

It is interesting to observe that the singular harmonic function in Fig. 35 just fails to be integrable, since the function grows by a factor of 3 and the measure shrinks by a factor of 1/3 as we move up the infinite sequence of triangles toward the vertex. This yields a cheap analog of Fatou's theorem: an integrable harmonic function has boundary values (since the boundary is just 3 points, we drop the "almost everywhere"). The same is true for positive harmonic functions.

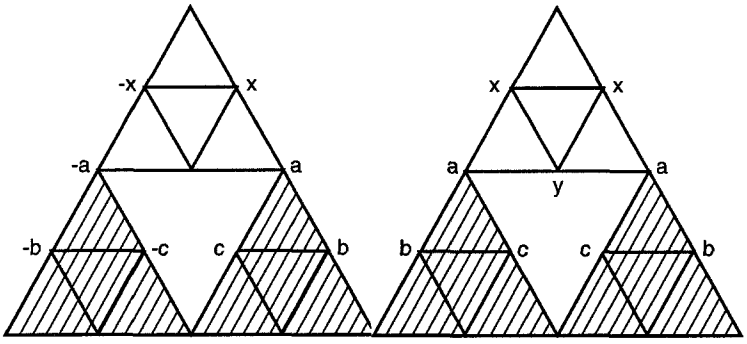

FIGURE 37 To extend a function harmonic in the shaded area, assumed either skew-symmetric or symmetric, to the next level, it suffices to compute the value of x (and y in the symmetric case). In the skew-symmetric case, $4a = x + b + c$ determines x. In the symmetric case, $4a = x + y + c + b$ and $4y = 2a + 2x$ determines x and y. The extension continues by induction.

5. Heat and Wave Equations

In this section $u(x, t)$ will denote a function defined for $x \in SG$ and $t \in \mathbb{R}$ (or $t \geq 0$). The heat equation is

$$\frac{\partial u}{\partial t} = \Delta_x u \,, \tag{5.1}$$

and the wave equation is

$$\frac{\partial^2 u}{\partial t^2} = \Delta_x u \,. \tag{5.2}$$

We will impose Dirichlet boundary conditions

$$u\left(p_j, t\right) = 0, \quad j = 0, 1, 2 \,, \tag{5.3}$$

and initial conditions

$$u(x, 0) = f(x) \tag{5.4}$$

for the heat equation, and

$$u(x, 0) = f(x), \quad \frac{\partial u}{\partial t}(x, 0) = g(x) \tag{5.5}$$

for the wave equation. For the heat equation we require $t \geq 0$, and define the *heat kernel* $H(t, x, y)$ to be the solution of (5.1), (5.3), and (5.4) with f equal to the δ-measure at the point y. It is known that $H(t, x, y)$ exists and is continuous for $t > 0$, and the unique solution of (5.1), (5.3), (5.4) for continuous f vanishing at the boundary is given by

$$u(x, t) = \int_{SG} H(t, x, y) f(y) d\mu(y) \,. \tag{5.6}$$

(Here μ is the Hausdorff measure of dimension $\alpha = \log 3 / \log 2$ on SG normalized to have total mass 1.) The analogous object for the wave equation is the *wave propagator* $P(t, x, y)$ defined to be the solution to (5.2), (5.3), and (5.5) for $f = 0$ and g equal to the δ-measure at the point y. We will see that $P(t, x, y)$ exists at least as an L^2 function of x, y for each t. At least formally, the solution to (5.2), (5.3), and (5.5) should be

$$u(x, t) = \int_{SG} P(t, x, y) g(y) d\mu(y) + \frac{\partial}{\partial t} \int_{SG} P(t, x, y) f(y) d\mu(y) \,. \tag{5.7}$$

[Similarly, Duhamel's formula would allow an inhomogeneous term $F(x, t)$ on the right side of (5.2) and an additional term

$$\int_0^t \int_{SG} P(t-s, x, y)F(y, s)d\mu(y)ds \tag{5.8}$$

on the right side of (5.7).] The exact meaning of these expressions awaits further development of the subject. In particular, we point out that at present there is no theory of distributions on SG.

The simplest way to get a formula for the heat kernel and the wave propagator is to use the Fourier sine series analogs discussed earlier. To simplify notation we denote by $\varphi_1, \varphi_2, \ldots$ an orthonormal basis of Dirichlet eigenfunctions with eigenvalues $\lambda_1, \lambda_2, \ldots$. Then

$$H(t, x, y) = \sum_{j=1}^{\infty} e^{-\lambda_j t}\varphi_j(x)\varphi_j(y) \tag{5.9}$$

and

$$P(t, x, y) = \sum_{j=1}^{\infty} \frac{\sin\sqrt{\lambda_j}t}{\sqrt{\lambda_j}}\varphi_j(x)\varphi_j(y)\,. \tag{5.10}$$

Since it is known [8] that

$$\lambda_j = O\left(j^{\beta}\right) \quad \text{for} \quad \beta = \log 5/\log 3 \approx 1.4649735 \tag{5.11}$$

the series both converge in L^2 norm. The crucial fact that gives the convergence in (5.10) is $\beta > 1$, and this is in fact true for all Laplacians on p.c.f. fractals [14]. This is equivalent to the condition that the spectral dimension ($= 2/\beta \approx 1.3652124$) is less than 2. In some ways, the propagation of waves on SG is closer to the situation for strings than for membranes or regions in higher dimensional Euclidean spaces.

For numerical purposes, the expansions (5.9) and (5.10) are useless. The number of terms that would be required for minimal accuracy would be quite large, even if one could solve the problem of getting an orthonormal basis. (It is not even clear how to compute inner products of eigenfunctions.) Instead, we use the analog of the finite difference method for partial differential equations to obtain approximate solutions. We choose a space scale by taking the graph G_m in place of SG, and approximating the solutions only for $x \in V_m$. We also choose a time scale h, and restrict t to integer multiples of h. The difference equations are then

$$u(x, (k+1)h) - u(x, kh) = h5^m \left(\left(\sum_{(x,y)\in E_m} u(y, kh)\right) - 4u(x, kh)\right) \tag{5.12}$$

for the heat equation, and

$$\begin{aligned} &u(x, (k+2)h) - 2u(x, (k+1)h) + u(x, kh) \\ &\quad = h^2 5^m \left(\left(\sum_{(x,y)\in E_m} u(y, kh)\right) - 4u(x, kh)\right) \end{aligned} \tag{5.13}$$

for the wave equation, where x is any vertex in V_m except the three boundary points where u is 0 by (5.3). The initial conditions for the heat equation are

$$u(x, 0) = f(x)\,, \tag{5.14}$$

and for the wave equation

$$u(x, 0) = f(x),\ u(x, h) - u(x, 0) = hg(x)\,. \tag{5.15}$$

(This enables us to solve (5.13) forward in time; a minor variation also allows the solution backward in time.) To approximate the δ-measure at a point y in V_m we take the function equal to 3^m at that point and 0 elsewhere.

An important question is what is the optimal relationship between m and h? One reasonable approach would be to choose a constant value for $h5^m$ (heat) or $h^2 5^m$ (wave). In practice, there are severe constraints on the size of m because of computation time. Our procedure was to choose values of m in-between 5 and 9 and then experiment with choices of h until there was no appreciable change in the approximation when h was reduced.

In our computations of the heat kernel and wave propagator, we chose the stimulus point y to be a midpoint of one of the edges of G_0. In Fig. 38 we show the restriction of the heat kernel to this edge for a succession of five equally spaced small times. As expected, there is a Guassian shape which spreads and flattens with time, with a peak at the point where the heat was applied. In Figs. 39 and 40 we restrict to an edge opposite the one where the heat was applied. At the early times in Fig. 39 we see the heat arriving on the left half and beginning to slowly work its way across the midpoint bottleneck. The graph increases with time. At the later times in Fig. 40 the graph has begun to decrease with time in the left half, but it is still increasing with time in the right half.

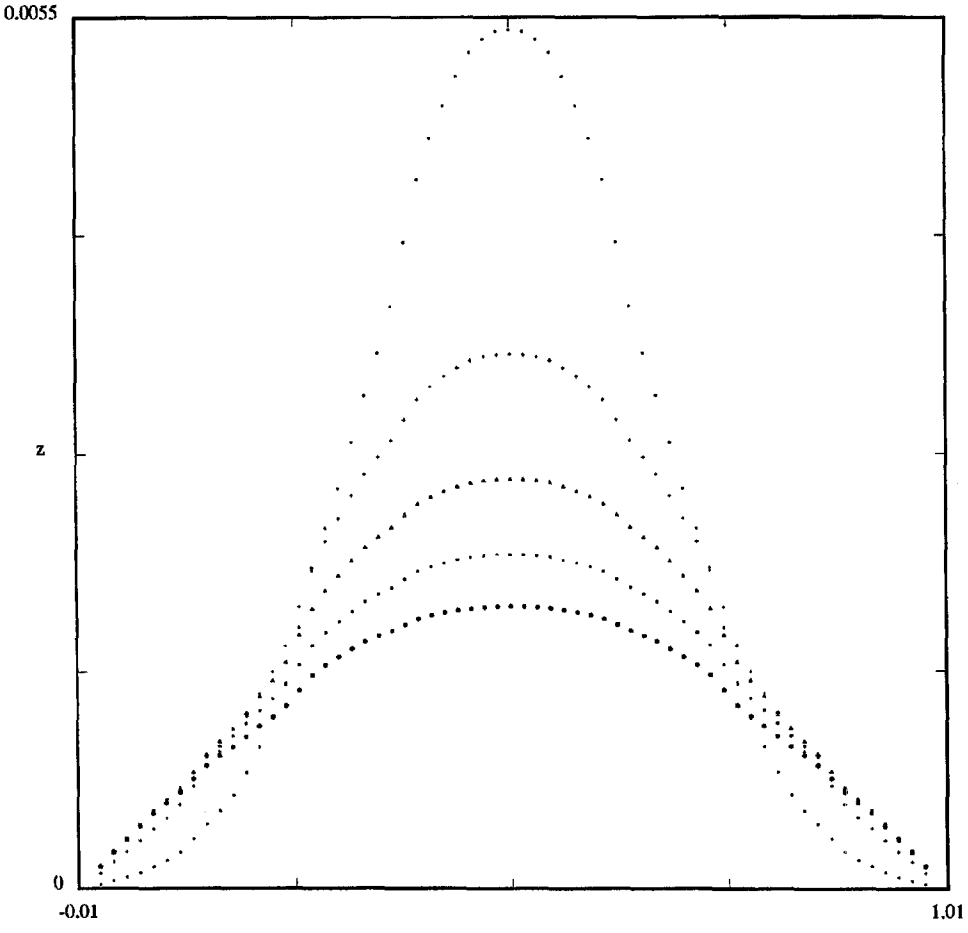

FIGURE 38 The heat kernel restricted to the edge containing the stimulus point in the middle, for times $t = .005, .01, .015, .02, .025$ (decreasing order at the midpoint).

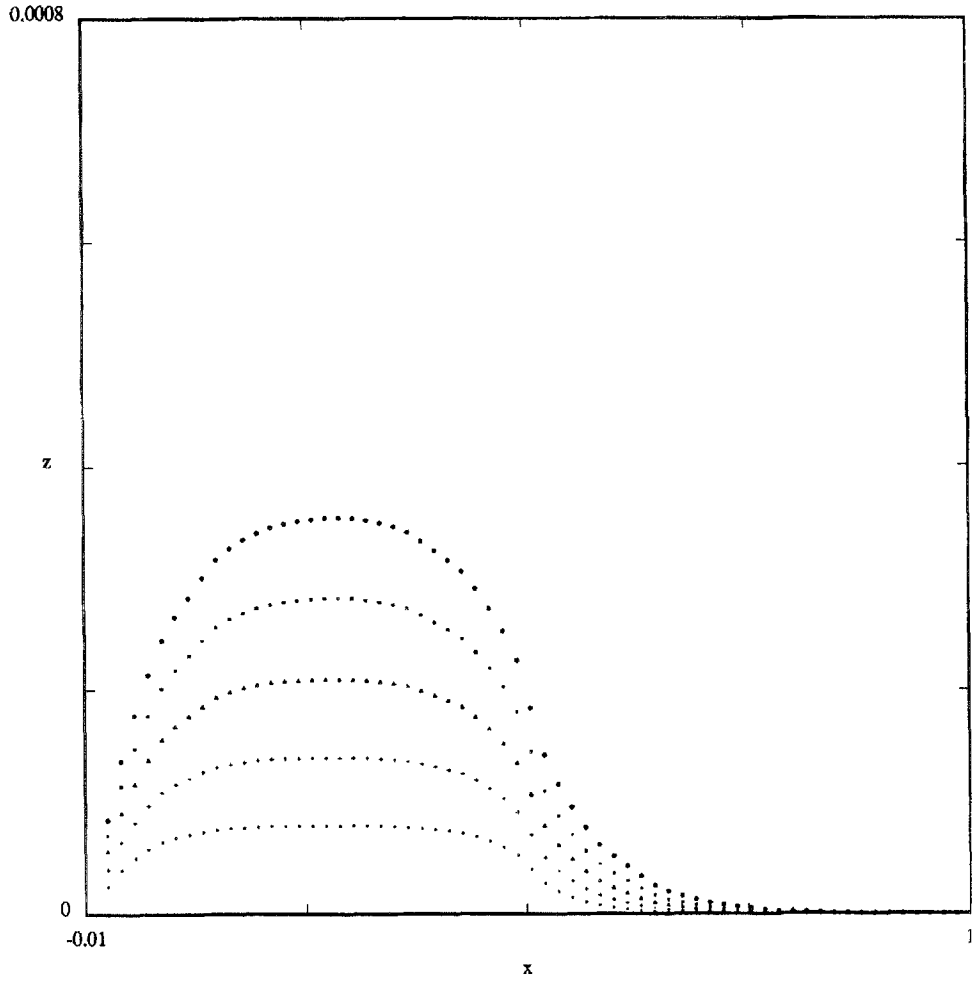

FIGURE 39 The heat kernel restricted to an edge opposite the stimulus point for times $t = .005, .006, .007, .008, .009$ (increasing order). The stimulus point is closest to the left half of the edge as shown. Note that some heat has already diffused across the midpoint bottleneck.

For the wave propagator, with stimulus at the midpoint of an edge, we restricted our computations to a minimal triangle in G_1 with one vertex at the stimulus point (the left corner in our figures). There is an obvious even symmetry about this point so the neighboring minimal triangle is just the mirror image of the one we show, and the third minimal triangle is far enough away from the stimulus point that the solution is extremely small for small times. In Fig. 41 we display the graph of our best approximation to $P(t, x, y)$ for a sequence of small times t. (We have reasons to believe that this is a rather inaccurate approximation, as will be explained below.)

We would like to compare our propagator with the analogous propagators on Euclidean space. Since SG is compact, it must be compared with a string or membrane with boundary. However, if we stay away from the boundary and take a small enough time, then the boundary effects are zero, and we can use the $\mathbb{R}^n$ propagator. For $n = 1$ and 2, with $y = 0$, these are

$$\frac{1}{2}\chi\,(|x| \leq |t|) \tag{5.16}$$

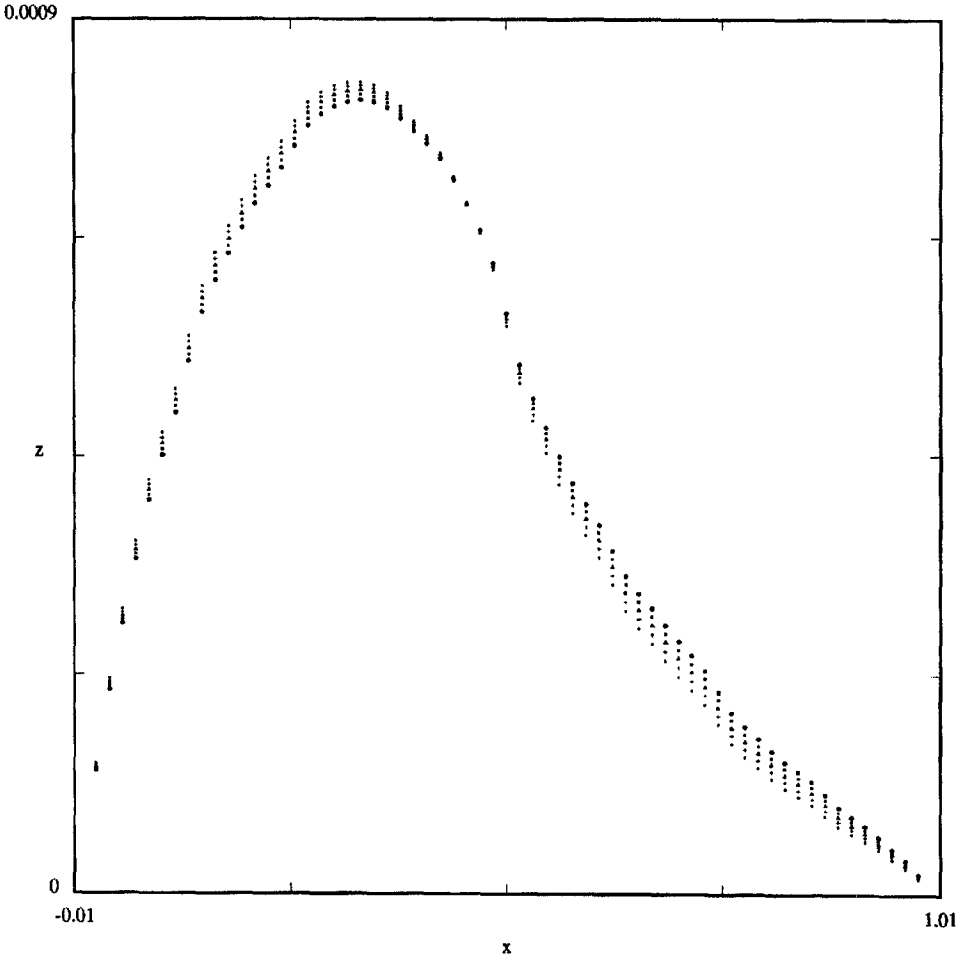

FIGURE 40 The heat kernel restricted to the same edge as in Fig. 39, for times $t = .03, .031, .032, .033, .034$. Note that the values are now decreasing on the left side, but are still increasing on the right side.

and

$$ct^{-1}\left(1-\frac{|x|^2}{t^2}\right)_+^{-1/2} = c\left(t^2-|x|^2\right)_+^{-1/2}. \tag{5.17}$$

By coincidence, these are nonnegative functions (no longer true in $\mathbb{R}^n$ for $n \geq 3$), but our data indicate that this is not the case on SG. The propagators (5.16) and (5.17) reveal the hyperbolicity of the wave equation in two striking properties: the support (for fixed t) is the ball of radius $|t|$, and the singular support is the boundary of the support. There does not appear to be any analogous behavior on SG. It does appear that $P(t, x, y)$ is localized to a neighborhood of $x = y$ for small t, with a sharper localization for smaller t, so we do have the general appearance of a wave spreading from the stimulus point y. But the spreading cannot occur at a constant speed.

Suppose it were true that for some t_0 and all times $|t| \leq t_0$ the propagator $P(t, x, y)$ had support (in x) contained in the two minimal G_1 triangles having vertex y. Choose coordinates so that $y = 0$. Then the function $\frac{\sqrt{5}}{3}P\left(\frac{t}{\sqrt{5}}, \frac{1}{2}x, y\right)$ (set equal to 0 on the third minimal triangle) would satisfy the same conditions as the propagator. Thus, we would have the scaling identity

$$P(t, x, 0) = \frac{\sqrt{5}}{3}P\left(\frac{t}{\sqrt{5}}, \frac{x}{2}, 0\right) \quad \text{for} \quad |t| \leq t_0 \tag{5.18}$$

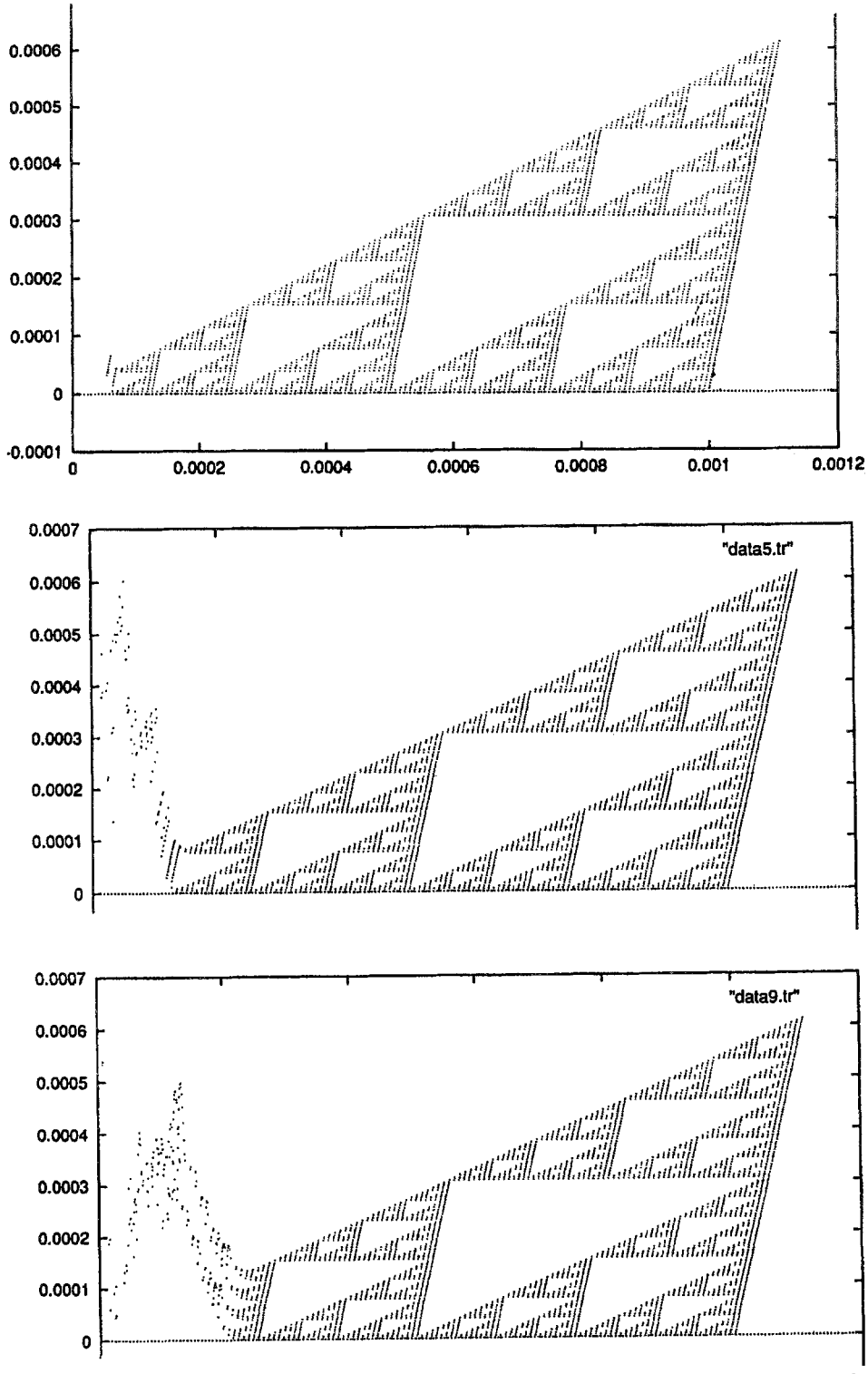

FIGURE 41 The wave propagator on a minimal G_1 triangle with stimulus point at the left vertex, for time $t = .02, .05, .09$.

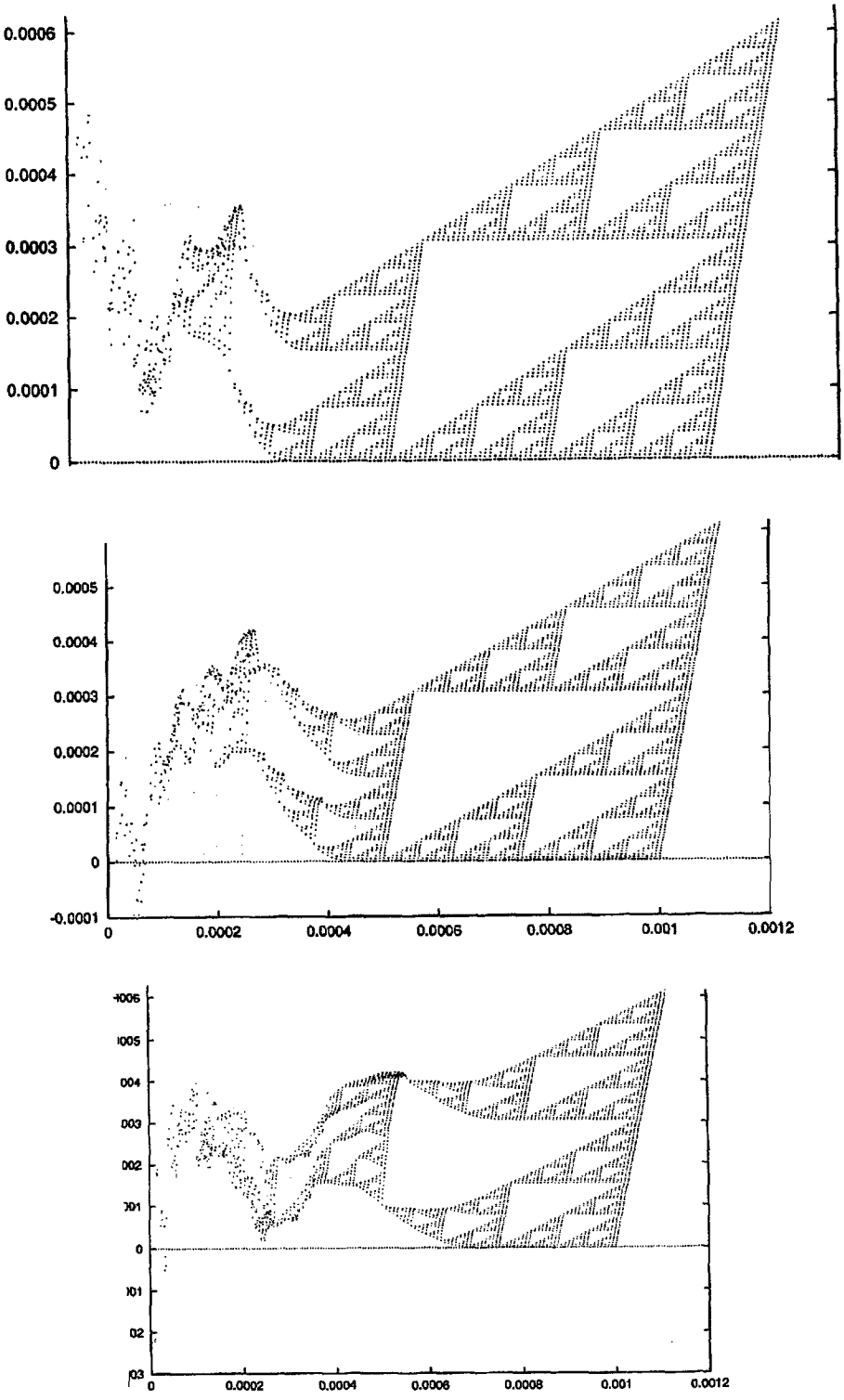

FIGURE 41 The wave propagator on a minimal G_1 triangle with stimulus point at the left vertex, for time $t = .15, .2, .35$.

on the two triangles. Suppose $\widetilde{x}$ is a point at time $\widetilde{t}$ for which $P(\widetilde{t}, \widetilde{x}, 0)$ is significantly different from zero. Then the wave has traveled at a speed of the order of $|\widetilde{x}|/\widetilde{t}$ to get from $y = 0$ to $\widetilde{x}$. But by (5.18), we would also have that $P(5^{-k/2}\widetilde{t}, 2^{-k}\widetilde{x}, 0)$ is significantly different from zero, so the wave has traveled at a speed of the order

$$\frac{|2^{-k}\widetilde{x}|}{5^{-k/2}\widetilde{t}} = \left(\frac{\sqrt{5}}{2}\right)^k \frac{|\widetilde{x}|}{\widetilde{t}}$$

to get from $y = 0$ to $2^{-k}\widetilde{x}$. This indicates that the speed of propagation increases as we pass to smaller scales. (The argument does not depend on using the exact Euclidean metric on SG, but only one that scales the same way under contractions. However, since SG contains lines, it is impossible to introduce a true metric on SG in which distances decrease any faster under contractions, so the increase in speed at smaller scales cannot be eliminated by choosing a different metric.)

This scaling argument shows that we cannot have a maximum propagation speed for the wave equation, but it does not conclusively rule out having a finite (but unbounded) propagation speed. There might be a function $a(t)$ such that $P(t, x, y)$ is supported in $|x - y| \leq a(t)$. In that case, (5.18) would imply

$$a\left(\frac{1}{\sqrt{5}}t\right) = \frac{a(t)}{2} \quad \text{for} \quad |t| < t_0 \tag{5.19}$$

which is consistent with

$$a(t) = O\left(t^\gamma\right) \quad \text{for} \quad \gamma = \frac{\log 2}{\log \sqrt{5}} .$$

But this seems very unlikely because (5.7) implies the semigroup property

$$P(t + s, x, y) = \frac{\partial}{\partial t} \int_{SG} P(t, x, z) P(s, z, y) d\mu(z) \tag{5.20}$$

which implies

$$a(t + s) \leq a(t) + a(s) , \tag{5.21}$$

with equality in (5.21) unless there is massive cancellation in (5.20). But (5.19) is inconsistent with equality in (5.21), so there would have to be massive cancellation in (5.20). While we cannot assert that this is impossible, we can make an analogy with the Lions–Titchmarsh Theorem for convolutions in $\mathbb{R}^n$: the convex hull of the support of a convolution of two distributions of compact support is exactly equal to the sum of the convex hulls of the supports of the distributions.

This argument, if it is valid, undermines the validity of (5.18), which was derived from a finite speed assumption. Thus, we do not believe that (5.18) is an exact equality. On the other hand, it seems likely that (5.18) is a good approximation, since the error would come from the influence of the Dirichlet boundary condition, and the boundary is relatively far away, at least for small t and x near y.

Since the wave propagator is known *a priori* to be only an L^2 function, it may be intrinsically very difficult to approximate accurately. Our data show extreme variability, and are very sensitive to the choice of m. Therefore, we also examined some less singular solutions to the wave equation. One way we tested for accuracy was to check the conservation of total energy

$$\mathcal{E}_m(t) = \sum_{p \in G_m} v(p, t)^2 + \frac{1}{2} 5^m \sum_{p \in G_m} \sum_{(p,q) \in E_m} (u(p, t) - u(q, t))^2 \tag{5.22}$$

where

$$v(p, kh) = h^{-1}(u(p, kh) - u(p, (k - 1)h)) \tag{5.23}$$

approximates $\partial u/\partial t$. We can also consider the portion of energy localized to any region in SG by restricting the sum to those values of p lying in the region.

We studied solutions of the wave equation obtained from zero initial position and velocity and boundary data, except that at one boundary point we specify the value of the solution by a driving function $\varphi(t)$. Let $U_{\varphi,m}(x, t)$ denote the resulting approximation at level m (we suppress the value of h, and choose space coordinates so that $x = 0$ corresponds to the driven boundary point). Figure 42 shows the graphs as a function of t for x the midpoint of one of the edges of G_0 containing $x = 0$, for $\varphi(t) = \sin \omega t$ and various choices of ω. Note the relative insensitivity of the change from $m = 3$ to $m = 4$, showing that, for these examples, a relatively small choice of m was sufficient.

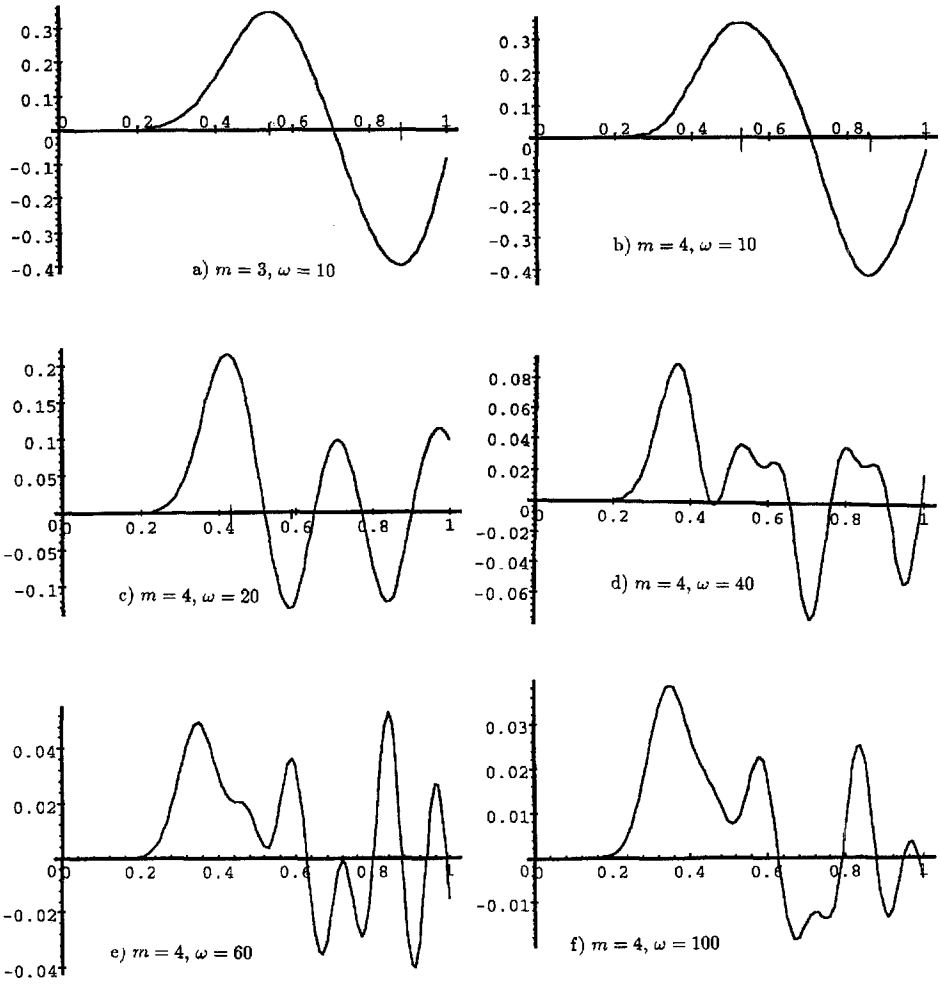

FIGURE 42 The graphs of $U_{\varphi,m}(x, t)$ as a function of t for x the midpoint of an edge of G_0 containing $x = 0$, and $\varphi(t) = \sin \omega t$, for various choices of m and ω. (a) $m = 3$, $\omega = 10$, (b) $m = 4$, $\omega = 10$, (c) $m = 4$, $\omega = 20$, (d) $m = 4$, $\omega = 40$, (e) $m = 4$, $\omega = 60$, and (f) $m = 4$, $\omega = 100$.

In general, the approximation is insensitive to m, and is therefore a good approximation, as long as the frequency of the driving function φ is significantly less than $5^{\frac{m}{2}}$. For such driving functions, high frequency noise develops near the point being driven, probably because of the introduction of

localized eigenfunctions. The major front of the wave, however, spreads outward from the driven point, its amplitude decreasing as it gets farther from the source.

In contrast, the approximations to the wave propagator show high sensitivity to the value of m. Figure 43 shows the position of the stimulated point as a function of time for several values of m. We observe that for higher values of m, the forces acting to restore the stimulated point are higher and thus the stimulated point oscillates more rapidly. Intuitively, a delta function of velocity on a coarse pre-gasket corresponds to a long wavelength and low frequency oscillation, while a velocity delta function on a refined pre-gasket is a high frequency stimulation. Based on Fig. 42, we conjecture that the energy from high frequency waves remains more localized than the energy from low frequency waves.

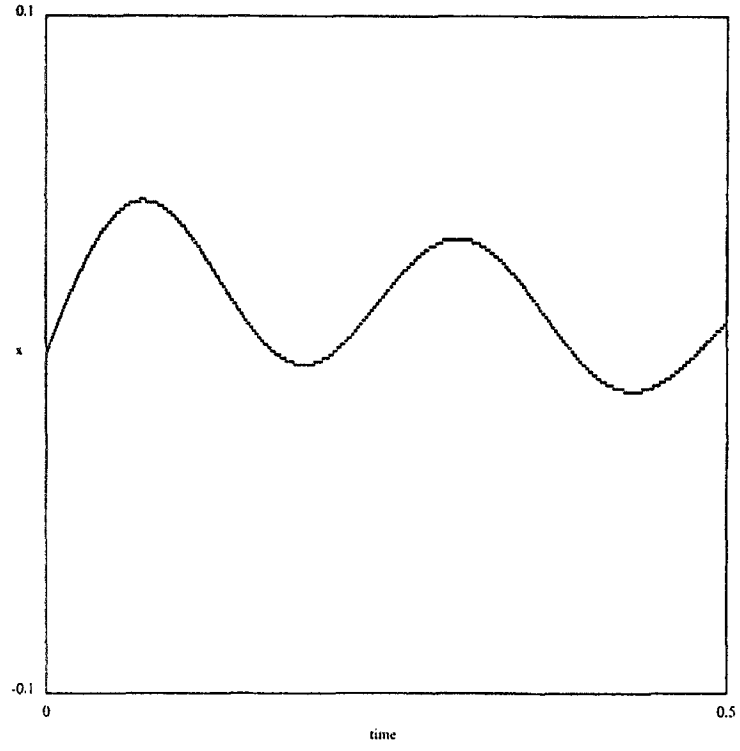

FIGURE 43 Approximations to the wave propagator at the stimulated point as a function of time, (a) $m = 3$.

To test our conjecture directly, we returned to the previous experiment of driving one of the boundary points. We used driving functions of the form

$$\varphi(t) = \begin{cases} \sin 2\pi\omega t & \text{if } 0 \leq t < 1/2\omega \\ 0 & \text{otherwise} \end{cases} \tag{5.24}$$

and varied the frequency. We measured the arrival times of the crest of the wave to the points p_1, p_2, p_3, (see Fig. 44) by noting the time at which the displacement of these points reached its first local maximum. From the arrival time we calculate the speed of the wave for that scale. We also recorded the amplitude of this first local maximum. In Fig. 45, we show for $m = 6$ the amplitude and speed of the wave at different points and for different frequencies. (The same computations for $m = 7$ yielded similar data, showing some evidence for the accuracy of our results.) This evidence supports our conjecture that the energy from high frequency waves remains more localized than the energy from low frequency waves. However, the data is disappointing in other respects. While a

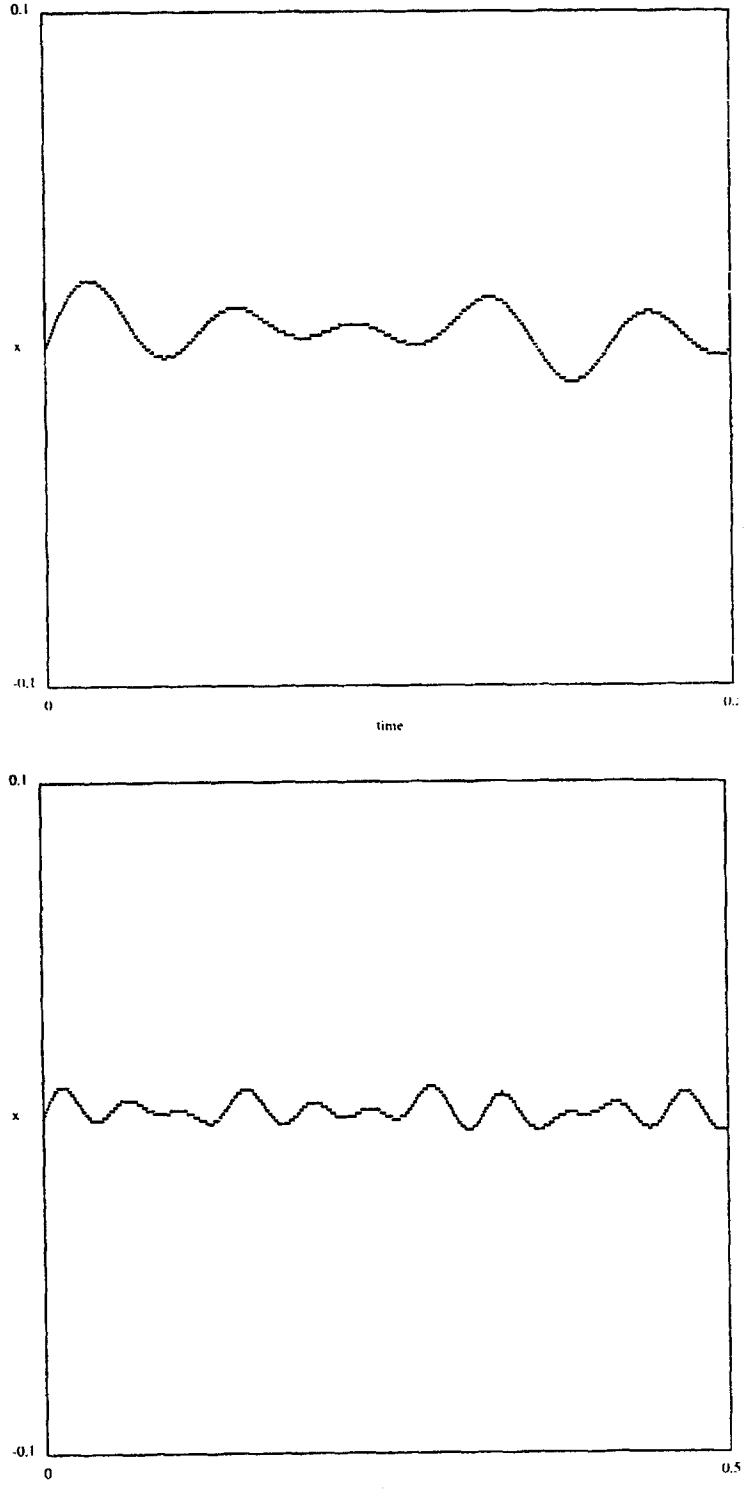

FIGURE 43 Approximations to the wave propagator at the stimulated point as a function of time, (b) $m = 4$ and (c) $m = 5$.

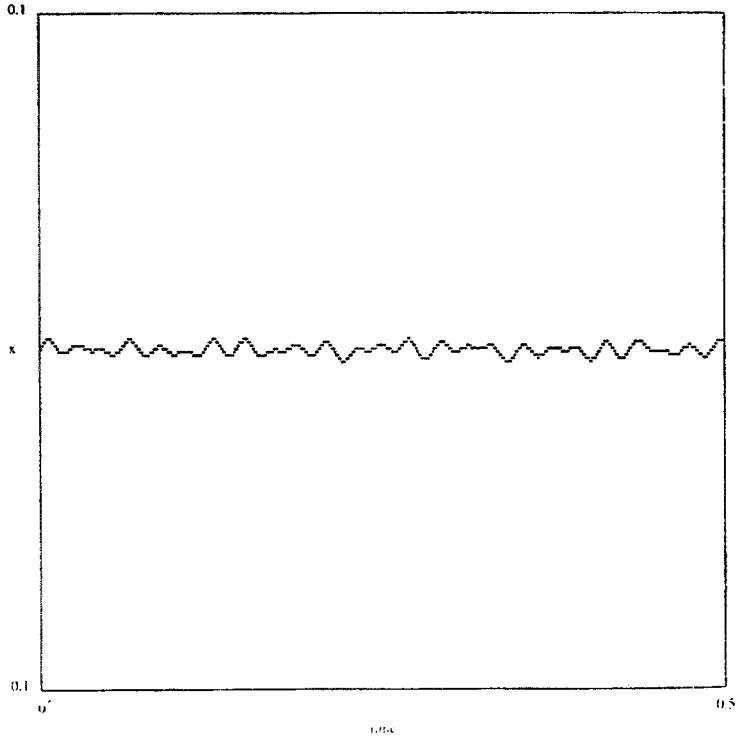

FIGURE 43 Approximations to the wave propagator at the stimulated point as a function of time, (d) $m = 6$.

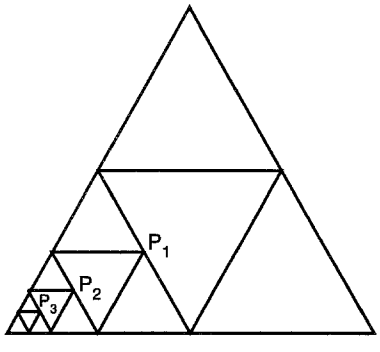

FIGURE 44 The sequence of points p_1, p_2, p_3 approaching the driving point.

speed-up is observed at smaller scales, it is somewhat more than the factor of $\sqrt{(5)}/2$ we predicted by using a scaling argument. It is not apparent from the figure, but the wavespeed is slightly sensitive to the depth m of the pre-gasket.

point	frequency(ω)	wave speed	maximum amplitude
p_1	3	1.384914	.316183
p_2	3	1.438159	.671578
p_3	3	1.705708	.874292
p_1	5	1.417033	.198700
p_2	5	1.485443	.420118
p_3	5	1.624431	.796316
p_1	10	1.420858	.102625
p_2	10	1.566907	.221725
p_3	10	1.655629	.471438
p_1	15	1.421599	.068883
p_2	15	1.569694	.151216
p_3	15	1.696833	.327375
p_1	20	1.421868	.051788
p_2	20	1.569859	.114424
p_3	20	1.707650	.250322
p_1	30	1.422138	.034587
p_2	30	1.570023	.076793
p_3	30	1.715070	.169459
p_1	40	1.422172	.025955
p_2	40	1.570105	.057730
p_3	40	1.716444	.127810

FIGURE 45 A table of values for wave speed and the first local maximum amplitude for solutions of the wave equation with driving term of the form (5.24). All data shown used an approximation $m = 6$ to the gasket (data for $m = 7$ is quite similar). The points p_j refer to Fig. 44.

Acknowledgments

We are grateful to Jun Kigami who read the original manuscript and suggested several improvements, and to John Hubbard for useful advice.

References

[1] Ayer, E. and Strichartz, R. Hausdorff measure and intervals of maximal density for Cantor sets, *Trans. Amer. Math. Soc.*, (to appear).

[2] Barlow, M.T. and Kigami, J. (1997). Localized eigenfunctions of the Laplacian on p.c.f. self-similar sets, *J. London Math. Soc.*

[3] Ben-Bassat, O., Strichartz, R., and Teplyaev, A. What is not in the domain of the Laplacian on a Sierpinski gasket type fractal, *J. Functional Anal.*, (to appear).

[4] Berry, M.V. (1980). Some geometric aspects of wave motion: wavefront dislocations, diffraction catastrophes, diffractals in Geometry of the Laplace Operator, *Proc. Symp. Pure Math.*, **36**, Amer. Math. Soc., Providence, 13–38.

[5] Brossard, J. and Carmona, R. (1986). Can one hear the dimension of a fractal? *Commun. Math. Phys.*, **104**, 103–122.

[6] Fleckinger, J., Levitin. M., and Vassiliev, D. (1995). Heat equation on the triadic von Koch snowflake, *Proc. London Math. Soc.*, (3)71, 372–396.

[7] Fleckinger, J. and Vassiliev, D. (1993). An example of a two-term asymptotics for the "counting function" of a fractal drum, *Trans. Amer. Math. Soc.*, **337**, 99–116.

[8] Fukushima, M. and Shima, T. (1992). On a spectral analysis for the Sierpinski gasket, *Potential Anal.*, **1**, 1–35.

[9] Jonsson, A. (1996). Brownian motion on fractals and function spaces, *Math. Zeit.*, **222**, 495–504.

[10] Kigami, J. Personal communication.

[11] Kigami, J. (1989). A harmonic calculus on the Sierpinski gasket, *Japan J. Appl. Math.*, **6**, 259–290.

[12] Kigami, J. (1993). Harmonic calculus on p.c.f. self-similar sets, *Trans. Amer. Math. Soc.*, **335**, 721–755.

[13] Kigami, J. (1993). Harmonic metric and Dirichlet form on the Sierpinski gasket, in Asymptotic problems in probability theory: stochastic models and diffusions on fractals, Elworthy, K.D. and Ikeda, N., Eds., *Pitman Research Notes in Math.*, **283**, 201–218.

[14] Kigami, J. and Lapidus, M. (1993). Weyl's problem for the spectral distribution of Laplacians on p.c.f. self-similar fractals, *Comm. Math. Phys.*, **158**, 93–125.

[15] Kusuoka, S. and Zhou X.Y. Waves on fractal-like manifolds and effective energy propagation, preprint.

[16] Levitin, M. and Vassiliev, D. (1996). Spectral asymptotics, renewal theorem, and the Berry conjecture for a class of fractals, *Proc. London Math. Soc.*, (3)72, 188–214.

[17] Lindstrom, T. (1990). Brownian motion on nested fractals, *Memoir AMS*, **83**(420).

[18] Milnor, J. (1990). *Dynamics in One Complex Variable: Introductory Lectures*, SUNY Stony Brook, Institute for Mathematical Sciences.

[19] Rammal, R. (1984). Spectrum of harmonic excitations on fractals, *J. Physique*, **45**, 191–206.

[20] Rammal, R. and Toulouse, G. (1982). Random walks on fractal structures and percolation clusters, *J. Physique Lett.*, **43**, L13–L22.

[21] Shima, T. (1991). On eigenvalue problems for the random walks on the Sierpinski pre-gaskets, *Japan J. Indust. Appl. Math.*, **8**, 127–141.

[22] Shima, T. (1996). On eigenvalue problems for Laplacians on p.c.f. self-similar sets, *Japan J. Indust. Appl. Math.*, **13**, 1–23.

[23] Strichartz, R. (1996). Fractals in the large, *Can. Math. J.*, **50**, 638–657.

[24] Strichartz, R. (1997). Piecewise linear wavelets on Sierpinski gasket type fractals, *J. Four. Anal. Appl.*, **3**, 387–416.

[25] Strichartz, R. Isoperimetric estimates on Sierpinski gasket type fractals *Trans. Amer. Math. Soc.*, (to appear).

[26] Strichartz, R. Some properties of Laplacians on fractals, *J. Functional Anal.*, (to appear).

[27] Teplyaev, A. (1998). Spectral analysis on infinite Sierpinski gaskets, *J. Functional Anal.*, **159**, 537–567.

Received June 23, 1997
Revision received Nov. 16, 1998

Polygon Network, Inc., 14142 Denver West Parkway, Bldg. 51, Ste225, Golden, CO 80401
e-mail: kyal@polygon.net

Mathematics Department, Cornell University, Ithaca, NY 14853
e-mail: str@math.cornell.edu

Department of Mathematics, Fine Hall, Washington Rd.,
Princeton University, Princeton, NJ 08544
e-mail: jpvinson@math.princeton.edu